

# A Critical Assessment of Electronic Structure Descriptors for Predicting Perovskite Catalytic Properties

**Authors:** Ryan Jacobs<sup>1,\*</sup>, Jian Liu<sup>2</sup>, Harry Abernathy<sup>2</sup>, Dane Morgan<sup>1</sup>

<sup>1</sup> Department of Materials Science and Engineering, University of Wisconsin-Madison, Madison, WI, 53706, USA.

<sup>2</sup> National Energy Technology Lab, Morgantown, WV, 26505, USA.

\*Corresponding author e-mail: [rjacobs3@wisc.edu](mailto:rjacobs3@wisc.edu)

**Keywords:** oxygen reduction reaction, perovskite, catalysis, density functional theory, electronic structure descriptor

## Abstract

The discovery and design of new materials which can efficiently catalyze the oxygen reduction and evolution reactions at reduced temperatures is important for facilitating the widespread adoption of fuel cell and electrolyzer technologies. Numerous studies have produced correlations between catalytic properties, such as oxygen surface exchange or electrode area specific resistance (ASR), and properties of the catalyst material. However, correlations have historically been limited in scope (e.g., using only a few materials or at a single temperature) and it has been difficult to provide detailed assessments of their robustness. Here, we assess the ability of the O p-band center electronic structure descriptor, obtained from density functional theory (DFT) calculations, to correlate with oxygen surface exchange rates, diffusivities, and area specific resistances for a large database of perovskite oxide catalytic properties. By data mining the literature, we obtain 747 catalytic property value data points spanning 299 unique perovskite compositions from 313 studies. We assess linear correlations of each property with the O p-band center and find generally modest correlations that are qualitatively useful (prediction mean absolute errors of about 0.5 log units are typical), where the correlations are improved at higher temperatures (e.g., 800 °C vs. 500 °C) and significantly improve when considering fits to the subset of materials which have multiple independent measurements. These findings suggest that the spread of property data is significantly influenced by experimental uncertainty, and subsequent measurements of additional materials will likely improve the O p-band center correlations.

## 1. Introduction

Oxygen-active materials that efficiently reduce, absorb, transport, and evolve oxygen are key components for energy devices such as solid oxide fuel cells (SOFCs), solid oxide electrolyzers (SOECs), reversible SOFCs (r-SOFCs), proton ceramic fuel cells (PCFCs),<sup>1–11</sup> solid oxide batteries,<sup>12–14</sup> memristors,<sup>15–17</sup> and oxygen separation membranes for high purity gas generation.<sup>18,19</sup> In this work, we focus on the perovskite oxide family of oxygen-active materials ( $A_{1-x}A'_xB_{1-y}B'_yO_3$  chemical formula). Perovskite oxides are the most explored candidate materials to replace precious metal catalysts for use in SOFCs and SOECs to catalyze the oxygen reduction reaction (ORR) and oxygen evolution reaction (OER), respectively. A tremendous body of research has been conducted in the past few decades, resulting in novel perovskite compounds for application as the electrode in a fuel cell and electrolyzer devices as well as the oxygen-transport mediating electrolyte material. Regarding the electrolyte, doped zirconia and ceria materials are often employed (e.g. yttria-stabilized zirconia (YSZ) as well as gadolinium- or samarium-doped ceria (GDC, SDC)), but occasionally Sr- and Mg-doped LaGaO<sub>3</sub> perovskite, La<sub>1-x</sub>Sr<sub>x</sub>Ga<sub>1-y</sub>Mg<sub>y</sub>O<sub>3</sub> (LSGM) is used, which remains one of the best oxygen-conducting electrolyte materials.<sup>20–22</sup> Perovskites have found more widespread use as the electrode material, where research has resulted in the development of current commercial SOFC materials like La<sub>1-x</sub>Sr<sub>x</sub>MnO<sub>3</sub> (LSM)<sup>23–25</sup> and La<sub>1-x</sub>Sr<sub>x</sub>Co<sub>1-y</sub>Fe<sub>y</sub>O<sub>3</sub> (LSCF),<sup>26–28</sup> and high-performing but presently non-commercial materials like Ba<sub>1-x</sub>Sr<sub>x</sub>Co<sub>1-y</sub>Fe<sub>y</sub>O<sub>3</sub> (BSCF)<sup>29–33</sup> and PrBaCo<sub>2</sub>O<sub>5+δ</sub> (PBCO).<sup>34–36</sup> Recently, it has been shown that some perovskites, like BaFe<sub>0.4</sub>Co<sub>0.4</sub>Zr<sub>0.1</sub>Y<sub>0.1</sub>O<sub>3</sub> (BFCZY),<sup>5,37,38</sup> Ba<sub>0.95</sub>La<sub>0.05</sub>Fe<sub>0.8</sub>Zn<sub>0.2</sub>O<sub>3</sub> (BLFZn)<sup>10,39</sup> and SrFe<sub>1.5</sub>Mo<sub>0.5</sub>O<sub>6-δ</sub>,<sup>40,41</sup> are highly oxygen-active materials which are also good incorporators and conductors of protons. Due to their ability to also transport electrons efficiently, these materials form a group of so-called triple conductors. Triple conducting materials are especially promising for use as electrodes in r-SOFCs and PCFCs, where the electrode must efficiently reduce and transport oxygen, protons and electrons simultaneously.<sup>42–45</sup>

In the past decade, a number of atomistic-scale computational investigations have been conducted to understand perovskite catalytic properties, primarily using first-principles density functional theory (DFT) methods. These computational studies sought to understand the origins of, and trends in, perovskite properties relevant to their desirable oxygen-active properties. In

such studies, electronic structure descriptors are commonly used to formulate and rationalize correlations between material structure and chemistry and a corresponding property of interest, like the oxygen surface exchange rate. Electronic structure descriptors are useful in part because they serve as a simple proxy for a more complex, difficult-to-acquire physical property, and they are important because they have enabled new understanding and a means to screen and predict new materials using DFT. While many descriptors have been proposed in the literature, such as O p-band center,<sup>46</sup> O p-band center weighted by the  $d_{xy}$  orbital band center,<sup>47</sup>  $e_g$  electron orbital occupancy,<sup>48,49</sup> charge transfer gap energy,<sup>50</sup> and  $G_{\max}$ , the maximum free energy of OER steps at zero overpotential,<sup>51</sup> among others, here we focus on the O p-band center as it has been previously shown to correlate well with a number of oxygen-active materials properties.<sup>52,53</sup> Properties shown to correlate with O p-band center include experimental surface exchange rates in perovskites and Ruddlesden-Popper oxides,<sup>46,54,55</sup> oxygen vacancy formation and migration energies,<sup>46,52,56</sup> calculated and experimental barriers for oxygen diffusion and surface exchange,<sup>46,53,55</sup> the electronic work function,<sup>57,58</sup> OER current densities and overpotential,<sup>47,53,59</sup> and the surface binding energies of numerous species such as O, H, OH, OOH.<sup>52,53,60</sup> The O p-band center has not only shed light on the above-mentioned correlations with material composition, but has also resolved trends in the coupling of lattice strain with changes in the electronic structure and resulting properties,<sup>61,62</sup> as well as distinguished surface-specific properties of work function<sup>58</sup> and adsorption energies.<sup>60</sup> There is also evidence suggesting that the O p-band center idea may be extensible beyond oxides as a more general anion p-band center descriptor, where it may find application to predict catalytic properties of sulfides, chlorides, and fluorides.<sup>52</sup> Further, the O p-band center correlation has enabled high-throughput DFT screening studies, such as the work by Jacobs et al.<sup>55</sup> who found new stable, highly active SOFC cathode materials<sup>63,64</sup> and Ma et al.,<sup>57</sup> who discovered a number of low work function perovskite materials for electron emission applications. While high-throughput computational screening using the O p-band center is more efficient than large-scale experimentation, a single prediction still requires at least one DFT calculation, which typically takes on the order of hours of computing time.

While previous studies employing descriptors like the O p-band center have resulted in new understanding and trends which have produced new promising materials, studies which

have examined correlations of the O p-band center with various properties tended to either focus on a limited set of the examined materials from the literature, provided values obtained under a single set of experimental conditions (e.g., one particular temperature), or lacked detailed estimates of the uncertainty both from the experimental values and predicted values from the correlations. These factors, in turn, raise questions about how accurate the O p-band descriptor is for calculating oxygen-active materials properties and whether such correlations are more suited for qualitative materials screening guidance rather than quantitative predictions of materials behavior. The first major result of this work is development and exploration of a large database of experimentally measured perovskite catalytic properties from the literature, including tracer and chemical surface exchange rates  $k^*$  and  $k_{\text{chem}}$ , tracer and chemical oxygen diffusivities  $D^*$  and  $D_{\text{chem}}$ , and the electrode cell area specific resistance (ASR). This database is expected to be widely useful for the broader research community for data-driven analysis, for example, assessing typical ranges of values of the most-studied materials, providing guidance for expected error levels of properties measured by different research groups on the same material, flagging potentially problematic measurements, forming lists of high-performing materials at various working temperatures, and more. The second main result of this work consists of using our new database to explore and quantitatively assess many previously proposed correlations, including the trends of  $k^*$  and ASR with O p-band center, trend of  $k^*$  versus  $D^*$ , and the relationships between  $D^*/D_{\text{chem}}$  and  $k^*/k_{\text{chem}}$ . We find that O p-band center trends worsen compared to previous studies with the addition of more data, but significantly improve when considering the subset of materials which have multiple experimental measurements. This finding suggests that experimental error plays a key role in determining the correlation quality, and that the O p-band center is still useful for qualitative assessment of perovskite catalytic properties.

## 2. Results and Discussion

### 2.1. Experimental property database development

Catalytic property data of perovskite oxide materials were collected from a total of 313 studies in the literature (the full database is available as part of the **Supplementary Information (SI)**, see **Data Availability**) (see **Methods** in **Section 4.2**). We believe this database of perovskite catalytic properties is the largest such database which has been collected to date. The data consist of chemical surface exchange ( $k_{\text{chem}}$ ) and diffusion ( $D_{\text{chem}}$ ) values from electrical conductivity relaxation (ECR) experiments, tracer surface exchange ( $k^*$ ) and diffusion ( $D^*$ ) values from isotope exchange depth profiling (IEDP) experiments, and ASR measurements from electrochemical impedance spectroscopy (EIS) experiments. From these 313 studies, a total of 749 data points on 299 unique perovskite compositions were obtained. For the properties of  $k_{\text{chem}}$ ,  $D_{\text{chem}}$ ,  $k^*$ ,  $D^*$  and ASR, a total of 98, 83, 80, 66 and 422 experimental measurements on various materials were obtained, respectively, which comprise 62, 58, 48, 42 and 257 unique materials for each property, respectively, as summarized in **Table 1**. As a visual overview of the collected data, in **Figure 1** we show a periodic table heatmap summarizing the occurrences of each element in our database. From **Figure 1**, we can observe that La is the most occurring rare earth element, and Sr, followed by Ba, are the most occurring alkaline earth elements. The elements Co and Fe are the most frequently occurring transition metal elements, and Nb is the most frequently occurring non-3d transition metal stabilizing element. The high frequency of these listed elements makes sense given the history of engineering new mixed ionic-electronic conductors, where perovskite  $\text{LaCoO}_3$  is a high-performing parent material which is often modified for increased activity by A-site doping with Sr or Ba and B-site doping with Fe and Nb. In **Figure 2** we show histograms of database catalytic property values at 500 °C and 800 °C, in conjunction with some basic statistics of the catalytic property distributions. Additional details and discussion of aspects of the collected database are presented in **Section S1** of the **SI**. This supplementary discussion includes an overall survey of basic statistics of each catalytic property in the database, including flagging potentially problematic measurements and enumerating the

best-performing materials at various temperatures based on each catalytic property (e.g., highest  $k_{\text{chem}}$  materials, lowest ASR materials).

**Table 1.** High-level summary of perovskite catalytic data extracted from the literature for this study.

Property	Number of studies examined	Number of measurements extracted	Number of unique materials
$k_{\text{chem}}$	70	98	62
$D_{\text{chem}}$	56	83	58
$k^*$	39	80	48
$D^*$	37	66	42
ASR	235	422	257

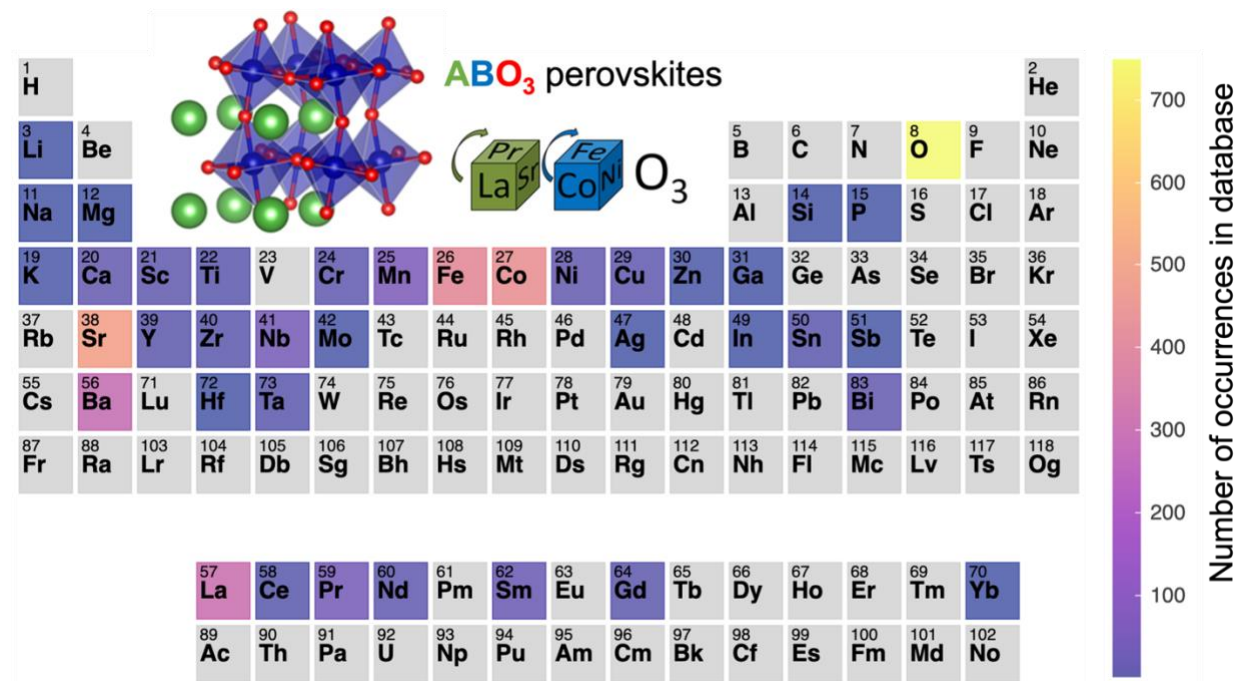


**Figure 1.** Periodic table heatmap summarizing the occurrences of different elements in the perovskite compositions comprising our catalytic property database.

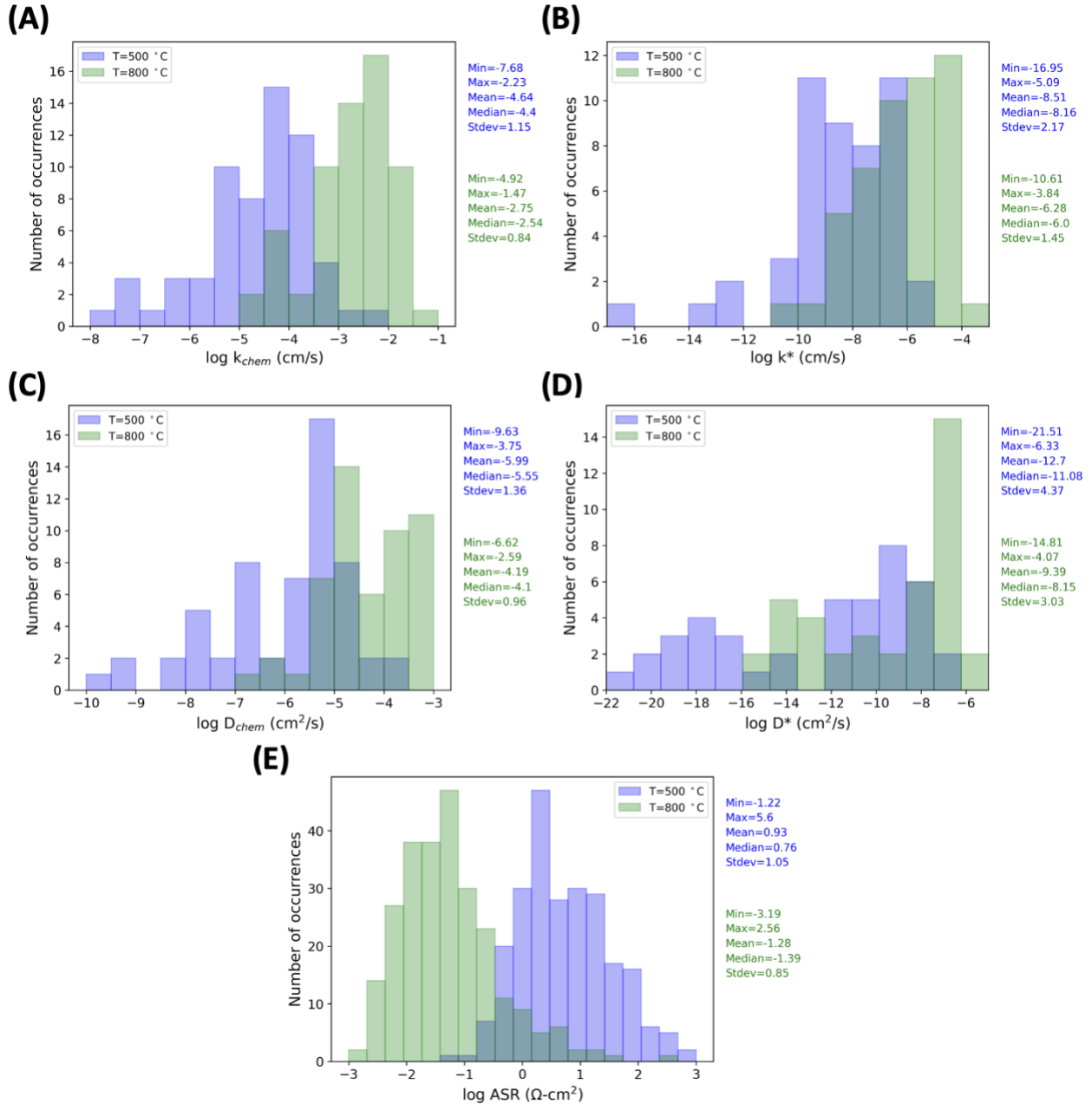


**Figure 2.** Histogram distributions of each perovskite catalytic property of interest from our collected database. In all plots, blue bars represent the distribution at 500 °C and green bars represent the distribution at 800 °C. (A):  $k_{chem}$  distribution, (B):  $k^*$  distribution, (C):  $D_{chem}$  distribution, (D):  $D^*$  distribution, (E): ASR distribution. Note that all values are plotted as the base-10 logarithm of the property value.

## 2.2. Assessment of O p-band center trends

In this section, we assess trends of our perovskite catalytic properties as a function of the DFT-calculated O p-band center (see **Methods in Section 4.1**). These assessments serve as a more detailed test of the O p-band center descriptor now that the perovskite catalytic property database has been significantly expanded compared to previous studies. Previous work by Lee et al.<sup>46</sup> formed correlations of  $k^*$  versus O p-band center for 9 materials and ASR versus O p-band center for 7 materials, resulting in linear  $R^2$  fit values of 0.87 and 0.99, respectively (note that LMO and LSM distinctly fall off the linear trend line of ASR versus O p-band in this example, and were not included in the fit). Subsequent work by Jacobs et al.<sup>55</sup> formed correlation of  $k^*$  versus O p-band center for 21 materials with a linear  $R^2$  fit of 0.86 and follow-on study of a subset of 9  $k^*$  measurements also had a linear  $R^2$  fit of 0.87.<sup>53</sup> These previous studies examined at least a 3-5 $\times$  smaller set of material than considered in this work, and only examined the trends at a single temperature.

**Figure 3** contains plots of perovskite catalytic properties from ECR ( $k_{\text{chem}}$ ,  $D_{\text{chem}}$ ), IEDP ( $k^*$ ,  $D^*$ ) and ASR values from EIS measurements as a function of the O p-band center calculated from DFT for each material. In **Figure 3**, the catalytic property trends are plotted at both 500 °C and 800 °C. Equivalent plots at 600 °C and 700 °C are provided in **Figure S2** of the **SI**. We observe from **Figure 3** that the quality of linear fit to the O p-band center is both property- and temperature-dependent. In general, the fit trends improve when considering data at higher temperatures. Based on the fit mean absolute error (MAE), when going from 500 °C to 800 °C the MAEs of fits to  $k_{\text{chem}}$  (0.68 vs. 0.49 cm/s),  $k^*$  (1.3 vs. 0.76 cm/s),  $D_{\text{chem}}$  (0.72 vs. 0.56 cm<sup>2</sup>/s),  $D^*$  (2.68 vs. 1.79 cm<sup>2</sup>/s) and ASR (0.69 vs. 0.57 Ohm-cm<sup>2</sup>) all decrease. We speculate the improved fits at higher temperature are a result of less experimental uncertainty in the measured values at higher temperature, producing less spread in the data and producing improved fits. The MAE values of  $k^*$  and  $D^*$  are higher than their  $k_{\text{chem}}$  and  $D_{\text{chem}}$  analogues, however this is likely a result of the larger dynamic range of the  $k^*$  and  $D^*$  data relative to  $k_{\text{chem}}$  and  $D_{\text{chem}}$ , because the reduced root mean square error (RMSE/ $\sigma$ ) ( $\sigma$ = dataset standard deviation) values for all properties are qualitatively similar, in the range of 0.6-0.8, indicating from this metric that the fits are statistically of similar quality.

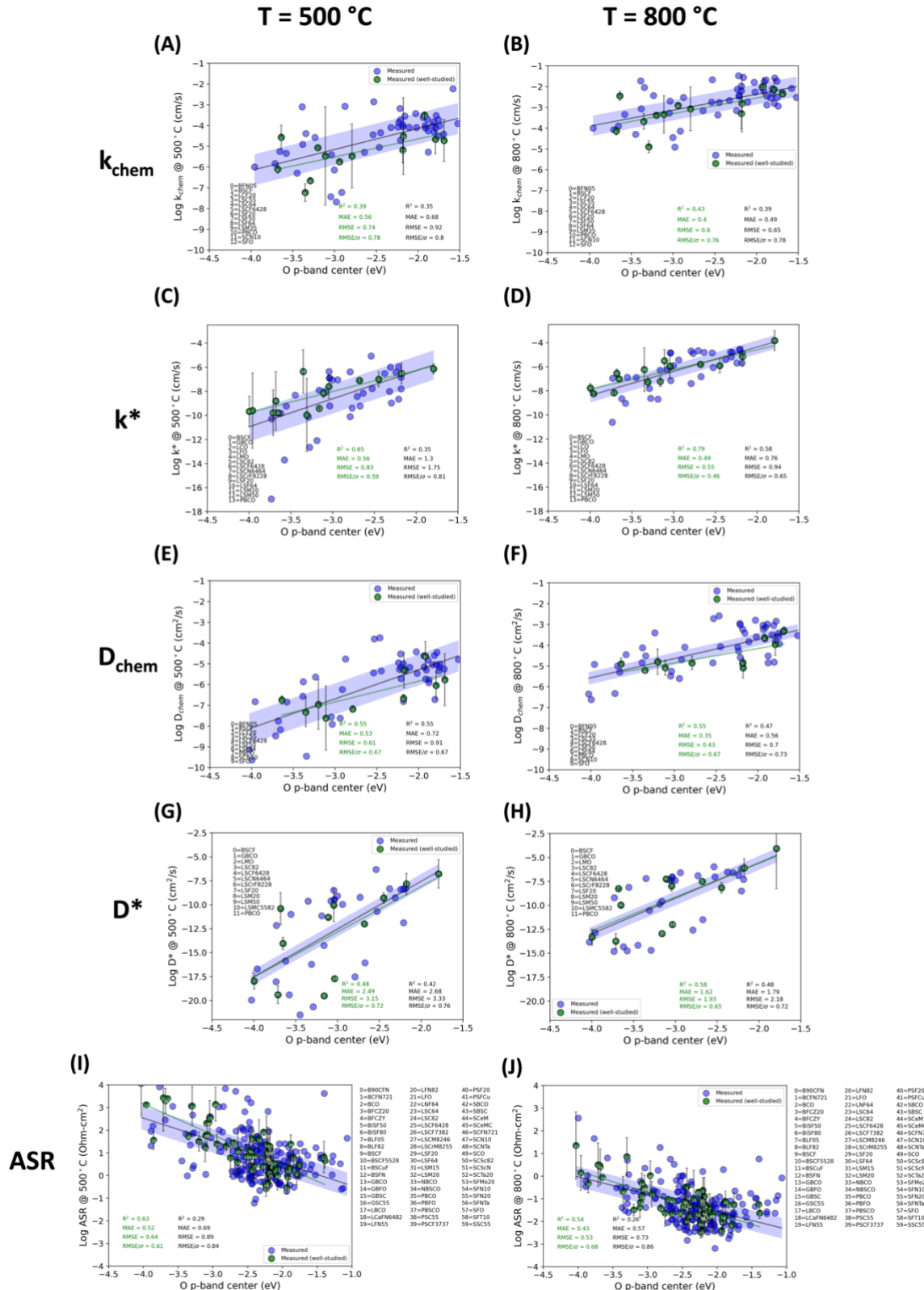


**Figure 3.** Trends of perovskite catalytic properties as a function of O p-band center. The left (right) column of plots is for T = 500 °C (T = 800 °C). The properties plotted are  $k_{\text{chem}}$  (A, B),  $k^*$  (C, D),  $D_{\text{chem}}$  (E, F),  $D^*$  (G, H), and ASR (I, J). The blue points and black fit line and statistics are for a linear fit to all the data. The green points and green fit line and statistics are for a linear fit to the subset of well-studied materials only (those materials with 2 or more measurements). The blue “x” points are outliers which were removed from the trend analysis. The blue shaded region is the average experimental error range, where the experimental error is calculated as the standard deviation of materials with multiple measurements. The average experimental error bars are 0.68 and 0.45 log units at 500 °C and 800 °C, respectively. For the ASR trend, ASR measurements of the same material with different electrolytes are averaged together. Data of the slopes and intercepts for all linear fits can be found in

The quality of the fits in **Figure 3** varies substantially when considering a fit to all materials (blue + green points) or just the subset of well-studied materials (green points), where here “well-studied” denotes materials with 2 or more independent measurements in the database. In **Figure 4**, the trend of improved fits both at higher temperatures and when considering only well-studied materials is shown more explicitly. In general, the well-studied materials have MAE smaller than fitting to all data points by about 10-50%, depending on the property and temperature. This result strongly suggests that a significant source of the errors in correlations with O p-band center is uncertainty in the experiments, where any given experimental data point may have an error bar of approximately 0.5-0.7 log units, depending on the temperature. We hypothesize that when a particular material is measured multiple times by different research groups, a more reliable average value emerges, and this causes the fits of O p-band center to have significantly less error. In **Figure 4** we alter the definition of “well-studied” to range from single measurements (the limiting case of considering all data in the database), up to the case where 5 or more independent measurements were conducted for a given material. Consistent with the above hypothesis, we find that model accuracy generally improves up to at least 3 or more measurements for a given material, as illustrated in **Figure 4F**. From **Figure 4F**, we can see that at 500 °C (800 °C), the MAE (in log units) of ASR is reduced from 0.58 to 0.38 (0.51 to 0.26) Ohm-cm<sup>2</sup>, corresponding to percentage reductions of about 35% (50%), respectively.

The quality of the linear fits in this work are slightly lower, but similar to, reliable values reported in previous studies discussed above when one takes into account that the previous studies were generally focused on high temperatures (about 800 °C) and values that came from

averaging multiple studies. Specifically, previous results found an  $R^2$  for  $k^*$  vs. p-band of 0.86–0.87<sup>46,53,55</sup> while the  $R^2$  for the well-studied materials at 800 °C from this work are 0.79 (**Figure 3D**). This modest reduction is likely due to the very high quality and limited data used in the earlier studies, leading to good correlations and significant sampling uncertainty. Previous studies found an  $R^2$  for ASR vs. p-band of 0.99<sup>46</sup>, which is much higher than the 0.44 (**Figure 3J**) found in this work. However, the extremely high 0.99 value is almost certainly an overestimate, likely caused by that study having removed selected data under the assumption that it followed a different model, some model tuning (as this result was the first O p-band center study), and the very limited size of the remaining data (just 7 points).

Overall, the O p-band center descriptor is useful in that it can provide a qualitative estimate of numerous catalytic properties at a given temperature of interest, where performing a single, bulk DFT calculation is generally much easier and faster (approximately 10 hours of computer time and can be done in parallel, with just minutes of human time for a properly automated setup) than synthesizing a material and performing the needed property measurements (possibly weeks of human time, typically done in serial). However, one should not expect quantitatively accurate predictions of key perovskite catalytic properties, at least estimates with error less than approximately 0.5 log units. Furthermore, it is likely that DFT-based descriptor approaches like the O p-band center are likely to be partially or totally replaced by more accurate and faster data-centric machine learning approaches as databases grow.

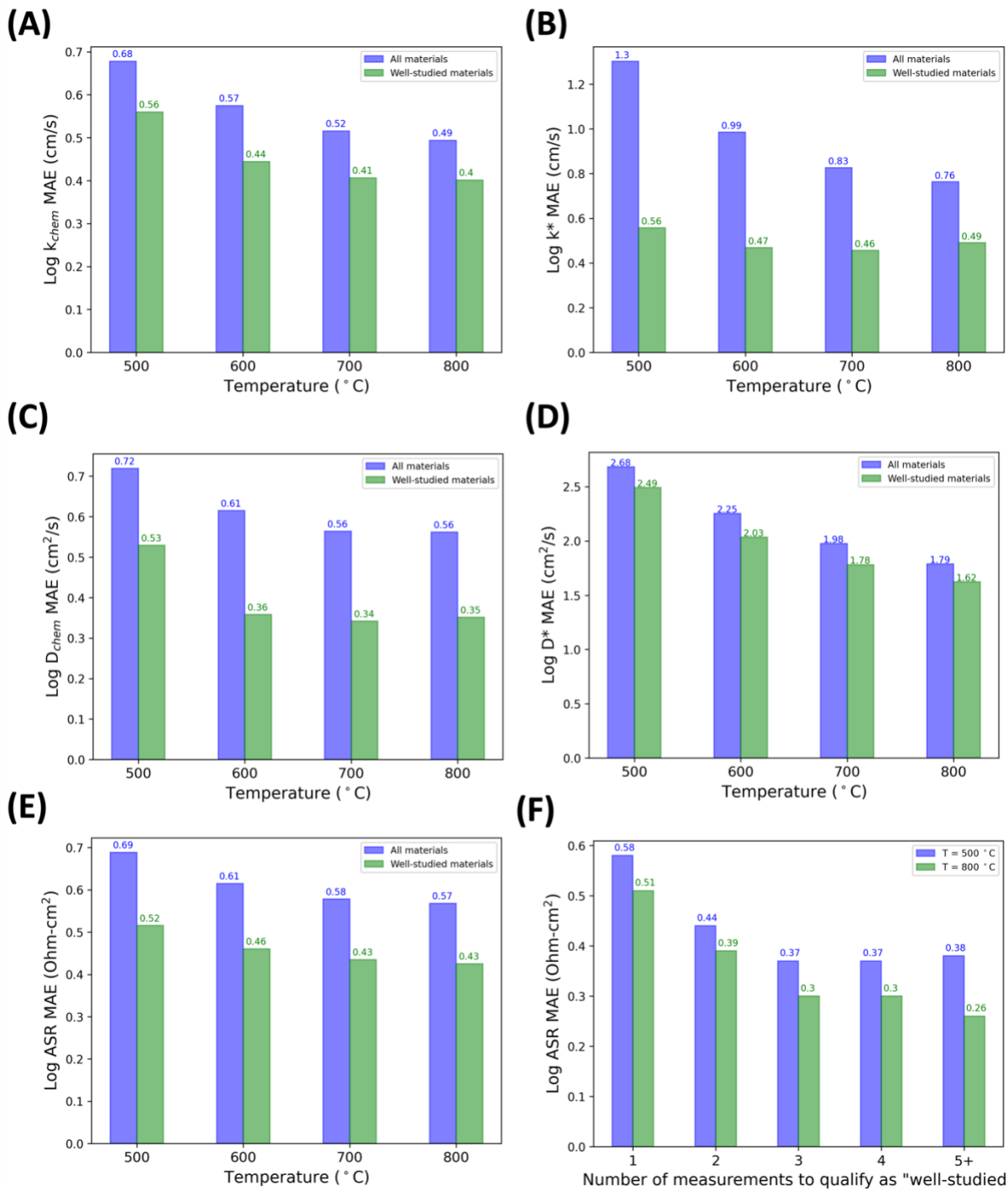


**Figure 4.** Bar charts summarizing the MAE values of linear fits to O p-band center of perovskite catalytic properties from ECR and IEDP experiments. In plots (A)-(E), the blue bars are MAE values of linear fits to all of the data, while the green bars are MAE values of linear fits to the subset of well-studied materials only (materials with 2 or more measurements). The properties are  $k_{\text{chem}}$  (A),  $k^*$  (B),  $D_{\text{chem}}$  (C),  $D^*$  (D), and ASR (E). Plot (F) further shows how the MAE on the ASR values varies when considering fits to materials containing increasing numbers of experimental measurements.

### 2.3. Summary of assessing relationships between catalytic properties

The database of perovskite catalytic properties developed in this work can be used to assess correlations between these properties proposed from previous studies. Such correlations can provide mechanistic insights and be used to fill in missing data with approximate values as a guide to material performance before performing a particular experiment or assessment of a result after experiment. In **Section S3** of the **SI**, we provide detailed discussion of assessing three inter-property relationships which have been proposed in the literature: First, the work of Kilner et al. showed there is a linear correlation between  $k^*$  and  $D^*$  for a set of  $\text{Sm}_{1-x}\text{Sr}_x\text{CoO}_3$ ,  $\text{La}_{1-x}\text{Sr}_x\text{CoO}_3$  and  $\text{La}_{1-x}\text{Sr}_x\text{MnO}_3$  perovskites.<sup>65</sup> Our analysis at 800 °C shows very good linear correlation similar to the work of Kilner et al.,<sup>65</sup> but with a wider range of perovskite compositions here ( $R^2 = 0.75$  for all materials,  $R^2=0.93$  for well-studied materials). Second, Lee et al. and Jacobs et al. showed correlations of  $k^*$  versus ASR for a limited set of materials.<sup>46,55</sup> This trend is particularly useful as it directly relates  $k^*$ , which is a materials property of the perovskite electrode catalyst, to ASR, which is related to the perovskite materials property but also includes additional confounding factors of the overall electrode device, such as its microstructure, the electrolyte it is bonded with, and any interfacial structure or phases at the electrode/electrolyte interface that may form. For this relationship of  $k^*$  versus ASR, our analysis at 800 °C results in an  $R^2=0.63$ , which increases to  $R^2=0.81$  for well-studied materials. Third, seminal work from Adler, Lane and Steele formulated a detailed model relating ASR with  $k^*$ ,  $D^*$ , and factors related to electrode microstructure, where this Adler-Lane-Steele<sup>66</sup> relationship stipulates that ASR is proportional to the inverse square root of the product of  $k^*$  and  $D^*$ . Similar with the other properties above, we find that this correlation persists but is improved when considering only well-studied materials, where at 800 °C we obtain  $R^2=0.68$ , increased slightly to  $R^2=0.7$  for well-studied materials. Overall, all of these property correlations follow the same two general principles discussed at length in **Section 2.2**: namely, the correlations are more robust at higher temperature and when considering fits to well-studied materials only, and show linear correlations of modest quality likely useful for qualitative materials property prediction.

## 2.4. Using thermodynamic factors and property correlations to predict new data

The inter-property correlations discussed in **Section 2.3** and **Section S3** of the **SI** provide one way to predict new property values given the corresponding property value forming the correlation. Here, we describe another approach to predict new materials property data by using the thermodynamic factor,  $\gamma$ , which relates the tracer surface exchange and diffusion with their chemical analogues, i.e.,  $k_{\text{chem}} = \gamma k^*$  and  $D_{\text{chem}} = \gamma D^*$ .<sup>27,67</sup> In this section, we first compare the values of  $\gamma$  obtained in three ways, then we use  $\gamma$  and the correlation of  $k^*$  versus ASR detailed in **Section S3** of the **SI** to obtain new predicted values of  $k^*$  using measurements of  $k_{\text{chem}}$  and ASR. Knowledge of  $\gamma$  can thus be used to fill in missing data values (e.g., obtain  $k^*$  if only  $k_{\text{chem}}$  is known), thus saving experimental time and aiding in screening for high-performing materials. Here, values of  $\gamma$  for a given material may be directly measured, which we refer to as “measured  $\gamma$ ”, the values of  $\gamma$  may be extracted from separate measurements of either  $k_{\text{chem}}/k^*$  or  $D_{\text{chem}}/D^*$ , which we refer to as “extracted  $\gamma$ ”, and, finally,  $\gamma$  may be predicted by taking the ratio of the linear fit lines from  $k_{\text{chem}}$  and  $k^*$  versus O p-band center (or  $D_{\text{chem}}$  and  $D^*$  versus O p-band center), which we refer to as “predicted  $\gamma$ ”.

It is worth noting that extracting  $\gamma$  from value pairs of  $k_{\text{chem}}/k^*$  or  $D_{\text{chem}}/D^*$  involves values taken from different research groups and different studies. Such a comparison may therefore add additional error as no two groups of people will make the exact same material or run a given experiment or analyze data in the same way. To our knowledge, there is only one case where  $\gamma$  was measured for a material, along with its  $k_{\text{chem}}$  and  $k^*$  values in the same study.<sup>33</sup> This study from Bucher et al.<sup>33</sup> sought to explicitly test the relationships of  $k_{\text{chem}} = \gamma k^*$  and  $D_{\text{chem}} = \gamma D^*$  against measuring  $\gamma$  using a precision thermobalance. They performed this test for BSCF. At  $T = 600$  °C they measured  $\gamma$  to be  $125 +/ - 2$ , and values of  $k_{\text{chem}}$  and  $k^*$  at  $600$  °C resulted in an extracted  $\gamma$  of about 110, and values of  $D_{\text{chem}}$  and  $D^*$  at  $600$  °C resulted in an extracted  $\gamma$  of 125, both of which showing essentially perfect agreement with the measured  $\gamma$ . In addition, a similar study from Saher et al. measured  $k^*$  and  $k_{\text{chem}}$  for LSCF and used  $\gamma$  values published in a separate study.<sup>68</sup> Both of these studies verified that the relationship between the tracer and chemical properties and  $\gamma$  is robust, and suggest that the differences of measured versus extracted  $\gamma$  we

show below in **Figure 5** are likely the result of differences of approach between various researchers.

**Figure 5** compares values of  $\gamma$  obtained from extraction of  $k_{\text{chem}}/k^*$  values,  $D_{\text{chem}}/D^*$  values, and predicted using the ratios of their respective O p-band center trendlines from **Figure 3**. For the data in **Figure 5**, a temperature of  $T = 800 \text{ } ^\circ\text{C}$  was used, because it resulted in the most experimentally measured  $\gamma$  values being available for comparison. Separately, in **Figure S5** of the **SI**, we plot the  $\gamma$  values extracted from  $k_{\text{chem}}/k^*$  as a function of temperature, with experimentally measured points overlaid. For the analysis shown in **Figure 5**, we were restricted to the set of materials in our database for which all of  $k_{\text{chem}}$ ,  $k^*$ ,  $D_{\text{chem}}$  and  $D^*$  had been measured, yielding only 12 materials. We were also able to compare these extracted and predicted  $\gamma$  values with those measured directly from experiment, of which data was available for 8 of the 12 materials. From the comparisons in **Figure 5**, we observe that the  $\gamma$  values extracted from  $k_{\text{chem}}/k^*$  measurements (dark green bars) are in closer agreement with the experimentally measured  $\gamma$  values (red bars) than those extracted from  $D_{\text{chem}}/D^*$  measurements (light green bars). More specifically, the MAE of  $\gamma$  in log units between these two values is 0.46 versus 1.29 for extracting  $\gamma$  from  $k_{\text{chem}}/k^*$  and  $D_{\text{chem}}/D^*$ , respectively. In addition, the predicted  $\gamma$  values from the O p-band center trends with  $k_{\text{chem}}$  and  $k^*$  also produce good agreement both with the extracted  $\gamma$  values from  $k_{\text{chem}}/k^*$  (dark purple bars) and the measured values (red bars) (MAE of 0.54 log units), while the predicted  $\gamma$  from the trends of  $D_{\text{chem}}$  and  $D^*$  (light purple bars) result in higher errors with many overestimations of the true  $\gamma$  values (MAE of 1.88 log units). The reason for the worse ability of using  $D_{\text{chem}}$  and  $D^*$  values to obtain  $\gamma$  is not totally clear but may be in part due to the larger spread of  $D^*$  values in experiment relative to  $k^*$  values, and the relatively worse correlation of  $D^*$  versus the O p-band center compared to the analogous  $k^*$  trend.

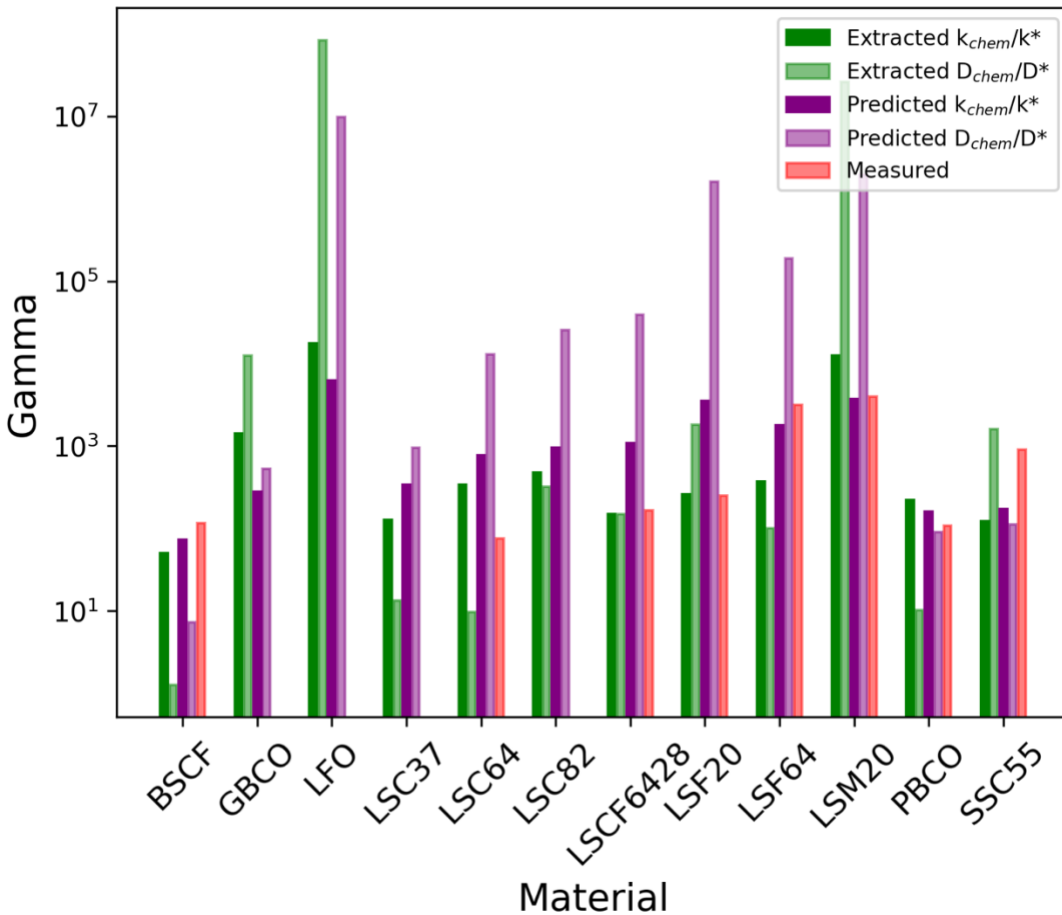


**Figure 5.** Bar chart summarizing thermodynamic factors ( $\gamma$ ) extracted from perovskite catalytic properties database, predicted from linear fits of catalytic properties with O p-band center, and from direct experimental measurements. All of these data are for a temperature of T = 800 °C.

While the use of the predicted  $\gamma$  from  $k_{chem}/k^*$  has slightly higher error than if measured values of  $k_{chem}$  and  $k^*$  were used, this method offers an avenue to convert between  $k_{chem}$  and  $k^*$  values using only a single experimental measurement and the DFT-calculated O p-band center, as opposed to needing to perform two separate experiments. In **Figure 6**, we take the 45  $k_{chem}$  values in our database for which there is no corresponding  $k^*$  value, and predict the corresponding  $k^*$  values by using the predicted  $\gamma$  value from the ratio of the O p-band center trend lines of  $k_{chem}$  and  $k^*$ . These 45 predicted  $k^*$  values are shown as purple dots in **Figure 6**. In addition, we use the inter-property correlation of  $k^*$  versus ASR from **Section S3** of the SI and predict  $k^*$  values for the 235 materials for which ASR data is known but no  $k^*$  value exists in the database. These 235  $k^*$  predictions are shown as red dots in **Figure 6** (they are also available as

part of the data files provided as part of the **SI**). This scheme provides quick qualitative estimates of catalytic property data and can be useful for fleshing out existing data, making decisions on key experiments to perform, or screening of top-performing materials based on specific performance metrics. From our list of newly predicted  $k^*$  values, the materials BiSFSb10, PSCF4628, BFZ90, and BiPBF (BiSFSb10, PSCF4628 are materials with low ASR in our database, while BFZ90 and BiPBF have high  $k_{\text{chem}}$ ) have predicted  $\log k^*$  values of -5.12, -5.28, -2.88, and -4.03 cm/s at  $T = 500$  °C, respectively, all of which are comparable or higher than the top  $k^*$  material, LSC37 (see discussion in **Section S1** of the **SI**), with a  $\log k^*$  value of -5.09 cm/s at 500 °C.

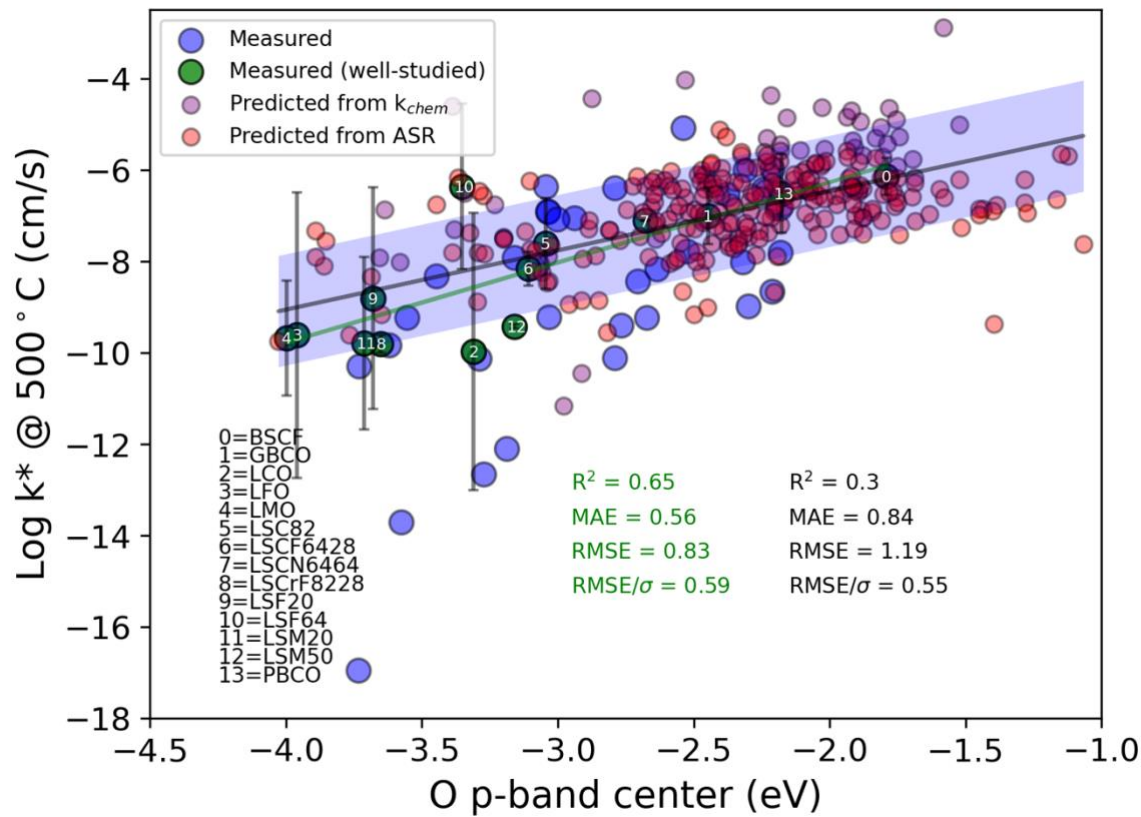


**Figure 6.** Trend of  $k^*$  with O p-band center at 500 °C with newly predicted data. The blue and green data are measured  $k^*$  values and well-studied measured  $k^*$  values, respectively. The purple data are predicted  $k^*$  values from measured  $k_{\text{chem}}$  and predicted  $\gamma$ . The red data are predicted  $k^*$  values from measured ASR values.

### 3. Summary and Conclusion

In this work, we constructed the largest database to-date of perovskite catalytic properties comprising oxygen surface exchange rates ( $k_{\text{chem}}$  and  $k^*$ ), oxygen diffusivity ( $D_{\text{chem}}$  and  $D^*$ ), and ASR data from ECR, IEDP, and EIS experiments. The database consists of nearly 750 measured property values spanning 299 unique perovskite materials from over 300 studies. By itself, the database is useful for examining typical value ranges at a given temperature, understanding typical ranges of experimental error from multiple independent measurements, flagging outlier data points as potentially problematic measurements, and listing top-performing materials based on each property. Using our database, we assess the ability of the O p-band center electronic structure descriptor, calculated using DFT methods, to correlate with  $k_{\text{chem}}$ ,  $k^*$ ,  $D_{\text{chem}}$ ,  $D^*$  and ASR values. We generally find that there are modest linear trends of each property with the O p-band center when considering fits to the full database of materials. We find that the fits are more robust at higher temperature, and significantly improve when considering fits to the subset of materials which have multiple independent measurements. These findings suggest that the spread of property data is largely the result of experimental uncertainty, and subsequent measurements of additional materials will continue to improve the O p-band center correlations. We also use our database to assess inter-property correlations, such as  $k^*$  versus  $D^*$ ,  $k^*$  versus ASR, and the Adler-Lane-Steele formula relating ASR to  $k^*$  and  $D^*$ . We broadly find that using the O p-band center results in property prediction mean absolute errors on the order of 0.5 log units, depending on the specific property and temperature considered. Further, we use our inter-property correlations with information of thermodynamic factor values extracted from the data and predicted from our O p-band correlations to make predictions of  $k^*$  for materials based on measured values of  $k_{\text{chem}}$  and ASR, and list several potential fast oxygen surface exchange materials which have not previously been explored using IEDP methods.

## 4. Data and Methods

### 4.1. Density Functional Theory (DFT) calculations

All Density functional theory (DFT) calculations were conducted using the Vienna Ab Initio Simulation Package (VASP).<sup>69</sup> Materials were modeled using a planewave basis set and the Generalized Gradient Approximation (GGA) exchange and correlation functional with Perdew-Burke-Ernzerhof (PBE) pseudopotentials.<sup>70</sup> The Hubbard U correction was not used in the present work following the study from Jacobs et al.,<sup>53</sup> who found the O p-band center trends were more robust over a range of properties for GGA-PBE compared to PBE+U. Spin polarization was enabled for all calculations. A planewave cutoff energy of 500 eV was used for all calculations. Perovskite materials were simulated using a  $2 \times 2 \times 2$  supercell (40 atoms) and a  $4 \times 4 \times 4$  Monkhorst-Pack<sup>71</sup> k-point mesh. To more accurately capture the experimental stoichiometry, for select materials, a larger  $2 \times 2 \times 4$  supercell (80 atoms) was used with a  $4 \times 4 \times 2$  Monkhorst-Pack k-point mesh was used. All perovskite compositions were first initially fully relaxed (volume + ions) to obtain the correct equilibrium volume. Then, a second run was performed where the cell parameters were set to be pseudocubic, that is, lattice parameters  $a = b = c$  but with the same equilibrium volume as obtained from the full relaxation run. For this second run, only ions were relaxed. The electronic density of states output from this second pseudocubic relaxation was used to calculate the O p-band center following previous studies.<sup>46,53,55</sup> All materials were simulated as fully stoichiometric with no oxygen vacancies. We acknowledge that these choices of simulating all materials as stoichiometric and pseudocubic is not physically rigorous for all systems, however doing so provides us a consistent set of calculations to more straightforwardly assess correlations between properties without introducing additional confounding factors from the simulation approach.

### 4.2. Database development

To extract perovskite catalytic data from the literature, each paper was manually evaluated and searched for data in the text, in tables, and in figures. Most of the data was found

to reside in figures, where typically data of any of the properties of interest is plotted as a function of temperature. We manually extracted measured property values at two different temperatures, so that an activation energy barrier could be obtained, and the property value for a given material could then be scaled to any desired temperature. For the ASR data, we did not explicitly differentiate data which originated from symmetrical cell tests versus full button cell tests, but most of the data came from symmetrical cell tests. In addition to extracting the ASR values, the microstructure type of the electrode studied (porous versus dense) and the electrolyte material used were also documented. There were some instances of studies where a property value was reported at only a single temperature. For these cases, we impute a value for the activation barrier. If the material for which the activation barrier requires imputation is present in our database, the average value of the activation barrier of the other measurements was used. If the material is not in the database, but a closely related material is (e.g., LSM35 not present, but LSM20 and LSM50 were), then the average of the nearby compounds was used. We note while this is a subjective designation, it was only needed for these cases: LSM20 (LSM35 closest), LSM35 (LSM20 and LSM50 closest), LSF30 (LSF20 and LSF50 closest), PBFO (PBCO closest), LSF64 (LSF20 and LSF10 closest), and LSMS<sub>c</sub> (LSMS<sub>c</sub>20 closest). Finally, if the material and no compositionally close material is present, the average activation barrier of the entire database was used. A comparison of 165 activation barriers obtained from the literature data versus the corresponding activation barrier values calculated from data extracted from figures resulted in a mean absolute error of 0.07 eV in the activation barrier, which is roughly 5% of a typical activation barrier value. We note that this error in the activation barrier is about the same level of error one may obtain from a linear fit to the data experimentally. For example, activation barrier error values quoted from Bucher et al.<sup>33</sup> and Saher et al.<sup>68</sup> were in the range of 7-12 kJ, which is 0.07-0.12 eV. Therefore, we expect our manual data extraction scheme to yield reasonably accurate property values as a function of temperature, as the activation barriers have about the same level of error as observed in typical experimental fits. It is worth noting that an activation barrier error of 0.07 eV, which, for a typical barrier of 1.2 eV, would yield a property change of +/- 0.3 log units at 800 °C. As discussed throughout this work, we believe a main source of error in our correlation fits is the result of such experimental uncertainty. Errors within about

0.3 log units may be a useful rule of thumb for establishing a lower bound on the precision one may obtain from such correlations, as any further error reduction would be within the uncertainty of what is typically measured experimentally.

In an effort to properly credit all original authors for their work performing the materials property measurements for all data used in this work, below we provide in **Table 2** a detailed record of references for each perovskite composition and the property which was measured.

**Table 2.** Detailed summary of original references examined in this work to obtain the present database of perovskite catalytic properties.

Material	Abbreviated composition	$k_{\text{chem}}$	$D_{\text{chem}}$	$k^*$	$D^*$	ASR
$\text{Ba}_{0.9}\text{Co}_{0.7}\text{Fe}_{0.2}\text{Nb}_{0.1}\text{O}_3$	B90CFN					72,73
$\text{Ba}_2\text{Bi}_{0.1}\text{Sc}_{0.2}\text{Co}_{1.7}\text{O}_5$	BBiScC					74
$\text{Ba}_{0.95}\text{Ca}_{0.05}\text{FeO}_3$	BCaF					75
$\text{Ba}_{0.95}\text{Ca}_{0.05}\text{Fe}_{0.95}\text{In}_{0.05}\text{O}_3$	BCaFln					75
$\text{BaCe}_{0.5}\text{Fe}_{0.5}\text{O}_3$	BCeF55	76				76
$\text{Ba}_{0.9}\text{Co}_{0.7}\text{Fe}_{0.2}\text{Mo}_{0.1}\text{O}_3$	BCFMo					77
$\text{BaCo}_{0.6}\text{Fe}_{0.3}\text{Nb}_{0.1}\text{O}_3$	BCFN631	78	78			78
$\text{BaCo}_{0.7}\text{Fe}_{0.2}\text{Nb}_{0.1}\text{O}_3$	BCFN721					72,73,79–81
$\text{BaCo}_{0.7}\text{Fe}_{0.22}\text{Sc}_{0.08}\text{O}_3$	BCFSc	82	82			82
$\text{BaCo}_{0.6}\text{Fe}_{0.2}\text{Sn}_{0.2}\text{O}_3$	BCFSn20	11	11			11
$\text{BaCo}_{0.6}\text{Fe}_{0.3}\text{Sn}_{0.1}\text{O}_3$	BCFSn631	78	78			78
$\text{BaCo}_{0.7}\text{Fe}_{0.2}\text{Sn}_{0.1}\text{O}_3$	BCFSn721	83	83			
$\text{BaCo}_{0.6}\text{Fe}_{0.2}\text{Sn}_{0.1}\text{Y}_{0.1}\text{O}_3$	BCFSnY	11	11			11
$\text{BaCo}_{0.7}\text{Fe}_{0.22}\text{Y}_{0.08}\text{O}_3$	BCFY	84	84			84
$\text{BaCo}_{0.6}\text{Fe}_{0.2}\text{Y}_{0.2}\text{O}_3$	BCFY20	11	11			11
$\text{BaCo}_{0.7}\text{Fe}_{0.2}\text{Yb}_{0.1}\text{O}_3$	BCFYb					85
$\text{BaCoO}_3$	BCO					86,87
$\text{BaCo}_{0.875}\text{Sc}_{0.125}\text{O}_3$	BCSc12					87
$\text{BaCo}_{0.75}\text{Sc}_{0.25}\text{O}_3$	BCSc25	87	87			87
$\text{BaCo}_{0.625}\text{Sc}_{0.375}\text{O}_3$	BCSc37					87
$\text{BaFe}_{0.9}\text{Bi}_{0.1}\text{O}_3$	BFBi					88
$\text{BaFe}_{0.6}\text{Co}_{0.3}\text{Ce}_{0.1}\text{O}_3$	BFCCe631					89
$\text{BaFe}_{0.95}\text{Ce}_{0.05}\text{O}_3$	BFCe05					90
$\text{BaFe}_{0.85}\text{Cu}_{0.15}\text{O}_3$	BFCu15					91
$\text{BaFe}_{0.75}\text{Cu}_{0.25}\text{O}_3$	BFCu25					91
$\text{BaFe}_{0.375}\text{Co}_{0.375}\text{Zr}_{0.25}\text{O}_3$	BFCZ20	63	63			92,93
$\text{BaCo}_{0.2}\text{Fe}_{0.5}\text{Zr}_{0.3}\text{O}_3$	BFCZ253					94
$\text{BaFe}_{0.25}\text{Co}_{0.25}\text{Zr}_{0.5}\text{O}_3$	BFCZ50	63	63			
$\text{BaCo}_{0.5}\text{Fe}_{0.2}\text{Zr}_{0.3}\text{O}_3$	BFCZ523					94
$\text{BaFe}_{0.125}\text{Co}_{0.125}\text{Zr}_{0.75}\text{O}_3$	BFCZ75	63	63			
$\text{BaFe}_{0.4}\text{Co}_{0.4}\text{Zr}_{0.1}\text{Y}_{0.1}\text{O}_3$	BFCZY	95	95			37,95
$\text{BaFe}_{0.95}\text{In}_{0.05}\text{O}_3$	BFIn05					75
$\text{BaFe}_{0.95}\text{Nb}_{0.05}\text{O}_3$	BFN05	96,97	96,97			96

BaFe <sub>0.9</sub> Nb <sub>0.1</sub> O <sub>3</sub>	BFN10	97	97			
BaFe <sub>0.8</sub> Nb <sub>0.2</sub> O <sub>3</sub>	BFN20	97	97			
BaFe <sub>0.75</sub> Ni <sub>0.25</sub> O <sub>3</sub>	BFNi82					98
BaFeO <sub>3</sub>	BFO					86
BaFe <sub>0.95</sub> Sn <sub>0.05</sub> O <sub>3</sub>	BFSn05					99
BaFe <sub>0.8</sub> Sn <sub>0.2</sub> O <sub>3</sub>	BFSn82					100
BaFe <sub>0.3</sub> Sn <sub>0.2</sub> Bi <sub>0.5</sub> O <sub>3</sub>	BFSnBi325					100
BaFe <sub>0.5</sub> Sn <sub>0.2</sub> Bi <sub>0.3</sub> O <sub>3</sub>	BFSnBi523					100
BaFe <sub>0.7</sub> Sn <sub>0.2</sub> Bi <sub>0.1</sub> O <sub>3</sub>	BFSnBi721					100
BaFe <sub>0.95</sub> Zr <sub>0.05</sub> O <sub>3</sub>	BFZ05					90
BaFe <sub>0.1</sub> Zr <sub>0.9</sub> O <sub>3</sub>	BFZ90	101				
BaFe <sub>0.8</sub> Zn <sub>0.1</sub> Bi <sub>0.1</sub> O <sub>3</sub>	BFZnBi					88
Ba <sub>0.95</sub> Gd <sub>0.05</sub> FeO <sub>3</sub>	BGF05					90
Bi <sub>0.7</sub> Pr <sub>0.1</sub> Ba <sub>0.2</sub> FeO <sub>3</sub>	BiPBF	102	102			102
Bi <sub>0.5</sub> Sr <sub>0.5</sub> Fe <sub>0.8</sub> Co <sub>0.2</sub> O <sub>3</sub>	BiSCF					103
Bi <sub>0.5</sub> Sr <sub>0.5</sub> FeO <sub>3</sub>	BiSF50	104,105	104,105			104–108
Bi <sub>0.2</sub> Sr <sub>0.8</sub> FeO <sub>3</sub>	BISF80					106,107
Bi <sub>0.5</sub> Sr <sub>0.5</sub> Fe <sub>0.8</sub> Cu <sub>0.2</sub> O <sub>3</sub>	BISFCu					109
Bi <sub>0.5</sub> Sr <sub>0.5</sub> Fe <sub>0.9</sub> Nb <sub>0.1</sub> O <sub>3</sub>	BISFN10					110
Bi <sub>0.5</sub> Sr <sub>0.5</sub> Fe <sub>0.9</sub> Sb <sub>0.1</sub> O <sub>3</sub>	BISFSb10					111
Bi <sub>0.5</sub> Sr <sub>0.5</sub> Fe <sub>0.9</sub> Ti <sub>0.1</sub> O <sub>3</sub>	BiSFT10					112
Bi <sub>0.5</sub> Sr <sub>0.5</sub> Fe <sub>0.8</sub> Ti <sub>0.2</sub> O <sub>3</sub>	BiSFT20					112
Bi <sub>0.5</sub> Sr <sub>0.5</sub> Fe <sub>0.9</sub> Ta <sub>0.1</sub> O <sub>3</sub>	BiSFTA10					108
Ba <sub>0.95</sub> La <sub>0.05</sub> FeO <sub>3</sub>	BLF05	113	113			90,113–115
Ba <sub>0.6</sub> La <sub>0.4</sub> FeO <sub>3</sub>	BLF64					116
Ba <sub>0.8</sub> La <sub>0.2</sub> FeO <sub>3</sub>	BLF82					116,117
Ba <sub>0.9</sub> La <sub>0.1</sub> FeO <sub>3</sub>	BLF91					116
Ba <sub>0.95</sub> La <sub>0.05</sub> Fe <sub>0.95</sub> P <sub>0.05</sub> O <sub>3</sub>	BLFP					114
(Ba <sub>0.5</sub> Sr <sub>0.5</sub> ) <sub>0.8</sub> Co <sub>0.8</sub> Fe <sub>0.2</sub> O <sub>3</sub>	BS0.8CF					118
		32,33,63,87,11 9–123	32,33,63,87,1 19,120,122,12 3	30,31,33	30,31	29,37,84,86,87,118 ,124–133
Ba <sub>0.5</sub> Sr <sub>0.5</sub> Co <sub>0.8</sub> Fe <sub>0.2</sub> O <sub>3</sub>	BSCF					134
Ba <sub>0.2</sub> Sr <sub>0.8</sub> Co <sub>0.8</sub> Fe <sub>0.2</sub> O <sub>3</sub>	BSCF2882					
Ba <sub>0.5</sub> Sr <sub>0.5</sub> Co <sub>0.2</sub> Fe <sub>0.8</sub> O <sub>3</sub>	BSCF5528					130,135
Ba <sub>0.5</sub> Sr <sub>0.5</sub> Co <sub>0.4</sub> Fe <sub>0.6</sub> O <sub>3</sub>	BSCF5546					130,136
Ba <sub>0.5</sub> Sr <sub>0.5</sub> Co <sub>0.7</sub> Fe <sub>0.2</sub> Ni <sub>0.1</sub> O <sub>3</sub>	BSCFN	136	136			136
Ba <sub>0.9</sub> Sr <sub>0.1</sub> Co <sub>0.9</sub> In <sub>0.1</sub> O <sub>3</sub>	BSCIn					137
Ba <sub>0.6</sub> Sr <sub>0.4</sub> Co <sub>0.9</sub> Nb <sub>0.1</sub> O <sub>3</sub>	BSCN641	138	138			138
Ba <sub>0.5</sub> Sr <sub>0.5</sub> Cu <sub>0.2</sub> Fe <sub>0.8</sub> O <sub>3</sub>	BSCuF					130,139
Ba <sub>0.5</sub> Sr <sub>0.5</sub> Cu <sub>0.4</sub> Fe <sub>0.6</sub> O <sub>3</sub>	BSCuF5546					130
Ba <sub>0.5</sub> Sr <sub>0.5</sub> Co <sub>0.1</sub> Zn <sub>0.1</sub> Fe <sub>0.8</sub> O <sub>3</sub>	BSCZnF					135
Ba <sub>0.5</sub> Sr <sub>0.5</sub> FeO <sub>3</sub>	BSF					140
		141	141			141
Ba <sub>0.5</sub> Sr <sub>0.5</sub> Fe <sub>0.8</sub> Cu <sub>0.1</sub> Ti <sub>0.1</sub> O <sub>3</sub>	BSFCuT					
Ba <sub>0.5</sub> Sr <sub>0.5</sub> Fe <sub>0.9</sub> Mo <sub>0.1</sub> O <sub>3</sub>	BSFMo10					142
Ba <sub>0.5</sub> Sr <sub>0.5</sub> Fe <sub>0.9</sub> Nb <sub>0.1</sub> O <sub>3</sub>	BSFN					143,144
Ba <sub>0.5</sub> Sr <sub>0.5</sub> Fe <sub>0.9</sub> Sb <sub>0.1</sub> O <sub>3</sub>	BSFSb10					140
Ba <sub>0.5</sub> Sr <sub>0.5</sub> Fe <sub>0.8</sub> Zn <sub>0.2</sub> O <sub>3</sub>	BSFZn					145
Ba <sub>0.4</sub> Sr <sub>0.4</sub> La <sub>0.2</sub> FeO <sub>3</sub>	BSLF					146

$Ba_{0.4}Sr_{0.4}La_{0.2}Fe_{0.9}Mn_{0.1}O_3$	BSLFM10					146
$Ba_{0.4}Sr_{0.4}La_{0.2}Fe_{0.9}Mn_{0.2}O_3$	BSLFM20					146
$Ba_{0.95}Sm_{0.05}FeO_3$	BSmF05					90
$Ba_{0.5}Sr_{0.5}Zn_{0.2}Fe_{0.8}O_3$	BSZnF					135
$CaMn_{0.9}Nb_{0.1}O_3$	CaMN91					147
$CaMnO_3$	CaMO					147
$GdBaCo_2O_5$	GBCO	148	148	34,149,150	34,149,150	34,127,151–153
$GdBaFe_2O_5$	GBFO					154,155
$GdBaMnFeO_5$	GBMF					156
$Gd_{0.5}Ba_{0.5}Mn_{0.5}Fe_{0.5}O_3$	GBMF5555					156
$GdBa_{0.5}Sr_{0.5}Co_2O_5$	GBSC					157,158
$GdBa_{0.5}Sr_{0.5}CoFeO_5$	GBSCF					157
$Gd_{0.5}Sr_{0.5}CoO_3$	GSC55					159,160
$Gd_{0.8}Sr_{0.2}CoO_3$	GSC82					161
$La_{0.5}Ba_{0.5}CoO_3$	LBC50					162
$La_{0.4}Ba_{0.6}CoO_3$	LBC60					163
$La_{0.1}Ba_{0.9}Co_{0.4}Fe_{0.6}O_3$	LBCF1946					164
$La_{0.3}Ba_{0.7}Co_{0.6}Fe_{0.4}O_3$	LBCF3764					164
$La_{0.6}Ba_{0.4}Co_{0.2}Fe_{0.8}O_3$	LBCF6428					129
$LaBaCo_2O_5$	LBCO					127,162,165
$LaBaFe_2O_5$	LBFO					154
$La_{0.4}Ba_{0.6}Fe_{0.8}Zn_{0.2}O_3$	LBFZh4682					166
$La_{0.4}Bi_{0.4}Sr_{0.2}FeO_3$	LBiSF					167
$La_{0.6}Ca_{0.4}Co_{0.2}Fe_{0.8}O_3$	LCaCF6428			66	66	
$La_{0.6}Ca_{0.4}Co_{0.8}Fe_{0.2}O_3$	LCaCF6482			66	66	
$La_{0.88}Ca_{0.12}CrO_3$	LCaCr12			168	168	
$La_{0.78}Ca_{0.22}CrO_3$	LCaCr22			168	168	169
$La_{0.7}Ca_{0.33}CrO_3$	LCaCr35	170		168	168	
$La_{0.6}Ca_{0.4}Fe_{0.8}Ni_{0.2}O_3$	LCaFN6482					171,172
$La_{0.6}Ca_{0.4}Co_{0.8}Fe_{0.2}O_3$	LCCF82			173	173	
$La_{0.9}Ca_{0.1}FeO_3$	LCF10	174	174			
$La_{0.8}Ca_{0.2}FeO_3$	LCF20	175,176	175,176			
$La_{0.9}Ca_{0.1}Fe_{0.9}Nb_{0.1}O_3$	LCFN10					177
$LaCo_{0.4}Ni_{0.4}Cu_{0.2}O_3$	LCNCu					178
$LaCoO_3$	LCO			179,180	179	181
$LaCrO_3$	LCrO					169
$LaFe_{0.5}Ni_{0.5}O_3$	LFN55					182
$LaFe_{0.8}Ni_{0.2}O_3$	LFN82					182
$LaFeO_3$	LFO	86	86	180,183	183	86,182
$LaMnO_3$	LMO		184	25,180,185	25,185	184
$LaNi_{0.6}Fe_{0.4}O_3$	LNF64					186,187
$(La_{0.75}Sr_{0.25})_{0.95}Cr_{0.5}Mn_{0.5}O_3$	LS0.95CrM			188	188	
$La_{0.7}Bi_{0.1}Sr_{0.2}FeO_3$	LSBiF12	189	189			
$La_{0.6}Bi_{0.2}Sr_{0.2}FeO_3$	LSBiF22	189	189			
$La_{0.4}Bi_{0.4}Sr_{0.2}FeO_3$	LSBiF42	189	189			
$La_{0.3}Sr_{0.7}CoO_3$	LSC37	190	190	191	191	
$La_{0.5}Sr_{0.5}CoO_3$	LSC55	190,192–195	190,192,193	196		
$La_{0.6}Sr_{0.4}CoO_3$	LSC64	192,197	192	28	28	198–201

$\text{La}_{0.8}\text{Sr}_{0.2}\text{CoO}_3$	LSC82	190	190	26,66,173,18 0,202	26,66,173,2 02	161,200,203,204
$\text{La}_{0.9}\text{Sr}_{0.1}\text{CoO}_3$	LSC91			205	205	
$\text{La}_{0.5}\text{Sr}_{0.5}\text{Co}_{0.8}\text{Fe}_{0.2}\text{O}_3$	LSCF5582					126
$\text{La}_{0.6}\text{Sr}_{0.4}\text{Co}_{0.2}\text{Fe}_{0.8}\text{O}_3$	LSCF6428	27,67,68,119,123,2 06–210	27,67,68,119,123, 206–210	27,68,180,206,2 11,212	27,68,180,206, 211,212	63,130,131,159– 161,212–219
$\text{La}_{0.6}\text{Sr}_{0.4}\text{Co}_{0.8}\text{Fe}_{0.2}\text{O}_3$	LSCF6482	220		221	221	
$\text{La}_{0.7}\text{Sr}_{0.3}\text{Co}_{0.8}\text{Fe}_{0.2}\text{O}_3$	LSCF7382					203
$\text{La}_{0.4}\text{Sr}_{0.6}\text{Co}_{0.2}\text{Fe}_{0.7}\text{Nb}_{0.1}\text{O}_3$	LSCFN					222
$\text{La}_{0.8}\text{Sr}_{0.2}\text{Co}_{0.4}\text{Mn}_{0.6}\text{O}_3$	LSCM8246					204
$\text{La}_{0.1}\text{Sr}_{0.9}\text{Co}_{0.85}\text{Nb}_{0.15}\text{O}_3$	LSCN					223
$\text{La}_{0.4}\text{Sr}_{0.6}\text{Co}_{0.6}\text{Ni}_{0.4}\text{O}_3$	LSCN4664			224	224	
$\text{La}_{0.4}\text{Sr}_{0.6}\text{Co}_{0.8}\text{Ni}_{0.2}\text{O}_3$	LSCN4682			224	224	
$\text{La}_{0.6}\text{Sr}_{0.4}\text{Co}_{0.4}\text{Ni}_{0.6}\text{O}_3$	LSCN6446			66	66	
$\text{La}_{0.6}\text{Sr}_{0.4}\text{Co}_{0.6}\text{Ni}_{0.4}\text{O}_3$	LSCN6464			66	66	
$\text{La}_{0.6}\text{Sr}_{0.4}\text{Co}_{0.8}\text{Ni}_{0.2}\text{O}_3$	LSCN6482				224	
$\text{La}_{0.8}\text{Sr}_{0.2}\text{Co}_{0.8}\text{Ni}_{0.2}\text{O}_3$	LSCN8282	225	225			225
$\text{La}_{0.2}\text{Sr}_{0.8}\text{Cr}_{0.2}\text{Fe}_{0.8}\text{O}_3$	LScrF2828	226	226			
$\text{La}_{0.3}\text{Sr}_{0.7}\text{Cr}_{0.3}\text{Fe}_{0.7}\text{O}_3$	LScrF3737					227
$\text{La}_{0.4}\text{Sr}_{0.6}\text{Cr}_{0.2}\text{Fe}_{0.8}\text{O}_3$	LScrF4628			228	228	
$\text{La}_{0.6}\text{Sr}_{0.4}\text{Cr}_{0.2}\text{Fe}_{0.8}\text{O}_3$	LScrF6428			228	228	
$\text{La}_{0.8}\text{Sr}_{0.2}\text{Cr}_{0.2}\text{Fe}_{0.8}\text{O}_3$	LScrF8228			228,229	228,229	
$\text{La}_{0.75}\text{Sr}_{0.25}\text{Cr}_{0.5}\text{Mn}_{0.5}\text{O}_3$	LScrM8255					230,231
$\text{La}_{0.7}\text{Sr}_{0.3}\text{CuO}_3$	LSCu73					232
$\text{La}_{0.6}\text{Sr}_{0.4}\text{Cu}_{0.2}\text{Fe}_{0.8}\text{O}_3$	LSCuF6428					233
$\text{La}_{0.7}\text{Sr}_{0.3}\text{Cu}_{0.4}\text{Fe}_{0.6}\text{O}_3$	LSCuF7346					232
$\text{La}_{0.8}\text{Sr}_{0.2}\text{Cu}_{0.2}\text{Fe}_{0.8}\text{O}_3$	LSCuF8228					219
$\text{La}_{0.9}\text{Sr}_{0.1}\text{FeO}_3$	LSF10			205	205	
$\text{La}_{0.8}\text{Sr}_{0.2}\text{FeO}_3$	LSF20	189,234	189	205	205	161,235
$\text{La}_{0.7}\text{Sr}_{0.3}\text{FeO}_3$	LSF30	210	210			
$\text{La}_{0.5}\text{Sr}_{0.5}\text{FeO}_3$	LSF50	105,226	105,226			105
$\text{La}_{0.6}\text{Sr}_{0.4}\text{FeO}_3$	LSF64	67,236	67,236	180,205	205	214,235
$\text{La}_{0.5}\text{Sr}_{0.5}\text{Fe}_{0.8}\text{Cu}_{0.2}\text{O}_3$	LSFCu					237
$\text{La}_{0.5}\text{Sr}_{0.5}\text{Fe}_{0.8}\text{Ga}_{0.2}\text{O}_3$	LSFG82	238				
$\text{La}_{0.5}\text{Sr}_{0.4}\text{Fe}_{0.8}\text{Mn}_{0.2}\text{O}_3$	LSFM6482	239	239			239
$\text{La}_{0.5}\text{Sr}_{0.5}\text{Fe}_{0.9}\text{Nb}_{0.1}\text{O}_3$	LSFN10					240
$\text{La}_{0.85}\text{Sr}_{0.15}\text{MnO}_3$	LSM15		184		241	184
$\text{La}_{0.8}\text{Sr}_{0.2}\text{MnO}_3$	LSM20	234	242	23,24,26,180 ,202	23,24,26,20 2,241	86,125,161,186,20 1,230,243–249
$\text{La}_{0.7}\text{Sr}_{0.3}\text{MnO}_3$	LSM35	250–252		173	173	253
$\text{La}_{0.5}\text{Sr}_{0.5}\text{MnO}_3$	LSM50			66,173,196	66,173	
$\text{La}_{0.5}\text{Sr}_{0.5}\text{Mn}_{0.8}\text{Co}_{0.2}\text{O}_3$	LSMC5582			173	173,196	
$\text{La}_{0.8}\text{Sr}_{0.2}\text{Mn}_{0.5}\text{Co}_{0.5}\text{O}_3$	LSMC8255			196	196	
$\text{La}_{0.8}\text{Sr}_{0.2}\text{Mn}_{0.8}\text{Co}_{0.2}\text{O}_3$	LSMC8282			196		
$\text{La}_{0.8}\text{Sr}_{0.2}\text{Mn}_{0.8}\text{Cu}_{0.2}\text{O}_3$	LSMCu					254
$\text{La}_{0.8}\text{Sr}_{0.2}\text{Mn}_{0.5}\text{Fe}_{0.5}\text{O}_3$	LSMF8255			247	247	
$\text{La}_{0.7}\text{Sr}_{0.3}\text{Mn}_{0.9}\text{Mg}_{0.1}\text{O}_3$	LSMMg10					253

$\text{La}_{0.7}\text{Sr}_{0.3}\text{Mn}_{0.8}\text{Mg}_{0.2}\text{O}_3$	LSMMg20					253
$\text{La}_{0.8}\text{Sr}_{0.2}\text{Mn}_{0.9}\text{Sc}_{0.1}\text{O}_3$	LSMSc					249
$\text{La}_{0.8}\text{Sr}_{0.2}\text{Sc}_{0.2}\text{Mn}_{0.8}\text{O}_3$	LSMSc20					255
$\text{La}_{0.4}\text{Sr}_{0.6}\text{Ni}_{0.2}\text{Fe}_{0.8}\text{O}_3$	LSNF4628					256
$\text{La}_{0.3}\text{Sr}_{0.7}\text{Ti}_{0.3}\text{Fe}_{0.7}\text{O}_3$	LSTF					257
$\text{NdBa}_{0.75}\text{Ca}_{0.25}\text{Co}_2\text{O}_5$	NBCaCO					258
$\text{NdBa}_{0.5}\text{Sr}_{0.5}\text{Co}_{1.5}\text{Fe}_{0.5}\text{O}_5$	NBCF1.5					259
$\text{NdBaCoMnO}_5$	NBCM					260
$\text{NdBaCo}_{1.5}\text{Mn}_{0.5}\text{O}_5$	NBCM1.5					260
$\text{NdBaCo}_2\text{O}_5$	NBCO					127,258,260–263
$\text{NdBaCu}_2\text{O}_5$	NBCuO					264
$\text{NdBaFe}_2\text{O}_5$	NBFO					154
$\text{NdBaMn}_2\text{O}_5$	NBMO					260
$\text{NdBa}_{0.5}\text{Sr}_{0.5}\text{Co}_{1.5}\text{Mn}_{0.5}\text{O}_5$	NBSCMO					265
$\text{NdBa}_{0.5}\text{Sr}_{0.5}\text{Co}_2\text{O}_5$	NBSKO					263,265–267
$\text{NdBa}_{0.5}\text{Sr}_{0.5}\text{Cu}_2\text{O}_5$	NBSCuO					264
$\text{NdCo}_3$	NCO					159
$\text{Nd}_{0.5}\text{Sr}_{0.5}\text{CoO}_3$	NSC55					159
$\text{Nd}_{0.5}\text{Sr}_{0.5}\text{Co}_{0.5}\text{Fe}_{0.5}\text{O}_3$	NSCF					268
$\text{NdSrCo}_2\text{O}_5$	NSCO					261
$\text{Nd}_{0.5}\text{Sr}_{0.5}\text{Fe}_{0.8}\text{Cu}_{0.2}\text{O}_3$	NSFCu					237
$\text{PrBa}_{0.8}\text{Ca}_{0.2}\text{Co}_{1.5}\text{Fe}_{0.5}\text{O}_5$	PBCCFO					269
$\text{PrBa}_{0.8}\text{Ca}_{0.2}\text{Co}_2\text{O}_5$	PBCCO					269
$\text{PrBaCoFeO}_5$	PBCF					270
$\text{PrBaCo}_{1.5}\text{Fe}_{0.5}\text{O}_5$	PBCF1.5					270
$\text{PrBaCo}_2\text{O}_5$	PBCO	270–274	270,273	36,150,271,273,	36,150,273,27	35,127,131,272,273,276
$\text{PrBaCo}_{1.9}\text{Sc}_{0.1}\text{O}_5$	PBCSc		275	5		–280
$\text{PrBaFe}_2\text{O}_5$	PBFO	281	281			154,282
$\text{PrBa}(\text{Fe}_{0.8}\text{Sc}_{0.2})_2\text{O}_5$	PBFSc					283
$\text{PrBaMn}_{1.5}\text{Fe}_{0.5}\text{O}_5$	PBMF1.5					284
$\text{PrBaMn}_2\text{O}_5$	PBMO					284
$\text{PrBa}_{0.5}\text{Sr}_{0.25}\text{Ca}_{0.25}\text{Co}_2\text{O}_5$	PBSCaCO					285
$\text{PrBa}_{0.5}\text{Sr}_{0.5}\text{CoCuO}_5$	PBSCCuO					286
$\text{PrBa}_{0.5}\text{Sr}_{0.5}\text{CoFeO}_5$	PBSCFO					287
$\text{PrBa}_{0.5}\text{Sr}_{0.5}\text{Co}_2\text{O}_5$	PBSCO					158,280,285–288
$\text{Pr}_{0.8}\text{Ca}_{0.2}\text{BaCo}_2\text{O}_5$	PCBCO					289
$\text{Pr}_{0.8}\text{Ca}_{0.2}\text{FeO}_3$	PCF20	175	175			
$\text{PrNi}_{0.6}\text{Co}_{0.4}\text{O}_3$	PNC64					290
$\text{Pr}_{0.3}\text{Sr}_{0.7}\text{CoO}_3$	PSC37					159
$\text{Pr}_{0.5}\text{Sr}_{0.5}\text{CoO}_3$	PSC55					159–161
$\text{Pr}_{0.8}\text{Sr}_{0.2}\text{CoO}_3$	PSC82					161
$\text{Pr}_{0.3}\text{Sr}_{0.7}\text{Co}_{0.3}\text{Fe}_{0.7}\text{O}_3$	PSCF3737					159,291
$\text{Pr}_{0.4}\text{Sr}_{0.6}\text{Co}_{0.2}\text{Fe}_{0.8}\text{O}_3$	PSCF4628					292
$\text{Pr}_{0.6}\text{Sr}_{0.4}\text{Co}_{0.2}\text{Fe}_{0.8}\text{O}_3$	PSCF6428					293
$\text{Pr}_{0.4}\text{Sr}_{0.6}\text{Co}_{0.16}\text{Fe}_{0.64}\text{Mo}_{0.2}\text{O}_3$	PSCFM20					292
$\text{Pr}_{0.4}\text{Sr}_{0.6}\text{Co}_{0.2}\text{Fe}_{0.7}\text{Nb}_{0.1}\text{O}_3$	PSCFN10					294
$\text{Pr}_{0.6}\text{Sr}_{0.4}\text{Co}_{0.18}\text{Fe}_{0.72}\text{Sc}_{0.1}\text{O}_3$	PSCFSc10					293
$\text{PrSrCo}_2\text{O}_5$	PSCO					280
$\text{Pr}_{0.8}\text{Sr}_{0.2}\text{FeO}_3$	PSF20					161,295

$\text{Pr}_{0.5}\text{Sr}_{0.5}\text{Fe}_{0.8}\text{Cu}_{0.2}\text{O}_3$	PSFCu					237,296
$\text{Pr}_{0.7}\text{Sr}_{0.3}\text{Fe}_{0.8}\text{Ni}_{0.2}\text{O}_3$	PSFN7382					297
$\text{Sr}_{0.95}\text{Co}_{0.8}\text{Nb}_{0.1}\text{Ta}_{0.1}\text{O}_3$	S95CNTa					298
$\text{Sr}_{0.95}\text{Ag}_{0.05}\text{Nb}_{0.1}\text{Co}_{0.9}\text{O}_3$	SAgCN	299				299
$\text{SmBaCo}_2\text{O}_5$	SBCO			150	150	127,300–302
$\text{SmBaFe}_2\text{O}_5$	SBFO					154
$\text{SmBa}_{0.5}\text{Sr}_{0.5}\text{Co}_2\text{O}_5$	SBSC					158,302–305
$\text{SmBa}_{0.5}\text{Sr}_{0.5}\text{Co}_{1.5}\text{Cu}_{0.5}\text{O}_5$	SBSCCu					303
$\text{SmBa}_{0.5}\text{Sr}_{0.5}\text{Cu}_2\text{O}_5$	SBSCu					306
$\text{SmBa}_{0.5}\text{Sr}_{0.5}\text{CuFeO}_5$	SBSCuF					306
$\text{Sr}_{0.9}\text{Ce}_{0.1}\text{CoO}_3$	SCeC10					161
$\text{Sr}_{0.9}\text{Ce}_{0.1}\text{Co}_{0.9}\text{Nb}_{0.1}\text{O}_3$	SCeCN10					307
$\text{Sr}_{0.9}\text{Ce}_{0.1}\text{FeO}_3$	SCeF10					161
$\text{Sr}_{0.9}\text{Ce}_{0.1}\text{Fe}_{0.8}\text{Ni}_{0.2}\text{O}_3$	SCeFN82					308
$\text{Sr}_{0.9}\text{Ce}_{0.1}\text{Fe}_{0.9}\text{Ni}_{0.1}\text{O}_3$	SCeFN91					308
$\text{Sr}_{0.8}\text{Ce}_{0.2}\text{MnO}_3$	SCeM					309,310
$\text{Sr}_{0.8}\text{Ce}_{0.2}\text{Mn}_{0.8}\text{Co}_{0.2}\text{O}_3$	SCeMC					309,310
$\text{SrCo}_{0.85}\text{Fe}_{0.15}\text{O}_3$	SCF15					311
$\text{SrCo}_{0.4}\text{Fe}_{0.5}\text{Nb}_{0.1}\text{O}_3$	SCFN451					312
$\text{SrCo}_{0.7}\text{Fe}_{0.2}\text{Nb}_{0.1}\text{O}_3$	SCFN721					312,313
$\text{SrCo}_{0.85}\text{Fe}_{0.1}\text{P}_{0.05}\text{O}_3$	SCFP					311
$\text{SrCo}_{0.9}\text{Nb}_{0.1}\text{O}_3$	SCN10	138,314	138,314			312,315–317
$\text{SrCo}_{0.8}\text{Nb}_{0.2}\text{O}_3$	SCN20	318	318			318
$\text{SrCo}_{0.8}\text{Nb}_{0.1}\text{Ta}_{0.1}\text{O}_3$	SCNTa					124,298
$\text{SrCoO}_3$	SCO	319	319			86,159,319
$\text{SrCo}_{0.8}\text{Sc}_{0.2}\text{O}_3$	SCSc82	319	319			319–321
$\text{SrCo}_{0.9}\text{Sc}_{0.1}\text{O}_3$	SCSc91	319	319			319
$\text{SrCo}_{0.75}\text{Sc}_{0.125}\text{Nb}_{0.125}\text{O}_3$	SCScN		322			322,323
$\text{SrSc}_{0.175}\text{Nb}_{0.025}\text{Co}_{0.8}\text{O}_3$	SCScN80					132
$\text{SrCo}_{0.9}\text{Ti}_{0.1}\text{O}_3$	SCT10					324
$\text{SrCo}_{0.8}\text{Ti}_{0.2}\text{O}_3$	SCT20					324
$\text{SrCo}_{0.9}\text{Ta}_{0.1}\text{O}_3$	SCTa10					325
$\text{SrCo}_{0.8}\text{Ta}_{0.2}\text{O}_3$	SCTa20	318	318			318
$\text{SrCo}_{0.6}\text{Ta}_{0.4}\text{O}_3$	SCTa40					325
$\text{SrCo}_{0.9}\text{Y}_{0.1}\text{O}_3$	SCY10					326
$\text{SrCo}_{0.8}\text{Y}_{0.2}\text{O}_3$	SCY20					326
$\text{SrFe}_{0.75}\text{Cr}_{0.25}\text{O}_3$	SFCr25					327
$\text{SrFe}_{0.9}\text{Hf}_{0.1}\text{O}_3$	SFH10	328	328			328
$\text{SrFe}_{0.8}\text{Mo}_{0.2}\text{O}_3$	SFMo20					327
$\text{SrFe}_{0.9}\text{Nb}_{0.1}\text{O}_3$	SFN10					329–332
$\text{SrFe}_{0.8}\text{Nb}_{0.2}\text{O}_3$	SFN20					329,333
$\text{SrFe}_{0.8}\text{Nb}_{0.1}\text{Ta}_{0.1}\text{O}_3$	SFNta					333,334
$\text{SrFeO}_3$	SFO	226,328	226,328	335		86,308,327,328,33 5–337
$\text{SrSc}_{0.175}\text{Nb}_{0.025}\text{Fe}_{0.8}\text{O}_3$	SFScN80					338
$\text{SrSc}_{0.025}\text{Nb}_{0.075}\text{Fe}_{0.9}\text{O}_3$	SFScN90					339
$\text{SrFe}_{0.9}\text{Si}_{0.1}\text{O}_3$	SFSi					337
$\text{SrFe}_{0.9}\text{Ti}_{0.1}\text{O}_3$	SFT10					340,341
$\text{SrFe}_{0.8}\text{Ta}_{0.2}\text{O}_3$	SFTa20					333

$\text{SrFe}_{0.9}\text{Zr}_{0.1}\text{O}_3$	SFZ10					336
$\text{SrFe}_{0.8}\text{Zr}_{0.2}\text{O}_3$	SFZ20					336
$\text{Sr}_{0.9}\text{K}_{0.1}\text{FeO}_3$	SKF					342
$\text{Sr}_{0.9}\text{K}_{0.1}\text{Fe}_{0.1}\text{Co}_{0.9}\text{O}_3$	SKFC19					342
$\text{Sr}_{0.9}\text{K}_{0.1}\text{Fe}_{0.3}\text{Co}_{0.7}\text{O}_3$	SKFC37					342
$\text{Sr}_{0.9}\text{K}_{0.1}\text{Fe}_{0.5}\text{Co}_{0.5}\text{O}_3$	SKFC55					342
$\text{Sr}_{0.95}\text{K}_{0.05}\text{Fe}_{0.8}\text{Nb}_{0.1}\text{Ta}_{0.1}\text{O}_3$	SKFNTa					334
$\text{Sr}_{0.95}\text{Li}_{0.05}\text{Fe}_{0.8}\text{Nb}_{0.1}\text{Ta}_{0.1}\text{O}_3$	SLiFNTa					334
$\text{SmCo}_3$	SmCO			343	343	159
$\text{Sr}_{0.95}\text{Na}_{0.05}\text{Fe}_{0.8}\text{Nb}_{0.1}\text{Ta}_{0.1}\text{O}_3$	SNaFNTa					334
$\text{Sm}_{0.2}\text{Sr}_{0.8}\text{CoO}_3$	SSC28					344
$\text{Sr}_{0.5}\text{Sm}_{0.5}\text{CoO}_3$	SSC55	345	345	343	343	159,344,346–350
$\text{Sm}_{0.8}\text{Sr}_{0.2}\text{CoO}_3$	SSC82			343	343	344
$\text{Sm}_{0.5}\text{Sr}_{0.5}\text{Co}_{0.8}\text{Fe}_{0.2}\text{O}_3$	SSCF5582					126,349
$\text{Sm}_{0.5}\text{Sr}_{0.5}\text{Co}_{0.9}\text{Nb}_{0.1}\text{O}_3$	SSCN					347
$\text{Sm}_{0.3}\text{Sr}_{0.7}\text{Nb}_{0.08}\text{Co}_{0.92}\text{O}_3$	SSCN10					351
$\text{SmSrCo}_2\text{O}_5$	SSCO					302
$\text{SrSc}_{0.075}\text{Ta}_{0.025}\text{Fe}_{0.9}\text{O}_3$	SScTaF					352
$\text{Sm}_{0.5}\text{Sr}_{0.5}\text{FeO}_3$	SSF					348
$\text{Sm}_{0.5}\text{Sr}_{0.5}\text{MnO}_3$	SSM					346
$\text{Sm}_{0.5}\text{Sr}_{0.5}\text{Fe}_{0.8}\text{Cu}_{0.2}\text{O}_3$	SSmFCu					353
$\text{Sm}_{0.5}\text{Sr}_{0.5}\text{NiO}_3$	SSN					348
$\text{SrTi}_{0.95}\text{Fe}_{0.05}\text{O}_3$	STF05			335		
$\text{SrTi}_{0.9}\text{Fe}_{0.1}\text{O}_3$	STF10			335		
$\text{SrTi}_{0.65}\text{Fe}_{0.35}\text{O}_3$	STF35			335		335
$\text{SrTi}_{0.5}\text{Fe}_{0.5}\text{O}_3$	STF50			335		
$\text{SrTi}_{0.2}\text{Fe}_{0.8}\text{O}_3$	STF80			335		335
$\text{Sr}_{0.7}\text{Y}_{0.3}\text{CoO}_3$	SYC					354
$\text{YBaCo}_2\text{O}_5$	YBCO					127,355,356
$\text{YBaFe}_2\text{O}_5$	YBFO					154
$\text{YBa}_{0.5}\text{Sr}_{0.5}\text{Co}_2\text{O}_5$	YBSKO					355

**Acknowledgements:** This project was funded by the United States Department of Energy, National Energy Technology Laboratory, in part, through a site support contract. Neither the United States Government nor any agency thereof, nor any of their employees, nor the support contractor, nor any of their employees, makes any warranty, express or implied, or assumes any legal liability or responsibility for the accuracy, completeness, or usefulness of any information, apparatus, product, or process disclosed, or represents that its use would not infringe privately owned rights. Reference herein to any specific commercial product, process, or service by trade name, trademark, manufacturer, or otherwise does not necessarily constitute or imply its endorsement, recommendation, or favoring by the United States Government or any agency

thereof. The views and opinions of authors expressed herein do not necessarily state or reflect those of the United States Government or any agency thereof.

### **Conflicts of Interest**

The authors of have no conflicts of interest to declare.

### **Data Availability**

The database of collected experimental measurements and all data used to construct the figures is publicly available on Figshare: <https://doi.org/10.6084/m9.figshare.24438079.v1>.

## **Supplementary Information for**

### **A Critical Assessment of Electronic Structure Descriptors for Predicting Perovskite Catalytic Properties**

**Authors:** Ryan Jacobs<sup>1,\*</sup>, Jian Liu<sup>2,\*</sup>, Harry Abernathy<sup>2</sup>, Dane Morgan<sup>1</sup>

<sup>1</sup> Department of Materials Science and Engineering, University of Wisconsin-Madison, Madison, WI, 53706, USA.

<sup>2</sup> National Energy Technology Lab, Morgantown, WV, 26505, USA.

## Section S1: Additional details of experimental property database development

In this section, we provide additional discussion of an overall survey of basic statistics of each catalytic property in the database, analysis of flagging potentially problematic measurements, and enumerating the best-performing materials at various temperatures based on each catalytic property (e.g., highest  $k_{\text{chem}}$  materials, lowest ASR materials). **Table 1** in the main text provides a high-level summary of the data collected in this work.

Assembling a large database of perovskite catalytic properties provides us with useful information, such as knowledge of typical ranges of each property at a given temperature, the best-performing materials at various working temperatures, the ability to flag outlier data points potentially indicative of problematic measurements, and information related to typical experimental measurement uncertainties by averaging measurements of the same material from multiple studies. Before performing additional analysis, we first average the measurements for the cases where the same material was measured across multiple studies. This averaging also provides an error bar for the measurements of these materials, which we calculate as the standard deviation of the measurements. From this, we find that the average experimental error bars across all properties at 500 °C, 600 °C, 700 °C and 800 °C are 0.68, 0.54, 0.47 and 0.45 log units, respectively. The above temperature values were chosen as they represent a typical operational range of SOFC, SOEC, r-SOFC and PCFC devices, where 500 °C is a desirable low temperature target for next-generation fuel cell and electrolyzer materials, and 800 °C is a more conventional intermediate-to-high temperature historically assessed in many experiments.

**Table S3** below provides a summary of some basic statistics of each perovskite catalytic property investigated in this work, including the minimum value, maximum value, average value, and standard deviation of all acquired values for 500 °C, 600 °C, 700 °C and 800 °C. The corresponding histogram distributions of property values at 500 °C and 800 °C are provided in **Figure 2** of the main text. The information shown in **Table S3** and **Figure 2** of the main text enables observations of characteristics of the data which will be important for understanding assessments of trends in property values with the O p-band center as discussed in **Section 2.2** of the main text. First, the dynamic range, and therefore, the standard deviation, of the data is

temperature-dependent. In general, the dynamic range and standard deviations of the data are larger at lower temperature for all five properties examined. For example, for the  $k_{\text{chem}}$  data from ECR, at 500 °C and 800 °C the data range over about 5.5 and 3.5 log units, respectively, and have standard deviations of 1.15 and 0.84 log units, respectively. Second, the dynamic range of the  $k^*$  and  $D^*$  values are larger than the  $k_{\text{chem}}$  and  $D_{\text{chem}}$  values. For example, at 500 °C and 800 °C the  $k^*$  values range over about 12 and 7 log units, respectively, which is about 3.5-5 log units larger than the  $k_{\text{chem}}$  ranges quoted above. This larger dynamic range of  $k^*$  data may make correlations with these data less susceptible to variations caused by experimental error (because the experimental error is a smaller fraction of the range of the data), which, as discussed above, can be on the order of 0.68 and 0.45 log units at 500 °C and 800 °C, respectively.

The property value distributions shown in **Figure 2** of the main text suggest that some measurements can be flagged as outliers as they may be potentially problematic. Here, we define a data point as being an outlier if its value is more than two standard deviations above or below the mean value of that property at a given temperature. For example, at 500 °C the minimum log  $k^*$  value of -16.95 cm/s is more than two standard deviations below the mean value (-8.52 cm/s -  $2 \times 2.16$  cm/s = -12.84 cm/s). Based on this definition of outlier points, at 500 °C there are 5 (BFZ90, LSC82, LSCN8282, LSF64, LSFG82), 3 (LMO, LSF30, LSM15), 2 (LCaCr12 and LCaCr22), 1 (LCaCr35) and 13 (LCaCr22, LCrO, LFN82, LFO, LMO, LNF64, LSF20, LSM15, LSM20, NCO, PSFN7382, SmCO, SSM, SSN) outlier materials for  $k_{\text{chem}}$ ,  $D_{\text{chem}}$ ,  $k^*$ ,  $D^*$ , and ASR, respectively. At 800 °C, there are 3 (LSCF6482, LSFG82, LSM35), 3 (LMO, LSM15, LSM20), 1 (LCaCr12), 0 and 13 (BCFY, CaMN91, LCaCr22, LCrO, LMO, LNF64, LSM15, LSM20, LSM35, LSMMg10, SmCO, SSM, SSN) outlier materials for  $k_{\text{chem}}$ ,  $D_{\text{chem}}$ ,  $k^*$ ,  $D^*$ , and ASR, respectively. Note that all of the data are used to fits throughout the main text and **SI**, and the above statements regarding outlier points is meant to illustrate a useful application of the database in understanding properties of the data.

**Table S3.** Overview of database statistics for each perovskite catalytic property investigated for temperatures in range of 500-800 °C. The order of the values given are minimum, maximum, average and standard deviation. All values are listed as base-10 logarithm.

	$k_{\text{chem}}$ (cm/s)	$D_{\text{chem}}$ (cm <sup>2</sup> /s)	$k^*$ (cm/s)	$D^*$ (cm <sup>2</sup> /s)	ASR (Ohm·cm <sup>2</sup> )
500 °C	-7.68, -2.23, -4.64, 1.15	-9.63, -3.75, -5.99, 1.36	-16.95, -5.09, -8.51, 2.17	-21.51, -6.33, -12.70, 4.37	-1.22, 5.60, 0.93, 1.05
600 °C	-6.55, -2.17, -3.87, 0.98	-8.40, -3.27, -5.26, 1.16	-14.36, -4.99, -7.60, 1.80	-18.50, -5.67, -11.35, 3.79	-1.52, 4.36, 0.02, 0.94
700 °C	-5.65, -1.93, -3.25, 0.89	-7.42, -2.89, -4.67, 1.04	-12.29, -4.18, -6.87, 1.57	-16.29, -4.79, -10.27, 3.35	-2.44, 3.36, - 0.69, 0.88
800 °C	-4.92, -1.47, -2.75, 0.84	-6.62, -2.59, -4.19, 0.96	-10.61, -3.38, -6.28, 1.45	-14.81, -4.07, -9.39, 3.03	-3.19, 2.56, - 1.28, 0.85

**Table S4** contains a summary of the top three best-performing materials in our database for each property for temperatures of 500 °C, 600 °C, 700 °C and 800 °C. We first discuss the top candidates with regard to  $k_{\text{chem}}$  and  $D_{\text{chem}}$  values. Based on these ECR measurements,  $\text{PrBaFe}_2\text{O}_{5+\delta}$  (PBFO),  $\text{Bi}_{0.7}\text{Pr}_{0.1}\text{Ba}_{0.2}\text{FeO}_3$  (BiPBF),  $\text{BaCo}_{0.7}\text{Fe}_{0.22}\text{Y}_{0.08}\text{O}_3$  (BCFY),  $\text{BaFe}_{0.4}\text{Co}_{0.4}\text{Zr}_{0.1}\text{Y}_{0.1}\text{O}_3$  (BFCZY),  $\text{BaCo}_{0.6}\text{Fe}_{0.2}\text{Sn}_{0.1}\text{Y}_{0.1}\text{O}_3$  (BCFSnY) and  $\text{BaFe}_{0.1}\text{Zr}_{0.9}\text{O}_3$  (BFZ90) are all top-performing materials. It is interesting that four of these six top materials are fully Ba A-site materials with a mixture of late transition metals and redox-inactive species like Zr, Y and Sn on the B-site. It is worth noting that stability and  $k_{\text{chem}}$  trends investigated by Jacobs et al. for the BFCZ system with varying Zr content also support this observation.<sup>63</sup> Further, it is worth noting the high performance of BiPBF as a Co-free material, where eliminating Co is attractive both from the standpoint of cost and for its relative scarcity compared to other transition metals like Fe and Mn. Finally, while BFZ90 is the highest  $k_{\text{chem}}$  material at low temperature, based on the outlier definition established above, it is anomalously high, indicating this material may benefit from additional study to confirm its potentially exceptional  $k_{\text{chem}}$  value.

Next, regarding the top candidate  $k^*$  and  $D^*$  materials, the materials  $\text{Ba}_{0.5}\text{Sr}_{0.5}\text{Co}_{0.8}\text{Fe}_{0.2}\text{O}_3$  (BSCF),  $\text{La}_{0.3}\text{Sr}_{0.7}\text{CoO}_3$  (LSC37),  $\text{PrBaCo}_2\text{O}_{5+\delta}$  (PBCO) and  $\text{Sm}_{0.5}\text{Sr}_{0.5}\text{CoO}_3$  (SSC55) are the most frequently occurring. These materials are all majority Co-doped on the B-site and have a mixture of alkaline earth and rare earth metals on the A-site. It is interesting to note the lack of overlap between the top candidates from the  $k^*/D^*$  list compared to the  $k_{\text{chem}}/D_{\text{chem}}$  list. From examining our database, this lack of overlap appears to be due to none of the top materials from the  $k_{\text{chem}}$

and  $D_{\text{chem}}$  lists being measured with IEDP (thus, no  $k^*$  and  $D^*$  measurements were made), as opposed to some fundamental difference in the underlying property measurement.

Finally, regarding ASR, many of the best materials like BCFY,  $\text{BaCo}_{0.7}\text{Fe}_{0.22}\text{Sc}_{0.08}\text{O}_3$  (BCFSc),  $\text{Ba}_{0.5}\text{Sr}_{0.5}\text{Co}_{0.7}\text{Fe}_{0.2}\text{Ni}_{0.1}\text{O}_3$  (BSCFN) are similar to the best  $k_{\text{chem}}/D_{\text{chem}}$  materials, suggesting that high  $k_{\text{chem}}$  and  $D_{\text{chem}}$  values may be more important for realizing low ASR than high  $k^*$  and  $D^*$  values. In addition, the materials  $\text{Pr}_{0.4}\text{Sr}_{0.6}\text{Co}_{0.2}\text{Fe}_{0.8}\text{O}_3$  (PSCF4628) and  $\text{Bi}_{0.5}\text{Sr}_{0.5}\text{Fe}_{0.9}\text{Sb}_{0.1}\text{O}_3$  (BiSFSb10) differ from the other materials in that they do not contain majority Ba. These materials are also the best performing materials at 500 °C with an ASR already lower than the 0.1 Ohm-cm<sup>2</sup> threshold enabling the desirable performance target of 1 W/cm<sup>2</sup> cells (assuming a typical 1 A/cm<sup>2</sup> current). It is somewhat surprising that PSCF4628 performs so well at 500 °C, because it is compositionally very similar to  $\text{La}_{0.6}\text{Sr}_{0.4}\text{Co}_{0.2}\text{Fe}_{0.8}\text{O}_3$  (LSCF6428), which has a much higher base-10 log ASR value of 1.23 at 500 °C. In addition, the very similar compound  $\text{Pr}_{0.6}\text{Sr}_{0.4}\text{Co}_{0.2}\text{Fe}_{0.8}\text{O}_3$  (PSCF6428) has a base-10 log ASR value of 1.60 at 500 °C. It is worth noting that PSCF4628 has only a single measurement in our database, so obtaining additional data on this material to further verify its excellent performance may be warranted. Finally, the high performance of BiSFSb10 is noteworthy because, like BiPBF, it is a Co-free material with desirable catalytic properties.

**Table S4.** Summary of top three best-performing materials in the database for each property for temperatures in range of 500-800 °C. All values are listed as base-10 logarithm. Materials marked with an asterisk (\*) were flagged as potentially problematic based on the outlier criteria of more than two standard deviations from the mean of the property data.

	$k_{\text{chem}}$ (cm/s)	$D_{\text{chem}}$ (cm <sup>2</sup> /s)	$k^*$ (cm/s)	$D^*$ (cm <sup>2</sup> /s)	ASR (Ω·cm <sup>2</sup> )
500 °C	*BFZ90: -2.23	PBFO: -3.75	LSC37: -5.09	LSC37: -6.33	BiSFSb10: -1.22
	BiPBF: -2.86	BiPBF: -3.81	SSC55: -5.98	BSCF: -6.79	PSCF4628: -1.04
	LSCrF2828: -3.07	BCFY: -4.42	LSCN4664: -6.00	PBCO: -7.84	BSCFN: -0.70
600 °C	BFZ90: -2.17	PBFO: -3.27	LSC37: -4.99	BSCF: -5.67	BCFY: -1.52
	BiPBF: -2.37	BiPBF: -3.36	BSCF: -5.20	LSC37: -6.19	BSCFN: -1.45
	BSCN641: -2.48	BCFY: -3.76	SSC55: -5.40	PBCO: -7.13	BCFSc: -1.44
700 °C	BSCN641: -1.93	PBFO: -2.89	BSCF: -4.45	BSCF: -4.79	BCFY: -2.44
	BiPBF: -1.99	BiPBF: -3.01	LSC37: -4.92	LSC37: -6.08	BCFSc: -2.17
	BFCZY: -2.08	BCFY: -3.23	SSC55: -4.94	PBCO: -6.56	SCeFN82: -2.06
800 °C	BSCN641: -1.48	PBFO: -2.59	BSCF: -3.84	BSCF: -4.08	BCFY: -3.19
	BFCZY: -1.56	BiPBF: -2.72	SSC55: -4.56	LSC37: -5.98	SCeFN82: -2.84
	BCFSnY: -1.59	BCFY: -2.80	SSC82: -4.60	PBCO: -6.10	BCFSc: -2.76

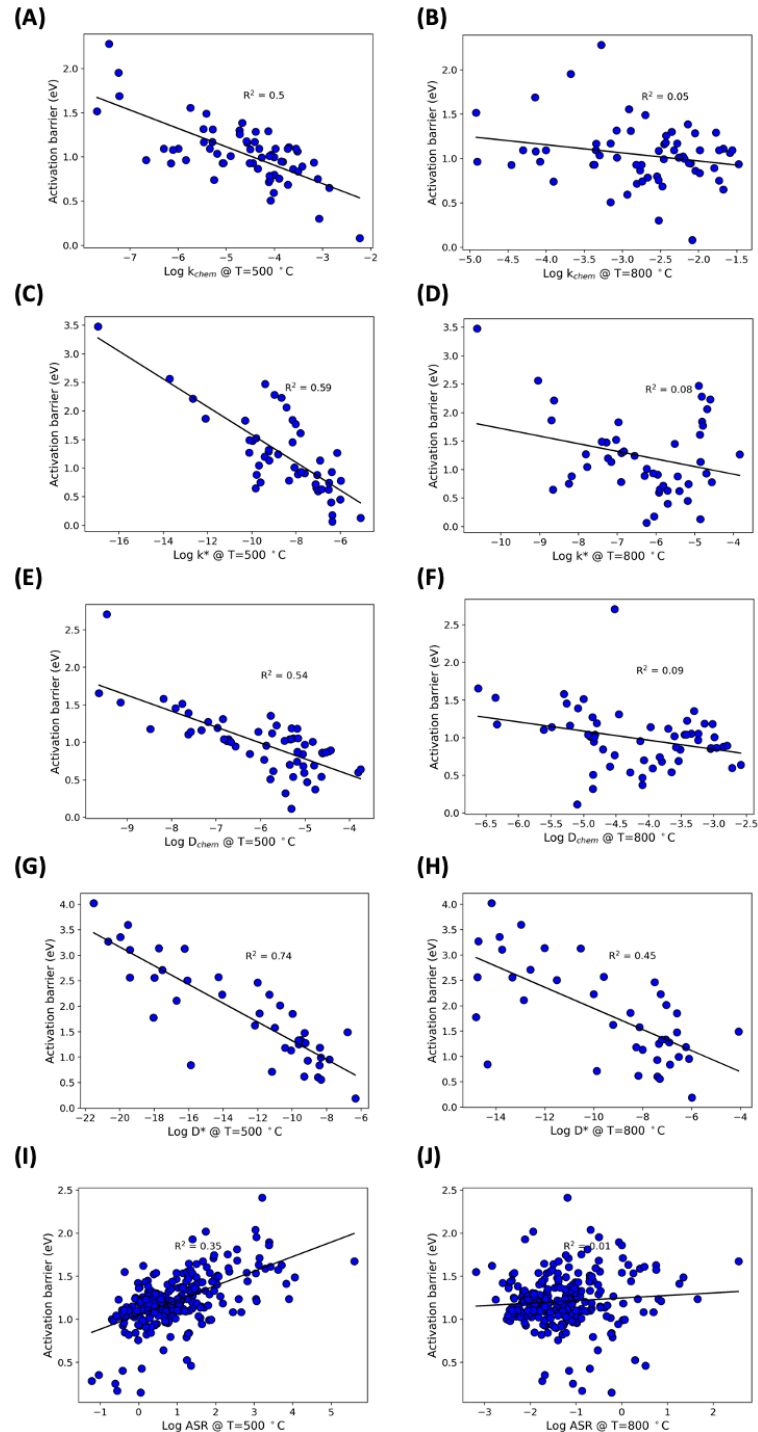


**Figure S7.** Plots of calculated activation energy barriers for each property, as a function of the property value at 500 °C and 800 °C. The left-hand column plots are all at 500 °C, while the right-hand column plots are at 800 °C. (A) and (B):  $k_{chem}$ , (C) and (D):  $k^*$ , (E) and (F):  $D_{chem}$ , (G) and (H):  $D^*$ , (I) and (J): ASR.

## Section S2: Additional details of O p-band center property trends

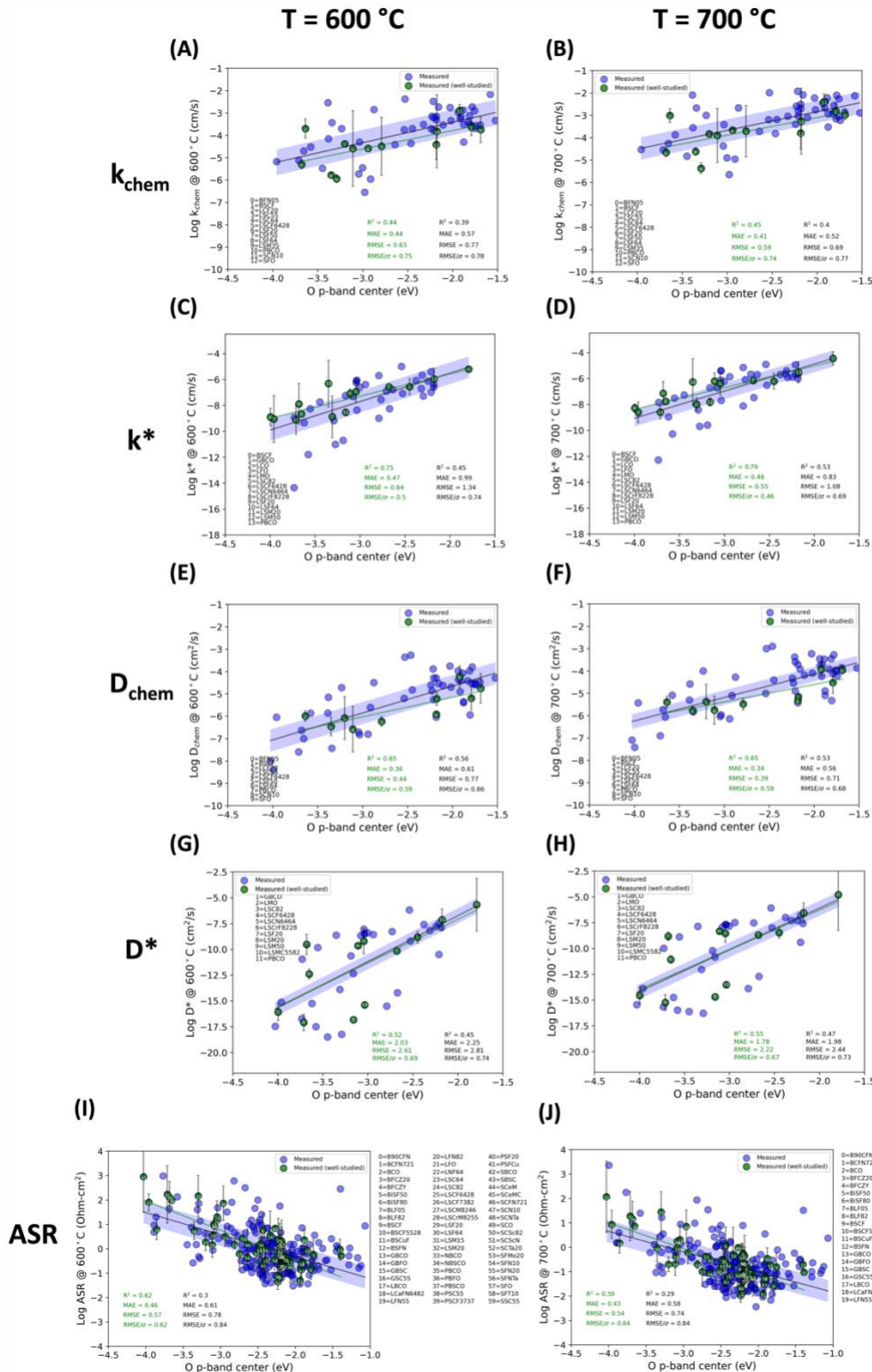


**Figure S8.** Trends of perovskite catalytic properties as a function of O p-band center. The left (right) column of plots is for  $T = 600\text{ }^\circ\text{C}$  ( $T = 700\text{ }^\circ\text{C}$ ). The properties plotted are  $k_{\text{chem}}$  (A, B),  $k^*$  (C, D),  $D_{\text{chem}}$  (E, F),  $D^*$  (G, H), and ASR (I, J).

D), D<sub>chem</sub> (E, F), D\* (G, H), and ASR (I, J). The blue points and black fit line and statistics are for a linear fit to all of the data. The green points and green fit line and statistics are for a linear fit to the subset of well-studied materials only (those materials with 2 or more measurements). The blue “x” points are outliers which were removed from the trend analysis. The blue shaded region is the average experimental error range, where the experimental error is calculated as the standard deviation of materials with multiple measurements. The average experimental error bars are 0.42 and 0.39 log units at 600 °C and 700 °C, respectively.

**Table S3.** Summary of O p-band linear fit slopes and intercepts.

Property	Temperature (°C)	Data	Slope	Intercept
k*	500	All	2.33	-1.65
		Outliers removed	1.74	-3.14
		Well-studied only	1.75	-2.76
	600	All	2.20	-1.12
		Outliers removed	1.75	-2.25
		Well-studied only	1.71	-2.17
	700	All	2.09	-0.70
		Outliers removed	1.76	-1.55
		Well-studied only	1.67	-1.69
	800	All	2.01	-0.36
		Outliers removed	1.85	-0.77
		Well-studied only	1.64	-1.30
k <sub>chem</sub>	500	All	1.01	-2.12
		Outliers removed	0.77	-2.61
		Well-studied only	0.87	-2.91
	600	All	0.91	-1.59
		Outliers removed	0.80	-1.78
		Well-studied only	0.82	-2.14
	700	All	0.83	-1.17
		Outliers removed	0.75	-1.31
		Well-studied only	0.78	-1.53
	800	All	0.77	-0.83
		Outliers removed	0.66	-1.02
		Well-studied only	0.75	-1.04
D*	500	All	4.98	2.40
		Outliers removed	4.77	1.92
		Well-studied only	4.73	1.35
	600	All	4.45	2.16
		Outliers removed	4.45	2.16
		Well-studied only	4.24	1.39
	700	All	4.04	1.98
		Outliers removed	4.04	1.98

		Well-studied only	3.84	1.41
D <sub>chem</sub>	800	All	3.70	1.82
		Outliers removed	3.70	1.82
		Well-studied only	3.53	1.43
		All	1.40	-2.49
ASR	500	Outliers removed	1.15	-3.00
		Well-studied only	1.00	-3.85
	600	All	1.20	-2.24
		Outliers removed	1.01	-2.66
		Well-studied only	0.87	-3.41
	700	All	1.05	-2.04
		Outliers removed	0.86	-2.44
		Well-studied only	0.78	-3.05
	800	All	0.92	-1.89
		Outliers removed	0.75	-2.26
		Well-studied only	0.70	-2.77
ASR	500	All	-1.00	-1.45
		Outliers removed	-0.65	-0.78
		Well-studied only	-1.36	-2.30
	600	All	-0.90	-2.13
		Outliers removed	-0.65	-1.63
		Well-studied only	-1.19	-2.81
	700	All	-0.83	-2.68
		Outliers removed	-0.62	-2.26
		Well-studied only	-1.05	-3.22
	800	All	-0.77	-3.12
		Outliers removed	-0.55	-2.66
		Well-studied only	-0.94	-3.55

### Section S3: Additional details of catalytic property relationship trends

**Figure S9** contains plots assessing the above-mentioned correlations at both T = 500 °C (left column) and T = 800 °C (right column). All of these property correlations follow the same two general principles discussed at length in **Section 2.2** of the main text: the correlations are more robust at higher temperature, and more robust when considering fits to well-studied materials only. First, regarding the correlation of k\* versus D\* (**Figure S9A** and **Figure S9B**), the fit at 800 °C shows a very good linear correlation similar to the work of Kilner et al.,<sup>65</sup> but with a

wider range of perovskite compositions here. At 500 °C, the correlation is modest and still quite good if one only considers well-studied materials.

Next, regarding the correlation of  $k^*$  versus ASR (**Figure S9C** and **Figure S9D**), at both low (500 °C) and high (800 °C) temperatures the fits show reasonably good correlation, where  $k^*$  can be predicted from ASR and vice versa with MAE values in the range of 0.5-0.7 log units, depending on the temperature and set of data considered. This trend is particularly useful as it directly relates  $k^*$ , which is a materials property of the perovskite electrode catalyst, to ASR, which is related to the perovskite materials property but also includes additional confounding factors of the overall electrode device, such as its microstructure, the electrolyte it is bonded with, and any interfacial structure or phases at the electrode/electrolyte interface that may form.

Finally, we will refer to the relationship suggested by the Adler-Lane-Steele<sup>66</sup> formula, which is that  $ASR = A \times (k^* \times D^*)^{-1/2}$  ( $A = \text{constant}$ ) as the Adler-Lane-Steele relationship. The Adler-Lane-Steele formula was developed under very specific assumptions of mechanisms and microstructures, and it is not expected to apply to all the ASR measurements in this work. However, we explore it here just in case it provides a particularly robust relationship. Regarding the correlation of ASR in the Adler-Lane-Steele relationship (**Figure S9E** and **Figure S9F**), like the trend of  $k^*$  versus ASR, there are reasonably good linear trends at both 500 °C and 800 °C. From **Figure S9E** and **Figure S9F**, when considering the subset of well-studied materials, the MAE values for predicting ASR from the Adler-Lane-Steele relationship are 0.55 and 0.37 log units at 500 °C and 800 °C, respectively. Inverting the correlations in **Figure S9C** and **Figure S9D** yields approximately the same MAE values of predicting ASR from just using  $k^*$  of 0.58 and 0.28 log units at 500 °C and 800 °C, respectively (see **Figure S10**). One potential disadvantage of using the Adler-Lane-Steele relationship to predict new data is that it requires knowledge of both  $k^*$  and  $D^*$  to obtain a predicted ASR value, while the correlation of  $k^*$  versus ASR does not require knowledge of  $D^*$ .

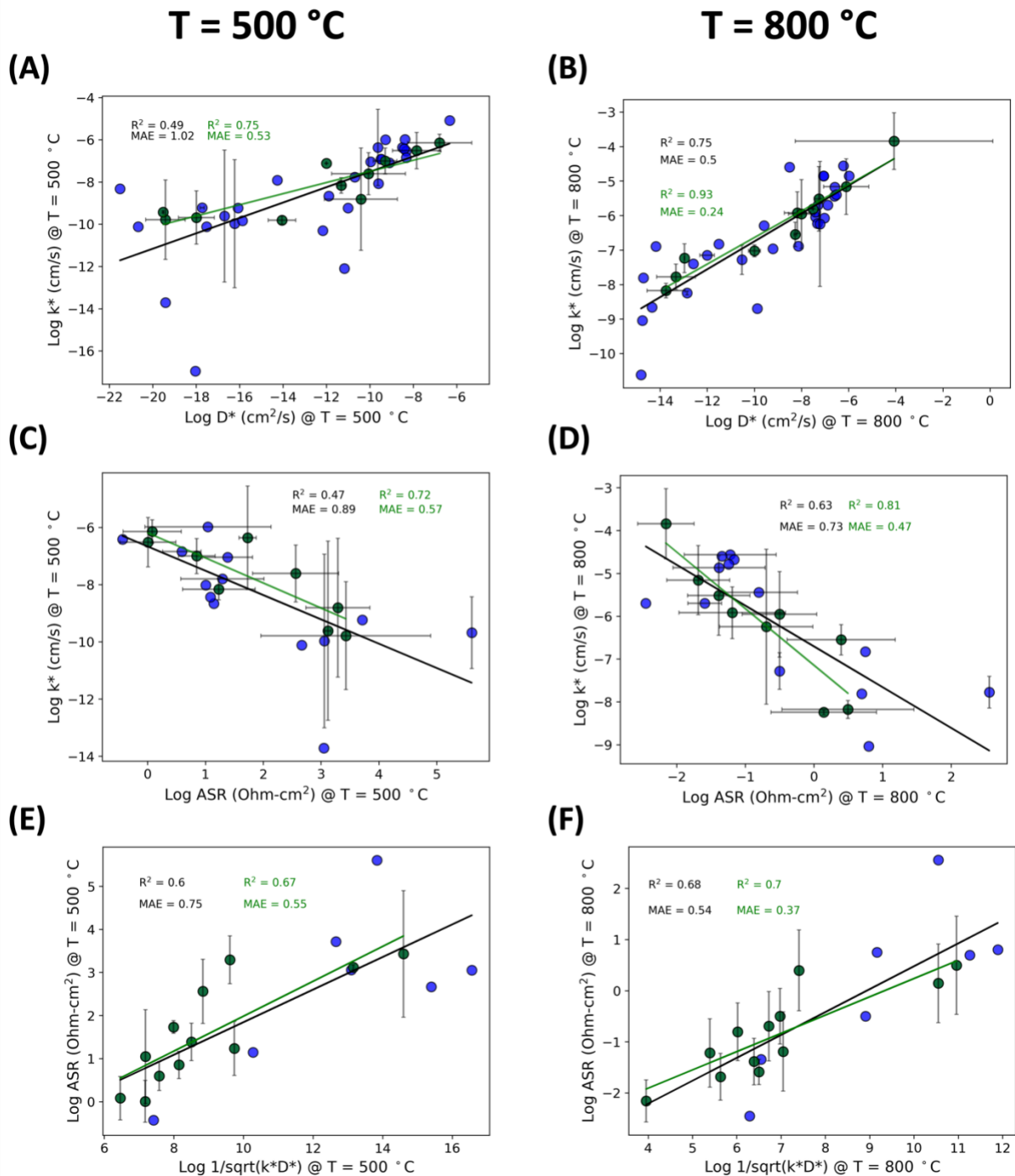


**Figure S9.** Assessments of correlations between perovskite catalytic properties. The left column of plots is at T = 500 °C, and the right column is at T = 800 °C. (A) and (B): Plots of k\* vs. D\* as proposed by Kilner et al.<sup>65</sup> at 500 °C and 800 °C, respectively. (C) and (D): Plots of k\* vs. ASR at 500 °C and 800 °C, respectively, (E) and (F): Assessments of Adler-Lane-Steele<sup>66</sup> relationship at 500 °C and 800 °C, respectively.

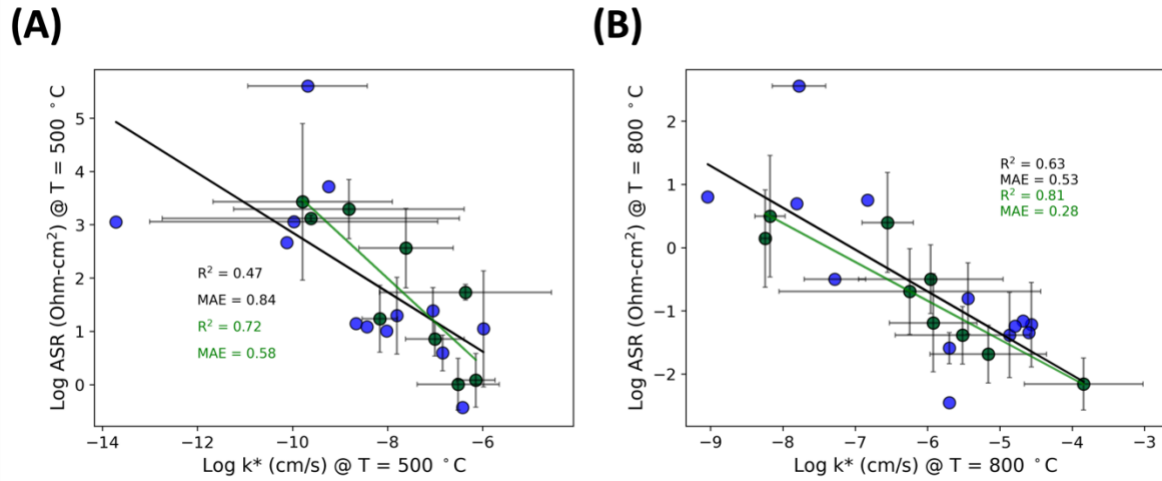


**Figure S10.** Plots of log  $k^*$  vs. log ASR at  $500^\circ\text{C}$  and  $800^\circ\text{C}$ .

## Section S4: Additional thermodynamic factor analysis

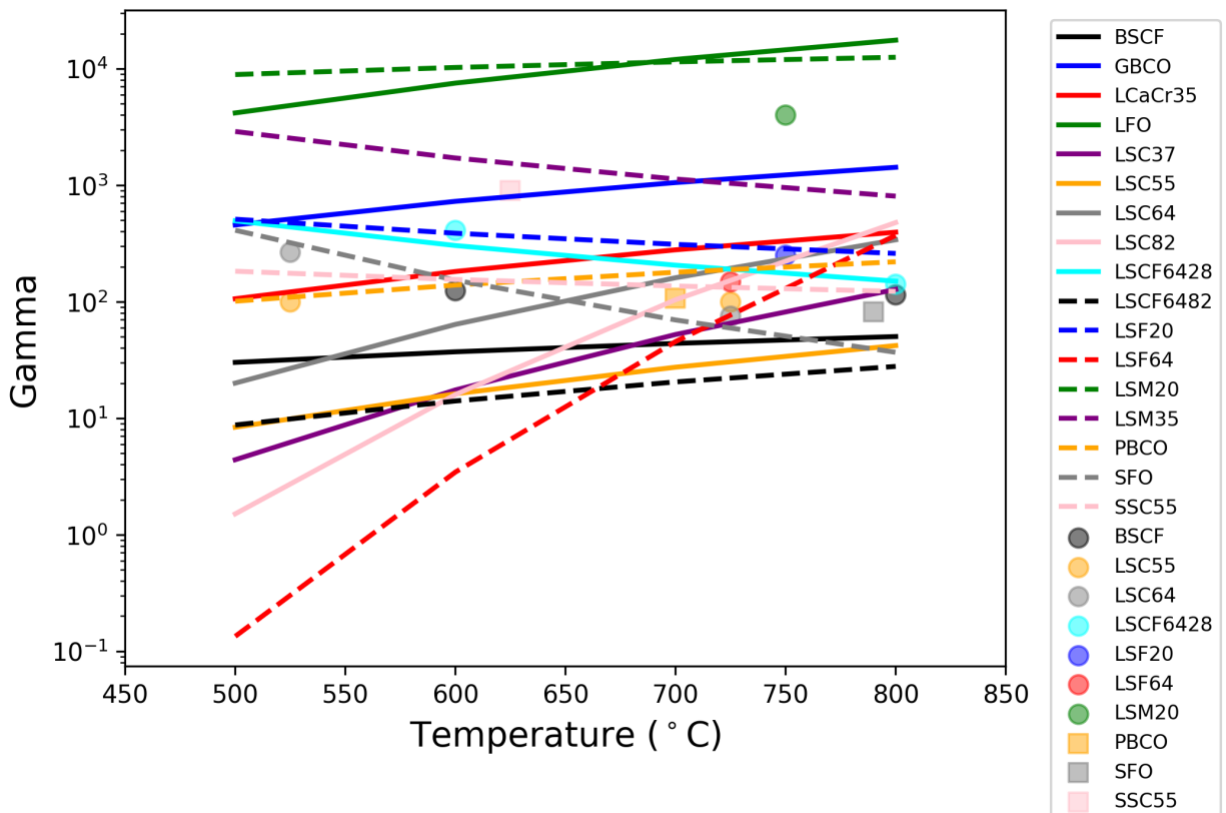


**Figure S5.** Plot of thermodynamic factor  $\gamma$  as a function of temperature using extracted values of  $k_{\text{chem}}/k^*$  at 500, 600, 700 and 800 °C. The data points signify experimentally measured  $\gamma$  values at the designated temperature.

## References

- (1) Ndubuisi, A.; Abouali, S.; Singh, K.; Thangadurai, V. Recent Advances, Practical Challenges, and Perspectives of Intermediate Temperature Solid Oxide Fuel Cell Cathodes. *Journal of Materials Chemistry A*. Royal Society of Chemistry February 7, 2022, pp 2196–2227. <https://doi.org/10.1039/d1ta08475e>.
- (2) Jacobson, A. J. Materials for Solid Oxide Fuel Cells. *Chemistry of Materials* **2010**, *22*, 660–674. <https://doi.org/10.1021/cm902640j>.
- (3) Haile, S. M. Fuel Cell Materials and Components. *Acta Mater* **2003**, *51*, 5981–6000. <https://doi.org/10.1016/j.actamat.2003.08.004>.
- (4) Wachsman, E. D.; Lee, K. T. Lowering the Temperature of Solid Oxide Fuel Cells. *Science (1979)* **2011**, *334* (6058), 935–939. <https://doi.org/10.1126/science.1204090>.
- (5) Duan, C.; Tong, J.; Shang, M.; Nikodemski, S.; Sanders, M.; Ricote, S.; Almansoori, A.; O’Hayre, R. Readily Processed Protonic Ceramic Fuel Cells with High Performance at Low Temperatures. *Science (1979)* **2015**, *349* (6254), 1321–1326. <https://doi.org/10.1126/science.aab3987>.
- (6) Li, Z.; Li, M.; Zhu, Z. Perovskite Cathode Materials for Low-Temperature Solid Oxide Fuel Cells: Fundamentals to Optimization. *Electrochemical Energy Reviews*. Springer June 1, 2022, pp 263–311. <https://doi.org/10.1007/s41918-021-00098-3>.
- (7) Gao, Z.; Mogni, L. V.; Miller, E. C.; Railsback, J. G.; Barnett, S. A. A Perspective on Low-Temperature Solid Oxide Fuel Cells. *Energy and Environmental Science*. Royal Society of Chemistry May 1, 2016, pp 1602–1644. <https://doi.org/10.1039/c5ee03858h>.
- (8) Vohs, J. M.; Gorte, R. J. High-Performance SOFC Cathodes Prepared by Infiltration. *Advanced Materials*. March 6, 2009, pp 943–956. <https://doi.org/10.1002/adma.200802428>.
- (9) Cao, J.; Ji, Y.; Shao, Z. Perovskites for Protonic Ceramic Fuel Cells: A Review. *Energy and Environmental Science*. Royal Society of Chemistry April 7, 2022, pp 2200–2232. <https://doi.org/10.1039/d2ee00132b>.
- (10) Merkle, R.; Hoedl, M. F.; Raimondi, G.; Zohourian, R.; Maier, J. Oxides with Mixed Protonic and Electronic Conductivity. *Annu Rev Mater Res* **2021**, *51*, 461–493. <https://doi.org/10.1146/annurev-matsci-091819-010219>.
- (11) Han, N.; Ren, R.; Ma, M.; Xu, C.; Qiao, J.; Sun, W.; Sun, K.; Wang, Z. Sn and Y Co-Doped BaCo<sub>0.6</sub>Fe<sub>0.4</sub>O<sub>3-δ</sub> Cathodes with Enhanced Oxygen Reduction Activity and CO<sub>2</sub> Tolerance for Solid Oxide Fuel Cells. *Chinese Chemical Letters* **2022**, *33* (5), 2658–2662. <https://doi.org/10.1016/j.cclet.2021.09.100>.
- (12) Zhang, C.; Huang, K. Solid-Oxide Metal–Air Redox Batteries. In *Solid Oxide-Based Electrochemical Devices*; Elsevier, 2020; pp 217–250. <https://doi.org/10.1016/B978-0-12-818285-7.00007-1>.

- (13) Zhao, X.; Gong, Y.; Li, X.; Xu, N.; Huang, K. A New Solid Oxide Molybdenum–Air Redox Battery. *J Mater Chem A Mater* **2013**, *1* (47), 14858. <https://doi.org/10.1039/c3ta12726e>.
- (14) Xu, N.; Li, X.; Zhao, X.; Goodenough, J. B.; Huang, K. A Novel Solid Oxide Redox Flow Battery for Grid Energy Storage. *Energy Environ Sci* **2011**, *4* (12), 4942. <https://doi.org/10.1039/c1ee02489b>.
- (15) Yang, J. J.; Strukov, D. B.; Stewart, D. R. Memristive Devices for Computing. *Nat Nanotechnol* **2013**, *8* (1), 13–24. <https://doi.org/10.1038/nnano.2012.240>.
- (16) Schweiger, S.; Pfenninger, R.; Bowman, W. J.; Aschauer, U.; Rupp, J. L. M. Designing Strained Interface Heterostructures for Memristive Devices. *Advanced Materials* **2017**, *29* (15), 1605049. <https://doi.org/10.1002/adma.201605049>.
- (17) Schmitt, R.; Spring, J.; Korobko, R.; Rupp, J. L. M. Design of Oxygen Vacancy Configuration for Memristive Systems. *ACS Nano* **2017**, *11* (9), 8881–8891. <https://doi.org/10.1021/acsnano.7b03116>.
- (18) Bouwmeester, H.; Burggraaf, A. Dense Ceramic Membranes for Oxygen Separation. In *Handbook of Solid State Electrochemistry*; CRC Press, 1997. <https://doi.org/10.1201/9781420049305.ch14>.
- (19) Koros, W. J.; Mahajan, R. Pushing the Limits on Possibilities for Large Scale Gas Separation: Which Strategies? *J Memb Sci* **2000**, *175* (2), 181–196. [https://doi.org/10.1016/S0376-7388\(00\)00418-X](https://doi.org/10.1016/S0376-7388(00)00418-X).
- (20) Ishihara, T.; Matsuda, H.; Takita, Y. Doped LaGaO<sub>3</sub> Perovskite Type Oxide as a New Oxide Ionic Conductor. *J Am Chem Soc* **1994**, *116*, 3801–3803.
- (21) Huang, K.; Goodenough, J. B. A Solid Oxide Fuel Cell Based on Sr-and Mg-Doped LaGaO<sub>3</sub> Electrolyte: The Role of a Rare-Earth Oxide Buffer. *J Alloys Compd* **2000**, 454–464.
- (22) Goodenough, J. B.; Manthiram, A.; Paranthaman, M.; Zhen, Y. S. Oxide Ion Electrolytes\*. *Materials Science and Engineering* **1992**, *12*, 357–364.
- (23) de Souza, R. A.; Kilner, J. A.; Walker, J. F. A SIMS Study of Oxygen Tracer Diffusion and Surface Exchange in La<sub>0.8</sub>Sr<sub>0.2</sub>MnO<sub>3+δ</sub>. *Mater Lett* **2000**, *43* (1–2), 43–52. [https://doi.org/10.1016/S0167-577X\(99\)00228-1](https://doi.org/10.1016/S0167-577X(99)00228-1).
- (24) Ji, Y.; Kilner, J. A.; Carolan, M. F. Electrical Properties and Oxygen Diffusion in Yttria-Stabilised Zirconia (YSZ)-La<sub>0.8</sub>Sr<sub>0.2</sub>MnO<sub>3±δ</sub> (LSM) Composites. *Solid State Ion* **2005**, *176* (9–10), 937–943. <https://doi.org/10.1016/j.ssi.2004.11.019>.
- (25) Berenov, A. v; MacManus-Driscoll, J. L.; Kilner, J. A. Oxygen Tracer Diffusion in Undoped Lanthanum Manganites. *Solid State Ion* **1999**, *122*, 41–49.
- (26) Kilner, J. A.; de Souza, R. A.; Fullarton, I. C. *Surface Exchange of Oxygen in Mixed Conducting Perovskite Oxides*; 1996.
- (27) Lane, J. A.; Benson, S. J.; Waller, D.; Kilner, J. A. Oxygen Transport in La<sub>0.6</sub>Sr<sub>0.4</sub>Co<sub>0.2</sub>Fe<sub>0.8</sub>O<sub>3-d</sub>. *Solid State Ion* **1999**, *121*, 201–208.
- (28) Berenov, A. V.; Atkinson, A.; Kilner, J. A.; Bucher, E.; Sitte, W. Oxygen Tracer Diffusion and Surface Exchange Kinetics in La<sub>0.6</sub>Sr<sub>0.4</sub>CoO<sub>3-δ</sub>. *Solid State Ion* **2010**, *181* (17–18), 819–826. <https://doi.org/10.1016/j.ssi.2010.04.031>.
- (29) Shao, Z.; Haile, S. M. A High-Performance Cathode for the next Generation of Solid-Oxide Fuel Cells. *Nature* **2004**, *431* (7005), 170–173. <https://doi.org/10.1038/nature02863>.
- (30) Berenov, A.; Atkinson, A.; Kilner, J.; Ananyev, M.; Eremin, V.; Porotnikova, N.; Farlenkov, A.; Kurumchin, E.; Bouwmeester, H. J. M.; Bucher, E.; Sitte, W. Oxygen Tracer Diffusion

- and Surface Exchange Kinetics in Ba<sub>0.5</sub>Sr<sub>0.5</sub>Co<sub>0.8</sub>Fe<sub>0.2</sub>O<sub>3</sub> - δ. *Solid State Ion* **2014**, 268 (Part A), 102–109. <https://doi.org/10.1016/j.ssi.2014.09.031>.
- (31) Wang, L.; Merkle, R.; Maier, J.; Acartürk, T.; Starke, U. Oxygen Tracer Diffusion in Dense Ba<sub>0.5</sub>Sr<sub>0.5</sub>Co<sub>0.8</sub>Fe<sub>0.2</sub>O<sub>3</sub>-δ Films. *Appl Phys Lett* **2009**, 94 (7). <https://doi.org/10.1063/1.3085969>.
- (32) Chen, D.; Shao, Z. Surface Exchange and Bulk Diffusion Properties of Ba<sub>0.5</sub>Sr<sub>0.5</sub>Co<sub>0.8</sub>Fe<sub>0.2</sub>O<sub>3</sub>-δ Mixed Conductor. *Int J Hydrogen Energy* **2011**, 36 (11), 6948–6956. <https://doi.org/10.1016/j.ijhydene.2011.02.087>.
- (33) Bucher, E.; Egger, A.; Ried, P.; Sitte, W.; Holtappels, P. Oxygen Nonstoichiometry and Exchange Kinetics of Ba<sub>0.5</sub>Sr<sub>0.5</sub>Co<sub>0.8</sub>Fe<sub>0.2</sub>O<sub>3</sub> - δ. *Solid State Ion* **2008**, 179 (21–26), 1032–1035. <https://doi.org/10.1016/j.ssi.2008.01.089>.
- (34) Tarancón, A.; Skinner, S. J.; Chater, R. J.; Hernández-Ramírez, F.; Kilner, J. A. Layered Perovskites as Promising Cathodes for Intermediate Temperature Solid Oxide Fuel Cells. *J Mater Chem* **2007**, 17 (30), 3175–3181. <https://doi.org/10.1039/b704320a>.
- (35) Wang, J.; Meng, F.; Xia, T.; Shi, Z.; Lian, J.; Xu, C.; Zhao, H.; Bassat, J. M.; Grenier, J. C. Superior Electrochemical Performance and Oxygen Reduction Kinetics of Layered Perovskite PrBa<sub>x</sub>Co<sub>2</sub>O<sub>5+δ</sub> (x = 0.90–1.0) Oxides as Cathode Materials for Intermediate-Temperature Solid Oxide Fuel Cells. *Int J Hydrogen Energy* **2014**, 39 (32), 18392–18404. <https://doi.org/10.1016/j.ijhydene.2014.09.041>.
- (36) Burriel, M.; Peña-Martínez, J.; Chater, R. J.; Fearn, S.; Berenov, A. v.; Skinner, S. J.; Kilner, J. A. Anisotropic Oxygen Ion Diffusion in Layered PrBa<sub>2</sub>Co<sub>2</sub>O<sub>5+δ</sub>. *Chemistry of Materials* **2012**, 24 (3), 613–621. <https://doi.org/10.1021/cm203502s>.
- (37) Duan, C.; Hook, D.; Chen, Y.; Tong, J.; O’Hayre, R. Zr and Y Co-Doped Perovskite as a Stable, High Performance Cathode for Solid Oxide Fuel Cells Operating below 500°C. *Energy Environ Sci* **2017**, 10 (1), 176–182. <https://doi.org/10.1039/c6ee01915c>.
- (38) Duan, C.; Kee, R.; Zhu, H.; Sullivan, N.; Zhu, L.; Bian, L.; Jennings, D.; O’Hayre, R. Highly Efficient Reversible Protonic Ceramic Electrochemical Cells for Power Generation and Fuel Production. *Nat Energy* **2019**, 4 (3), 230–240. <https://doi.org/10.1038/s41560-019-0333-2>.
- (39) Zohourian, R.; Merkle, R.; Raimondi, G.; Maier, J. Mixed-Conducting Perovskites as Cathode Materials for Protonic Ceramic Fuel Cells: Understanding the Trends in Proton Uptake. *Adv Funct Mater* **2018**, 28 (35). <https://doi.org/10.1002/adfm.201801241>.
- (40) Liu, Q.; Dong, X.; Xiao, G.; Zhao, F.; Chen, F. A Novel Electrode Material for Symmetrical SOFCs. *Advanced Materials* **2010**, 22 (48), 5478–5482. <https://doi.org/10.1002/adma.201001044>.
- (41) Muñoz-García, A. B.; Pavone, M. First-Principles Design of New Electrodes for Proton-Conducting Solid-Oxide Electrochemical Cells: A-Site Doped Sr<sub>2</sub>Fe<sub>1.5</sub>Mo<sub>0.5</sub>O<sub>6</sub>-δ Perovskite. *Chemistry of Materials* **2016**, 28 (2), 490–500. <https://doi.org/10.1021/acs.chemmater.5b03262>.
- (42) Kasyanova, A. v.; Tarutina, L. R.; Rudenko, A. O.; Lyagaeva, J. G.; Medvedev, D. A. Ba(Ce,Zr)O<sub>3</sub> -Based Electrodes for Protonic Ceramic Electrochemical Cells: Towards Highly Compatible Functionality and Triple-Conducting Behaviour . *Russian Chemical Reviews* **2020**, 89 (6), 667–692. <https://doi.org/10.1070/rctr4928>.

- (43) Tahir, N. N. M.; Baharuddin, N. A.; Samat, A. A.; Osman, N.; Somalu, M. R. A Review on Cathode Materials for Conventional and Proton-Conducting Solid Oxide Fuel Cells. *Journal of Alloys and Compounds*. Elsevier Ltd February 15, 2022. <https://doi.org/10.1016/j.jallcom.2021.162458>.
- (44) Papac, M.; Stevanović, V.; Zakutayev, A.; O’Hayre, R. Triple Ionic–Electronic Conducting Oxides for next-Generation Electrochemical Devices. *Nature Materials*. Nature Research March 1, 2021, pp 301–313. <https://doi.org/10.1038/s41563-020-00854-8>.
- (45) Kim, J.; Sengodan, S.; Kwon, G.; Ding, D.; Shin, J.; Liu, M.; Kim, G. Triple-Conducting Layered Perovskites as Cathode Materials for Proton-Conducting Solid Oxide Fuel Cells. *ChemSusChem* **2014**, 7 (10), 2811–2815. <https://doi.org/10.1002/cssc.201402351>.
- (46) Lee, Y.-L.; Kleis, J.; Rossmeisl, J.; Shao-Horn, Y.; Morgan, D. Prediction of Solid Oxide Fuel Cell Cathode Activity with First-Principles Descriptors. *Energy Environ Sci* **2011**, 4, 3966–3970. <https://doi.org/10.1039/c1ee02032c>.
- (47) Kim, Y.; Ha, M.; Anand, R.; Zafari, M.; Baik, J. M.; Park, H.; Lee, G. Unveiling a Surface Electronic Descriptor for Fe-Co Mixing Enhanced the Stability and Efficiency of Perovskite Oxygen Evolution Electrocatalysts. *ACS Catal* **2022**, 14698–14707. <https://doi.org/10.1021/acscatal.2c04424>.
- (48) Suntivich, J.; May, K. J.; Gasteiger, H. A.; Goodenough, J. B.; Shao-Horn, Y. A Perovskite Oxide Optimized for Oxygen Evolution Catalysis from Molecular Orbital Principles. *Science (1979)* **2011**, 334 (6061), 1383–1385. <https://doi.org/10.1126/science.1212858>.
- (49) Suntivich, J.; Gasteiger, H. A.; Yabuuchi, N.; Nakanishi, H.; Goodenough, J. B.; Shao-horn, Y. Design Principles for Oxygen-Reduction Activity on Perovskite Oxide Catalysts for Fuel Cells and Metal – Air Batteries. *Nat Chem* **2011**, 3 (7), 546–550. <https://doi.org/10.1038/nchem.1069>.
- (50) Hong, W. T.; Stoerzinger, K. A.; Lee, Y. L.; Giordano, L.; Grimaud, A.; Johnson, A. M.; Hwang, J.; Crumlin, E. J.; Yang, W.; Shao-Horn, Y. Charge-Transfer-Energy-Dependent Oxygen Evolution Reaction Mechanisms for Perovskite Oxides. *Energy Environ Sci* **2017**, 10 (10), 2190–2200. <https://doi.org/10.1039/c7ee02052j>.
- (51) Exner, K. S. A Universal Descriptor for the Screening of Electrode Materials for Multiple-Electron Processes: Beyond the Thermodynamic Overpotential. *ACS Catalysis*. American Chemical Society November 6, 2020, pp 12607–12617. <https://doi.org/10.1021/acscatal.0c03865>.
- (52) Giordano, L.; Akkiraju, K.; Jacobs, R.; Vivona, D.; Morgan, D.; Shao-Horn, Y. Electronic Structure-Based Descriptors for Oxide Properties and Functions. *Acc Chem Res* **2022**, 55 (3), 298–308.
- (53) Jacobs, R.; Hwang, J.; Hong, W.; Shao-Horn, Y.; Morgan, D. Assessing Correlations with Electronic Structure Descriptors for Perovskite Catalytic Performance. *Chemistry of Materials* **2019**, 31 (3), 785–797. <https://doi.org/10.1021/acs.chemmater.8b03840>.
- (54) Lee, Y. L.; Lee, D.; Wang, X. R.; Lee, H. N.; Morgan, D.; Shao-Horn, Y. Kinetics of Oxygen Surface Exchange on Epitaxial Ruddlesden-Popper Phases and Correlations to First-Principles Descriptors. *Journal of Physical Chemistry Letters* **2016**, 7 (2), 244–249. <https://doi.org/10.1021/acs.jpcllett.5b02423>.

- (55) Jacobs, R.; Mayeshiba, T.; Booske, J.; Morgan, D. Material Discovery and Design Principles for Stable, High Activity Perovskite Cathodes for Solid Oxide Fuel Cells. *Adv Energy Mater* **2018**, *8* (11), 1–27. <https://doi.org/10.1002/aenm.201702708>.
- (56) Mayeshiba, T. T.; Morgan, D. D. Factors Controlling Oxygen Migration Barriers in Perovskites. *Solid State Ion* **2016**, *296*, 71–77. <https://doi.org/10.1016/j.ssi.2016.09.007>.
- (57) Ma, T.; Jacobs, R.; Booske, J.; Morgan, D. Discovery and Engineering of Low Work Function Perovskite Materials. *J Mater Chem C Mater* **2021**, *9* (37), 12778–12790. [https://doi.org/https://doi.org/10.1039/D1TC01286J](https://doi.org/10.1039/D1TC01286J).
- (58) Jacobs, R.; Booske, J.; Morgan, D. Understanding and Controlling the Work Function of Perovskite Oxides Using Density Functional Theory. *Adv Funct Mater* **2016**, *26* (30). <https://doi.org/10.1002/adfm.201600243>.
- (59) Grimaud, A.; May, K. J.; Carlton, C. E.; Lee, Y.-L.; Risch, M.; Hong, W. T.; Zhou, J.; Shao-Horn, Y. Double Perovskites as a Family of Highly Active Catalysts for Oxygen Evolution in Alkaline Solution. *Nat Commun* **2013**, *4*, 1–7. <https://doi.org/10.1038/ncomms3439>.
- (60) Lee, Y.; Gadre, M. J.; Shao-horn, Y.; Morgan, D. Ab Initio GGA+U Study of Oxygen Evolution and Oxygen Reduction Electrocatalysis on the (001) Surfaces of Lanthanum Transition Metal Perovskites  $\text{LaBO}_3$  ( $B = \text{Cr}, \text{Mn}, \text{Fe}, \text{Co}$  and  $\text{Ni}$ ). *Physical Chemistry Chemical Physics* **2015**, *17*, 21643–21663. <https://doi.org/10.1039/C5CP02834E>.
- (61) Lee, D.; Jacobs, R.; Jee, Y.; Seo, A.; Sohn, C.; levlev, A. v; Ovchinnikova, O. S.; Huang, K.; Morgan, D.; Lee, H. N. Stretching Epitaxial  $\text{La}_0.6\text{Sr}_0.4\text{CoO}_3\text{-d}$  for Fast Oxygen Reduction. *Journal of Physical Chemistry C* **2017**, *121*, 25651–25658. <https://doi.org/10.1021/acs.jpcc.7b06374>.
- (62) Hwang, J.; Feng, Z.; Charles, N.; Wang, X. R.; Lee, D.; Stoerzinger, K. A.; Muy, S.; Rao, R. R.; Lee, D.; Jacobs, R.; Morgan, D.; Shao-Horn, Y. Tuning Perovskite Oxides by Strain: Electronic Structure, Properties, and Functions in (Electro)Catalysis and Ferroelectricity. *Materials Today* **2019**, *31*. <https://doi.org/10.1016/j.mattod.2019.03.014>.
- (63) Jacobs, R.; Liu, J.; Na, B. T.; Guan, B.; Yang, T.; Lee, S.; Hackett, G.; Kalapos, T.; Abernathy, H.; Morgan, D. Unconventional Highly Active and Stable Oxygen Reduction Catalysts Informed by Computational Design Strategies. *Adv Energy Mater* **2022**.
- (64) Sanchez-Ahijon, E.; Marin-Gamero, R.; Molero-Sanchez, B.; Avila-Brande, D.; Manjon-Sanz, A.; Fernandez-Dianz, M. T.; Moran, E.; Schmidt, R.; Prado-Gonjal, J. From Theory to Experiment:  $\text{BaFe}_{0.125}\text{Co}_{0.125}\text{Zr}_{0.75}\text{O}_3\text{-d}$ , a Highly Promising Cathode for Intermediate Temperature SOFCs. *J Mater Chem A Mater* **2020**. <https://doi.org/10.7551/mitpress/9780262019453.003.0012>.
- (65) Kilner, J. A.; de Souza, R. A.; Fullarton, I. C. Surface Exchange of Oxygen in Mixed Conducting Perovskite Oxides. *Solid State Ion* **1996**, *86–88* (PART 2), 703–709. [https://doi.org/10.1016/0167-2738\(96\)00153-1](https://doi.org/10.1016/0167-2738(96)00153-1).
- (66) Adler, S.; Lane, J.; Steele, B. Electrode Kinetics of Porous Mixed-Conducting Oxygen Electrodes. *J Electrochem Soc* **1996**, *143* (11), 3554–3564.
- (67) ten Elshof, J. E.; Lankhorst, M. H. R.; Bouwmeester, H. J. M. Oxygen Exchange and Diffusion Coefficients of Strontium-Doped Lanthanum Ferrites by Electrical Conductivity Relaxation. *J Electrochem Soc* **1997**, *144* (3), 1060–1067.
- (68) Saher, S.; Naqash, S.; Boukamp, B. A.; Hu, B.; Xia, C.; Bouwmeester, H. J. M. Influence of Ionic Conductivity of the Nano-Particulate Coating Phase on Oxygen Surface Exchange of

- La<sub>0.58</sub>Sr<sub>0.4</sub>Co<sub>0.2</sub>Fe<sub>0.8</sub>O<sub>3-δ</sub>. *J Mater Chem A Mater* **2017**, 5 (10), 4991–4999.  
<https://doi.org/10.1039/c6ta10954c>.
- (69) Kresse, G.; Furthmüller, J. Efficient Iterative Schemes for Ab Initio Total-Energy Calculations Using a Plane-Wave Basis Set. *Phys. Rev. B* **1996**, 54 (16), 11169–11186.
- (70) Perdew, J.; Burke, K.; Ernzerhof, M. Generalized Gradient Approximation Made Simple. *Phys Rev Lett* **1996**, 77 (18), 3865–3868. <https://doi.org/10.1103/PhysRevLett.77.3865>.
- (71) Monkhorst, H.; Pack, J. Special Points for Brillouin Zone Integrations. *Phys Rev B* **1976**, 13 (12), 5188–5192. <https://doi.org/10.1103/PhysRevB.13.5188>.
- (72) Wang, F.; Chen, D.; Shao, Z. Composition and Microstructure Optimization and Operation Stability of Barium Deficient Ba<sub>1-X</sub>Co<sub>0.7</sub>Fe<sub>0.2</sub>Nb<sub>0.1</sub>O<sub>3-δ</sub> Perovskite Oxide Electrodes. *Electrochim Acta* **2013**, 103, 23–31. <https://doi.org/10.1016/j.electacta.2013.04.054>.
- (73) Liu, Z.; Cheng, L. Z.; Han, M. F. A-Site Deficient Ba<sub>1-X</sub>Co<sub>0.7</sub>Fe<sub>0.2</sub>Ni<sub>0.1</sub>O<sub>3-δ</sub> Cathode for Intermediate Temperature SOFC. *J Power Sources* **2011**, 196 (2), 868–871. <https://doi.org/10.1016/j.jpowsour.2010.05.051>.
- (74) Zhou, W.; Sunarso, J.; Chen, Z. G.; Ge, L.; Motuzas, J.; Zou, J.; Wang, G.; Julbe, A.; Zhu, Z. Novel B-Site Ordered Double Perovskite Ba<sub>2</sub>Bi<sub>0.1</sub>Sc<sub>0.2</sub>Co<sub>1.7</sub>O<sub>6-x</sub> for Highly Efficient Oxygen Reduction Reaction. *Energy Environ Sci* **2011**, 4 (3), 872–875. <https://doi.org/10.1039/c0ee00451k>.
- (75) Wang, J.; Lam, K. Y.; Saccoccia, M.; Gao, Y.; Chen, D.; Ciucci, F. Ca and In Co-Doped BaFeO<sub>3-δ</sub> as a Cobalt-Free Cathode Material for Intermediate-Temperature Solid Oxide Fuel Cells. *J Power Sources* **2016**, 324, 224–232. <https://doi.org/10.1016/j.jpowsour.2016.05.089>.
- (76) Zhu, L.; Hong, T.; Xu, C.; Cheng, J. A Novel Dual Phase BaCe<sub>0.5</sub>Fe<sub>0.5</sub>O<sub>3-δ</sub> Cathode with High Oxygen Electrocatalysis Activity for Intermediate Temperature Solid Oxide Fuel Cells. *Int J Hydrogen Energy* **2019**, 44 (29), 15400–15408. <https://doi.org/10.1016/j.ijhydene.2019.04.060>.
- (77) Huang, S.; Lu, Q.; Feng, S.; Li, G.; Wang, C. Ba 0.9 Co 0.7 Fe 0.2 Mo 0.1 O 3-δ: A Promising Single-Phase Cathode for Low Temperature Solid Oxide Fuel Cells. *Adv Energy Mater* **2011**, 1 (6), 1094–1096. <https://doi.org/10.1002/aenm.201100497>.
- (78) Qian, B.; Chen, Y.; Tade, M. O.; Shao, Z. BaCo<sub>0.6</sub>Fe<sub>0.3</sub>Sn<sub>0.1</sub>O<sub>3-δ</sub> Perovskite as a New Superior Oxygen Reduction Electrode for Intermediate-to-Low Temperature Solid Oxide Fuel Cells. *J Mater Chem A Mater* **2014**, 2 (36), 15078–15086. <https://doi.org/10.1039/c4ta02869d>.
- (79) Yang, Z.; Yang, C.; Xiong, B.; Han, M.; Chen, F. BaCo<sub>0.7</sub>Fe<sub>0.2</sub>Nb<sub>0.1</sub>O<sub>3-δ</sub> as Cathode Material for Intermediate Temperature Solid Oxide Fuel Cells. *J Power Sources* **2011**, 196 (22), 9164–9168. <https://doi.org/10.1016/j.jpowsour.2011.06.096>.
- (80) Yang, Z.; Yang, C.; Jin, C.; Han, M.; Chen, F. Ba<sub>0.9</sub>Co<sub>0.7</sub>Fe<sub>0.2</sub>Nb<sub>0.1</sub>O<sub>3-δ</sub> as Cathode Material for Intermediate Temperature Solid Oxide Fuel Cells. *Electrochim commun* **2011**, 13 (8), 882–885. <https://doi.org/10.1016/j.elecom.2011.05.029>.
- (81) Zhu, C.; Liu, X.; Yi, C.; Pei, L.; Yan, D.; Niu, J.; Wang, D.; Su, W. Novel BaCo<sub>0.7</sub>Fe<sub>0.3</sub>-YNbyO<sub>3-δ</sub> (y = 0-0.12) as a Cathode for Intermediate Temperature Solid Oxide Fuel Cell. *Electrochim commun* **2009**, 11 (5), 958–961. <https://doi.org/10.1016/j.elecom.2009.02.034>.

- (82) He, W.; Dong, F. F.; Wu, X. L.; Ni, M. A Highly Active Perovskite Cathode for Low-Temperature Solid Oxide Fuel Cells: BaCo<sub>0.7</sub>Fe<sub>0.22</sub>Sc<sub>0.08</sub>O<sub>3-δ</sub>. *Adv Sustain Syst* **2017**, *1* (5). <https://doi.org/10.1002/adstu.201700005>.
- (83) Zhang, Z.; Chen, Y.; Tade, M. O.; Hao, Y.; Liu, S.; Shao, Z. Tin-Doped Perovskite Mixed Conducting Membrane for Efficient Air Separation. *J Mater Chem A Mater* **2014**, *2* (25), 9666–9674. <https://doi.org/10.1039/c4ta00926f>.
- (84) He, W.; Wu, X.; Yang, G.; Shi, H.; Dong, F.; Ni, M. BaCo<sub>0.7</sub>Fe<sub>0.22</sub>Y<sub>0.08</sub>O<sub>3-δ</sub> as an Active Oxygen Reduction Electrocatalyst for Low-Temperature Solid Oxide Fuel Cells below 600 °c. *ACS Energy Letters*. American Chemical Society February 10, 2017, pp 301–305. <https://doi.org/10.1021/acsenergylett.6b00617>.
- (85) Yang, C.; Gan, Y.; Lee, M.; Ren, C.; Xue, X. Yb Doping Effects on Structure and Performance of BaCo 0.7 Fe 0.3-x Yb x O 3-δ Perovskite . *J Electrochem Soc* **2018**, *165* (13), F1032–F1042. <https://doi.org/10.1149/2.0251813jes>.
- (86) Dong, F.; Chen, Y.; Chen, D.; Shao, Z. Surprisingly High Activity for Oxygen Reduction Reaction of Selected Oxides Lacking Long Oxygen-Ion Diffusion Paths at Intermediate Temperatures: A Case Study of Cobalt-Free BaFeO<sub>3-δ</sub>. *ACS Appl Mater Interfaces* **2014**, *6* (14), 11180–11189. <https://doi.org/10.1021/am502240m>.
- (87) Liu, B.; Sunarso, J.; Zhang, Y.; Yang, G.; Zhou, W.; Shao, Z. Highly Oxygen Non-Stoichiometric BaSc<sub>0.25</sub>Co<sub>0.75</sub>O<sub>3-δ</sub> as a High-Performance Cathode for Intermediate-Temperature Solid Oxide Fuel Cells. *ChemElectroChem* **2018**, *5* (5), 785–792. <https://doi.org/10.1002/celc.201701309>.
- (88) Xia, Y.; Xu, X.; Teng, Y.; Lv, H.; Jin, Z.; Wang, D.; Peng, R.; Liu, W. A Novel BaFe<sub>0.8</sub>Zn<sub>0.1</sub>Bi<sub>0.1</sub>O<sub>3-δ</sub> Cathode for Proton Conducting Solid Oxide Fuel Cells. *Ceram Int* **2020**, *46* (16), 25453–25459. <https://doi.org/10.1016/j.ceramint.2020.07.015>.
- (89) Zhang, L.; Li, J.; Yang, J.; Shen, H. BaFe<sub>0.6</sub>Ce<sub>0.1</sub>Co<sub>0.3</sub>O<sub>3-δ</sub> as a High-Performance Cathode for Intermediate-Temperature Solid Oxide Fuel Cells. *Electrochim Acta* **2015**, *154*, 244–248. <https://doi.org/10.1016/j.electacta.2014.12.060>.
- (90) Wang, J.; Saccoccio, M.; Chen, D.; Gao, Y.; Chen, C.; Ciucci, F. The Effect of A-Site and B-Site Substitution on BaFeO<sub>3-δ</sub>: An Investigation as a Cathode Material for Intermediate-Temperature Solid Oxide Fuel Cells. *J Power Sources* **2015**, *297*, 511–518. <https://doi.org/10.1016/j.jpowsour.2015.08.016>.
- (91) Xie, D.; Guo, W.; Guo, R.; Liu, Z.; Sun, D.; Meng, L.; Zheng, M.; Wang, B. Synthesis and Electrochemical Properties of BaFe<sub>1-x</sub>Cu<sub>x</sub>O<sub>3-δ</sub>Perovskite Oxide for IT-SOFC Cathode. *Fuel Cells* **2016**, *16* (6), 829–838. <https://doi.org/10.1002/fuce.201600149>.
- (92) Shang, M.; Tong, J.; O’Hayre, R. A Promising Cathode for Intermediate Temperature Protonic Ceramic Fuel Cells: BaCo<sub>0.4</sub>Fe<sub>0.4</sub>Zr<sub>0.2</sub>O<sub>3-δ</sub>. *RSC Adv* **2013**, *3* (36), 15769–15775. <https://doi.org/10.1039/c3ra41828f>.
- (93) Zhang, L.; Shan, J.; Wang, Q. BaCo<sub>0.4</sub>Fe<sub>0.4</sub>Zr<sub>0.2</sub>O<sub>3-δ</sub>: Evaluation as a Cathode for Ceria-Based Electrolyte IT-SOFCs. *J Alloys Compd* **2019**, *771*, 221–227. <https://doi.org/10.1016/j.jallcom.2018.08.232>.
- (94) Lv, H.; Jin, Z.; Peng, R.; Liu, W.; Gong, Z. BaC<sub>x</sub>Fe<sub>0.7-X</sub>Zr<sub>0.3</sub>O<sub>3-δ</sub>(0.2≤x≤0.5) as Cathode Materials for Proton-Based SOFCs. *Ceram Int* **2019**, *45* (18), 23948–23953. <https://doi.org/10.1016/j.ceramint.2019.08.096>.

- (95) Meng, Y.; Duffy, J.; Na, B. T.; Gao, J.; Yang, T.; Tong, J.; Lee, S.; Brinkman, K. S. Oxygen Exchange and Bulk Diffusivity of BaCo $0.4$ Fe $0.4$ Zr $0.1$ Y $0.1$ O $3-\delta$ : Quantitative Assessment of Active Cathode Material for Protonic Ceramic Fuel Cells. *Solid State Ion* **2021**, 368. <https://doi.org/10.1016/j.ssi.2021.115639>.
- (96) Dong, F.; Chen, Y.; Ran, R.; Chen, D.; Tadé, M. O.; Liu, S.; Shao, Z. BaNb $0.05$ Fe $0.95$ O $3-\delta$  as a New Oxygen Reduction Electrocatalyst for Intermediate Temperature Solid Oxide Fuel Cells. *J Mater Chem A Mater* **2013**, 1 (34), 9781–9791. <https://doi.org/10.1039/c3ta11447c>.
- (97) Xu, D.; Dong, F.; Chen, Y.; Zhao, B.; Liu, S.; Tade, M. O.; Shao, Z. Cobalt-Free Niobium-Doped Barium Ferrite as Potential Materials of Dense Ceramic Membranes for Oxygen Separation. *J Memb Sci* **2014**, 455, 75–82. <https://doi.org/10.1016/j.memsci.2013.12.030>.
- (98) Gao, L.; Zhu, M.; Xia, T.; Li, Q.; Li, T.; Zhao, H. Ni-Doped BaFeO $3-\delta$  Perovskite Oxide as Highly Active Cathode Electrocatalyst for Intermediate-Temperature Solid Oxide Fuel Cells. *Electrochim Acta* **2018**, 289, 428–436. <https://doi.org/10.1016/j.electacta.2018.09.096>.
- (99) Dong, F.; Ni, M.; He, W.; Chen, Y.; Yang, G.; Chen, D.; Shao, Z. An Efficient Electrocatalyst as Cathode Material for Solid Oxide Fuel Cells: BaFe $0.95$ Sn $0.05$ O $3-\delta$ . *J Power Sources* **2016**, 326, 459–465. <https://doi.org/10.1016/j.jpowsour.2016.07.023>.
- (100) Xia, Y.; Jin, Z.; Wang, H.; Gong, Z.; Lv, H.; Peng, R.; Liu, W.; Bi, L. A Novel Cobalt-Free Cathode with Triple-Conduction for Proton-Conducting Solid Oxide Fuel Cells with Unprecedented Performance. *J Mater Chem A Mater* **2019**, 7 (27), 16136–16148. <https://doi.org/10.1039/c9ta02449b>.
- (101) Zhang, H.; Suresh, A.; Carter, C. B.; Wilhite, B. A. Materials Synthesis, Electrochemical Characterization and Oxygen Permeation Properties of Fe-Doped BaZrO $3$ . *Solid State Ion* **2014**, 266, 58–67. <https://doi.org/10.1016/j.ssi.2014.08.011>.
- (102) Li, L.; Kong, Z.; Yao, B.; Yang, H.; Gao, Z.; Xu, L.; Dong, F.; Ni, M.; Lin, Z. An Efficient and Durable Perovskite Electrocatalyst for Oxygen Reduction in Solid Oxide Fuel Cells. *Chemical Engineering Journal* **2020**, 396. <https://doi.org/10.1016/j.cej.2020.125237>.
- (103) Huang, S.; Gao, F.; Meng, Z.; Feng, S.; Sun, X.; Li, Y.; Wang, C. Bismuth-Based Pervoskite as a High-Performance Cathode for Intermediate-Temperature Solid-Oxide Fuel Cells. *ChemElectroChem* **2014**, 1 (3), 554–558. <https://doi.org/10.1002/celc.201300070>.
- (104) Niu, Y.; Zhou, W.; Sunarso, J.; Ge, L.; Zhu, Z.; Shao, Z. High Performance Cobalt-Free Perovskite Cathode for Intermediate Temperature Solid Oxide Fuel Cells. *J Mater Chem* **2010**, 20 (43), 9619–9622. <https://doi.org/10.1039/c0jm02816a>.
- (105) Niu, Y.; Sunarso, J.; Liang, F.; Zhou, W.; Zhu, Z.; Shao, Z. A Comparative Study of Oxygen Reduction Reaction on Bi- and La-Doped SrFeO $[Sub\ 3-\delta]$  Perovskite Cathodes. *J Electrochem Soc* **2011**, 158 (2), B132. <https://doi.org/10.1149/1.3521316>.
- (106) Niu, Y.; Sunarso, J.; Zhou, W.; Liang, F.; Ge, L.; Zhu, Z.; Shao, Z. Evaluation and Optimization of Bi $1-X$ SrxFeO $3-\delta$  Perovskites as Cathodes of Solid Oxide Fuel Cells. *Int J Hydrogen Energy* **2011**, 36 (4), 3179–3186. <https://doi.org/10.1016/j.ijhydene.2010.11.109>.

- (107) Wedig, A.; Merkle, R.; Stuhlhofer, B.; Habermeier, H. U.; Maier, J.; Heifets, E. Fast Oxygen Exchange Kinetics of Pore-Free Bi<sub>1-X</sub>Sr<sub>X</sub>FeO<sub>3-δ</sub> Thin Films. *Physical Chemistry Chemical Physics* **2011**, *13* (37), 16530–16533. <https://doi.org/10.1039/c1cp21684h>.
- (108) Gao, J.; Li, Q.; Sun, L.; Huo, L.; Zhao, H. Enhanced Electrocatalytic Activity and CO<sub>2</sub> Tolerant Bi<sub>0.5</sub>Sr<sub>0.5</sub>Fe<sub>1-X</sub>TaxO<sub>3-δ</sub> as Cobalt-Free Cathode for Intermediate-Temperature Solid Oxide Fuel Cells. *Ceram Int* **2019**, *45* (16), 20226–20233. <https://doi.org/10.1016/j.ceramint.2019.06.295>.
- (109) Gao, L.; Zhu, M.; Li, Q.; Sun, L.; Zhao, H.; Grenier, J. C. Electrode Properties of Cu-Doped Bi<sub>0.5</sub>Sr<sub>0.5</sub>FeO<sub>3-δ</sub>cobalt-Free Perovskite as Cathode for Intermediate-Temperature Solid Oxide Fuel Cells. *J Alloys Compd* **2017**, *700*, 29–36. <https://doi.org/10.1016/j.jallcom.2017.01.026>.
- (110) Gao, L.; Li, Q.; Sun, L.; Zhang, X.; Huo, L.; Zhao, H.; Grenier, J. C. A Novel Family of Nb-Doped Bi<sub>0.5</sub>Sr<sub>0.5</sub>FeO<sub>3-Δ</sub> Perovskite as Cathode Material for Intermediate-Temperature Solid Oxide Fuel Cells. *J Power Sources* **2017**, *371*, 86–95. <https://doi.org/10.1016/j.jpowsour.2017.10.036>.
- (111) Gao, L.; Li, Q.; Sun, L.; Xia, T.; Huo, L.; Zhao, H.; Grenier, J. C. Antimony-Doped Bi<sub>0.5</sub>Sr<sub>0.5</sub>FeO<sub>3-δ</sub> as a Novel Fe-Based Oxygen Reduction Electrocatalyst for Solid Oxide Fuel Cells below 600 °c. *J Mater Chem A Mater* **2018**, *6* (31), 15221–15229. <https://doi.org/10.1039/c8ta04222e>.
- (112) Gao, J.; Li, Q.; Xia, W.; Sun, L.; Huo, L. H.; Zhao, H. Advanced Electrochemical Performance and CO<sub>2</sub> Tolerance of Bi<sub>0.5</sub>Sr<sub>0.5</sub>Fe<sub>1-X</sub>TixO<sub>3-δ</sub> Perovskite Materials as Oxygen Reduction Cathodes for Intermediate-Temperature Solid Oxide Fuel Cells. *ACS Sustain Chem Eng* **2019**, *7* (22), 18647–18656. <https://doi.org/10.1021/acssuschemeng.9b05086>.
- (113) Dong, F.; Chen, D.; Chen, Y.; Zhao, Q.; Shao, Z. La-Doped BaFeO<sub>3-δ</sub> Perovskite as a Cobalt-Free Oxygen Reduction Electrode for Solid Oxide Fuel Cells with Oxygen-Ion Conducting Electrolyte. *J Mater Chem* **2012**, *22* (30), 15071–15079. <https://doi.org/10.1039/c2jm31711g>.
- (114) Liu, J.; Wang, J.; Belotti, A.; Ciucci, F. P-Substituted Ba<sub>0.95</sub>La<sub>0.05</sub>FeO<sub>3-?</sub> As a Cathode Material for SOFCs. *ACS Appl Energy Mater* **2019**, *2* (8), 5472–5480. <https://doi.org/10.1021/acsaelm.9b00624>.
- (115) Chen, D.; Chen, C.; Dong, F.; Shao, Z.; Ciucci, F. Cobalt-Free Polycrystalline Ba<sub>0.95</sub>La<sub>0.05</sub>FeO<sub>3-δ</sub> Thin Films as Cathodes for Intermediate-Temperature Solid Oxide Fuel Cells. *J Power Sources* **2014**, *250*, 188–195. <https://doi.org/10.1016/j.jpowsour.2013.11.010>.
- (116) Ding, X.; Gao, X.; Zhu, W.; Wang, J.; Jiang, J. Electrode Redox Properties of Ba<sub>1-X</sub>LaxFeO<sub>3-δ</sub> as Cobalt Free Cathode Materials for Intermediate- Temperature SOFCs. *Int J Hydrogen Energy* **2014**, *39* (23), 12092–12100. <https://doi.org/10.1016/j.ijhydene.2014.06.009>.
- (117) Liu, P.; Zhu, H.; Kong, J.; Wei, N.; Wang, C.; Yang, X.; Liu, Q. Preparation and Electrochemical Properties of Ba<sub>0.8</sub>La<sub>0.2</sub>FeO<sub>3-δ</sub> Cathode for Intermediate-Temperature Solid Oxide Fuel Cells. *J Solgel Sci Technol* **2017**, *82* (1), 233–238. <https://doi.org/10.1007/s10971-016-4300-0>.

- (118) Zhou, W.; Ran, R.; Shao, Z.; Jin, W.; Xu, N. Evaluation of A-Site Cation-Deficient  $(\text{Ba}_0.5\text{Sr}_0.5)_1\text{XCo}_0.8\text{Fe}_0.2\text{O}_3-\delta$  ( $\text{x} > 0$ ) Perovskite as a Solid-Oxide Fuel Cell Cathode. *J Power Sources* **2008**, *182* (1), 24–31. <https://doi.org/10.1016/j.jpowsour.2008.04.012>.
- (119) Ried, P.; Holtappels, P.; Wichser, A.; Ulrich, A.; Graule, T. Synthesis and Characterization of  $\text{La}_0.6\text{Sr}_0.4\text{Co}_0.2\text{Fe}_0.8\text{O}_3-\delta$  and  $\text{Ba}_0.5\text{Sr}_0.5\text{Co}_0.8\text{Fe}_0.2\text{O}_3-\delta$ . *J Electrochem Soc* **2008**, *155* (10), B1029. <https://doi.org/10.1149/1.2960873>.
- (120) Yakovlev, S.; Yoo, C. Y.; Fang, S.; Bouwmeester, H. J. M. Phase Transformation and Oxygen Equilibration Kinetics of Pure and Zr-Doped  $\text{Ba}_0.5\text{Sr}_0.5\text{Co}_0.8\text{Fe}_0.2\text{O}_3-\delta$  Perovskite Oxide Probed by Electrical Conductivity Relaxation. *Appl Phys Lett* **2010**, *96* (25). <https://doi.org/10.1063/1.3455908>.
- (121) Burriel, M.; Niedrig, C.; Meneskou, W.; Wagner, S. F.; Santiso, J.; Ivers-Tiffée, E. BSCF Epitaxial Thin Films: Electrical Transport and Oxygen Surface Exchange. *Solid State Ion* **2010**, *181* (13–14), 602–608. <https://doi.org/10.1016/j.ssi.2010.03.005>.
- (122) Girdauskaite, E.; Ullmann, H.; Vashook, V. v.; Guth, U.; Caraman, G. B.; Bucher, E.; Sitte, W. Oxygen Transport Properties of  $\text{Ba}_0.5\text{Sr}_0.5\text{Co}_0.8\text{Fe}_0.2\text{O}_3 - \text{x}$  and  $\text{Ca}_0.5\text{Sr}_0.5\text{Mn}_0.8\text{Fe}_0.2\text{O}_3 - \text{x}$  Obtained from Permeation and Conductivity Relaxation Experiments. *Solid State Ion* **2008**, *179* (11–12), 385–392. <https://doi.org/10.1016/j.ssi.2008.02.042>.
- (123) Ried, P.; Bucher, E.; Preis, W.; Sitte, W.; Holtappels, P. Characterisation of  $\text{La}_0.6\text{Sr}_0.4\text{Co}_0.2\text{Fe}_0.8\text{O}_3-\delta$  and  $\text{Ba}_0.5\text{Sr}_0.5\text{Co}_0.8\text{Fe}_0.2\text{O}_3-\delta$  as Cathode Materials for the Application in Intermediate Temperature Fuel Cells. *ECS Trans* **2007**, *7* (1), 1217–1224. <https://doi.org/10.1149/1.2729221>.
- (124) Li, M.; Zhao, M.; Li, F.; Zhou, W.; Peterson, V. K.; Xu, X.; Shao, Z.; Gentle, I.; Zhu, Z. A Niobium and Tantalum Co-Doped Perovskite Cathode for Solid Oxide Fuel Cells Operating below 500 °C. *Nat Commun* **2017**, *8*. <https://doi.org/10.1038/ncomms13990>.
- (125) Tarancón, A.; Burriel, M.; Santiso, J.; Skinner, S. J.; Kilner, J. A. Advances in Layered Oxide Cathodes for Intermediate Temperature Solid Oxide Fuel Cells. *J Mater Chem* **2010**, *20* (19), 3799–3813. <https://doi.org/10.1039/b922430k>.
- (126) Peña-Martínez, J.; Marrero-López, D.; Pérez-Coll, D.; Ruiz-Morales, J. C.; Núñez, P. Performance of  $\text{XScOF}$  ( $\text{X} = \text{Ba}, \text{La}$  and  $\text{Sm}$ ) and  $\text{LSCrX}'$  ( $\text{X}' = \text{Mn}, \text{Fe}$  and  $\text{Al}$ ) Perovskite-Structure Materials on LSGM Electrolyte for IT-SOFC. *Electrochim Acta* **2007**, *52* (9), 2950–2958. <https://doi.org/10.1016/j.electacta.2006.09.004>.
- (127) Zhang, K.; Ge, L.; Ran, R.; Shao, Z.; Liu, S. Synthesis, Characterization and Evaluation of Cation-Ordered  $\text{LnBaCo}_2\text{O}_5+\delta$  as Materials of Oxygen Permeation Membranes and Cathodes of SOFCs. *Acta Mater* **2008**, *56* (17), 4876–4889. <https://doi.org/10.1016/j.actamat.2008.06.004>.
- (128) Chen, C. H.; Chang, C. L.; Hwang, B. H. Electrochemical and Microstructure Characteristics of  $\text{Ba}_0.5\text{Sr}_0.5\text{Co}_0.8\text{Fe}_0.2\text{O}_3-\delta$  (BSCF) Cathodes Prepared by Citrate Precursor Method for SOFCs. *Mater Chem Phys* **2009**, *115* (1), 478–482. <https://doi.org/10.1016/j.matchemphys.2009.01.018>.
- (129) Lee, S.; Lim, Y.; Lee, E. A.; Hwang, H. J.; Moon, J. W.  $\text{Ba}_0.5\text{Sr}_0.5\text{Co}_0.8\text{Fe}_0.2\text{O}_3-\delta$  (BSCF) and  $\text{La}_0.6\text{Ba}_0.4\text{Co}_0.2\text{Fe}_0.8\text{O}_3-\delta$  (LBCF) Cathodes Prepared by Combined Citrate-EDTA Method for IT-SOFCs. *J Power Sources* **2006**, *157* (2), 848–854. <https://doi.org/10.1016/j.jpowsour.2005.12.028>.

- (130) Song, K. W.; Lee, K. T. Characterization of Ba<sub>0.5</sub>Sr<sub>0.5</sub>M<sub>1-X</sub>Fe<sub>X</sub>O<sub>3-δ</sub> (M = Co and Cu) Perovskite Oxide Cathode Materials for Intermediate Temperature Solid Oxide Fuel Cells. *Ceram Int* **2012**, *38* (6), 5123–5131. <https://doi.org/10.1016/j.ceramint.2012.03.015>.
- (131) Grimaud, A.; Mauvy, F.; Bassat, J. M.; Fourcade, S.; Rocheron, L.; Marrony, M.; Grenier, J. C. Hydration Properties and Rate Determining Steps of the Oxygen Reduction Reaction of Perovskite-Related Oxides as H<sub>+</sub>-SOFC Cathodes. *J Electrochem Soc* **2012**, *159* (6), B683–B694. <https://doi.org/10.1149/2.101205jes>.
- (132) Zhang, Y.; Yang, G.; Chen, G.; Ran, R.; Zhou, W.; Shao, Z. Evaluation of the CO<sub>2</sub> Poisoning Effect on a Highly Active Cathode SrSc<sub>0.175</sub>Nb<sub>0.025</sub>Co<sub>0.8</sub>O<sub>3-δ</sub> in the Oxygen Reduction Reaction. *ACS Appl Mater Interfaces* **2016**, *8* (5), 3003–3011. <https://doi.org/10.1021/acsami.5b09780>.
- (133) Zhou, W.; Shao, Z.; Ran, R.; Jin, W.; Xu, N. A Novel Efficient Oxide Electrode for Electrocatalytic Oxygen Reduction at 400–600°C. *Chemical Communications* **2008**, No. 44, 5791–5793. <https://doi.org/10.1039/b813327a>.
- (134) Ahmadrezaei, M.; Muchtar, A.; Muhamad, N.; Tan, C. Y.; Herianto Majlan, E. Electrochemical and Microstructural Characteristics of Nanoperovskite Oxides Ba<sub>0.2</sub>Sr<sub>0.8</sub>Co<sub>0.2</sub>Fe<sub>0.8</sub>O<sub>3-δ</sub> (BSCF) for Solid Oxide Fuel Cells. *Ceram Int* **2013**, *39* (1), 439–444. <https://doi.org/10.1016/j.ceramint.2012.06.045>.
- (135) Park, J.; Zou, J.; Yoon, H.; Kim, G.; Chung, J. S. Electrochemical Behavior of Ba<sub>0.5</sub>Sr<sub>0.5</sub>Co<sub>0.2</sub>-XZnxFe<sub>0.8</sub>O<sub>3-δ</sub> (x = 0–0.2) Perovskite Oxides for the Cathode of Solid Oxide Fuel Cells. *Int J Hydrogen Energy* **2011**, *36* (10), 6184–6193. <https://doi.org/10.1016/j.ijhydene.2011.01.142>.
- (136) Li, L.; Yang, H.; Gao, Z.; Zhang, Y.; Dong, F.; Yang, G.; Ni, M.; Lin, Z. Nickel-Substituted Ba<sub>0.5</sub>Sr<sub>0.5</sub>Co<sub>0.8</sub>Fe<sub>0.2</sub>O<sub>3-δ</sub>: A Highly Active Perovskite Oxygen Electrode for Reduced-Temperature Solid Oxide Fuel Cells. *J Mater Chem A Mater* **2019**, *7* (19), 12343–12349. <https://doi.org/10.1039/c9ta02548k>.
- (137) Cheng, Y.; Zhou, Q.; Li, W.; Wei, T.; Li, Z.; An, D.; Tong, X.; Ji, Z.; Han, X. Ba<sub>0.9</sub>Sr<sub>0.1</sub>Co<sub>0.9</sub>In<sub>0.1</sub>O<sub>3-δ</sub> Perovskite as Cathode Material for IT-SOFC. *J Alloys Compd* **2015**, *641*, 234–237. <https://doi.org/10.1016/j.jallcom.2015.03.257>.
- (138) Huang, C.; Chen, D.; Lin, Y.; Ran, R.; Shao, Z. Evaluation of Ba<sub>0.6</sub>Sr<sub>0.4</sub>Co<sub>0.9</sub>Nb<sub>0.1</sub>O<sub>3-δ</sub> Mixed Conductor as a Cathode for Intermediate-Temperature Oxygen-Ionic Solid-Oxide Fuel Cells. *J Power Sources* **2010**, *195* (16), 5176–5184. <https://doi.org/10.1016/j.jpowsour.2010.02.080>.
- (139) Zhao, L.; He, B.; Zhang, X.; Peng, R.; Meng, G.; Liu, X. Electrochemical Performance of Novel Cobalt-Free Oxide Ba<sub>0.5</sub>Sr<sub>0.5</sub>Fe<sub>0.8</sub>Cu<sub>0.2</sub>O<sub>3-δ</sub> for Solid Oxide Fuel Cell Cathode. *J Power Sources* **2010**, *195* (7), 1859–1861. <https://doi.org/10.1016/j.jpowsour.2009.09.078>.
- (140) Ling, Y.; Lu, X.; Niu, J.; Chen, H.; Ding, Y.; Ou, X.; Zhao, L. Antimony Doped Barium Strontium Ferrite Perovskites as Novel Cathodes for Intermediate-Temperature Solid Oxide Fuel Cells. *J Alloys Compd* **2016**, *666*, 23–29. <https://doi.org/10.1016/j.jallcom.2016.01.122>.
- (141) Yang, G.; Shen, J.; Chen, Y.; Tadé, M. O.; Shao, Z. Cobalt-Free Ba<sub>0.5</sub>Sr<sub>0.5</sub>Fe<sub>0.8</sub>Cu<sub>0.1</sub>Ti<sub>0.1</sub>O<sub>3-δ</sub> as a Bi-Functional Electrode Material for Solid Oxide Fuel

- Cells. *J Power Sources* **2015**, *298*, 184–192.  
<https://doi.org/10.1016/j.jpowsour.2015.08.064>.
- (142) Ling, Y.; Zhang, X.; Wang, Z.; Wang, S.; Zhao, L.; Liu, X.; Lin, B. Potentiality of Cobalt-Free Perovskite Ba<sub>0.5</sub>Sr<sub>0.5</sub>Fe<sub>0.9</sub>Mo<sub>0.1</sub>O<sub>3-δ</sub> as a Single-Phase Cathode for Intermediate-to-Low-Temperature Solid Oxide Fuel Cells. *Int J Hydrogen Energy* **2013**, *38* (33), 14323–14328. <https://doi.org/10.1016/j.ijhydene.2013.08.089>.
- (143) Wang, S. Evaluation of a Cobalt-Free Ba<sub>0.5</sub>Sr<sub>0.5</sub>Fe<sub>0.9</sub>Nb<sub>0.1</sub>O<sub>3-δ</sub> Cathode Material for Intermediate-Temperature Solid Oxide Fuel Cells. *Ionics (Kiel)* **2012**, *18* (8), 777–780. <https://doi.org/10.1007/s11581-012-0750-8>.
- (144) Huang, S.; Wang, G.; Sun, X.; Lei, C.; Li, T.; Wang, C. Cobalt-Free Perovskite Ba<sub>0.5</sub>Sr<sub>0.5</sub>Fe<sub>0.9</sub>Nb<sub>0.1</sub>O<sub>3-δ</sub> as a Cathode Material for Intermediate Temperature Solid Oxide Fuel Cells. *J Alloys Compd* **2012**, *543*, 26–30. <https://doi.org/10.1016/j.jallcom.2012.07.115>.
- (145) Wei, B.; Lü, Z.; Huang, X.; Liu, M.; Li, N.; Su, W. Synthesis, Electrical and Electrochemical Properties of Ba<sub>0.5</sub>Sr<sub>0.5</sub>Zn<sub>0.2</sub>Fe<sub>0.8</sub>O<sub>3-δ</sub> Perovskite Oxide for IT-SOFC Cathode. *J Power Sources* **2008**, *176* (1), 1–8. <https://doi.org/10.1016/j.jpowsour.2007.09.120>.
- (146) Hung, I. M.; Ciou, C. J.; Zeng, Y. J.; Wu, J. S.; Lee, Y. C.; Su, A.; Chan, S. H. Conductivity and Electrochemical Performance of (Ba<sub>0.5</sub>Sr<sub>0.5</sub>)<sub>0.8</sub>La<sub>0.2</sub>Fe<sub>1-X</sub>Mn<sub>X</sub>O<sub>3-δ</sub> Cathode Prepared by the Citrate-EDTA Complexing Method. *J Eur Ceram Soc* **2011**, *31* (16), 3095–3101. <https://doi.org/10.1016/j.jeurceramsoc.2011.04.029>.
- (147) Ni, C.; Irvine, J. T. S. Calcium Manganite as Oxygen Electrode Materials for Reversible Solid Oxide Fuel Cell. *Faraday Discuss* **2015**, *182*, 289–305. <https://doi.org/10.1039/C5FD00026B>.
- (148) Taskin, A. A.; Lavrov, A. N.; Ando, Y. Achieving Fast Oxygen Diffusion in Perovskites by Cation Ordering. *Appl Phys Lett* **2005**, *86* (9), 1–3. <https://doi.org/10.1063/1.1864244>.
- (149) Téllez, H.; Druce, J.; Kilner, J. A.; Ishihara, T. Relating Surface Chemistry and Oxygen Surface Exchange in LnBaCo<sub>2</sub>O<sub>5+δ</sub> Air Electrodes. *Faraday Discuss* **2015**, *182*, 145–157. <https://doi.org/10.1039/c5fd00027k>.
- (150) Ananyev, M. v.; Eremin, V. A.; Tsvetkov, D. S.; Porotnikova, N. M.; Farlenkov, A. S.; Zuev, A. Y.; Fetisov, A. v.; Kurumchin, E. K. Oxygen Isotope Exchange and Diffusion in LnBaCo<sub>2</sub>O<sub>6 - δ</sub> (Ln = Pr, Sm, Gd) with Double Perovskite Structure. *Solid State Ion* **2017**, *304*, 96–106. <https://doi.org/10.1016/j.ssi.2017.03.022>.
- (151) Tarancón, A.; Morata, A.; Dezanneau, G.; Skinner, S. J.; Kilner, J. A.; Estradé, S.; Hernández-Ramírez, F.; Peiró, F.; Morante, J. R. GdBaCo<sub>2</sub>O<sub>5+x</sub> Layered Perovskite as an Intermediate Temperature Solid Oxide Fuel Cell Cathode. *J Power Sources* **2007**, *174* (1), 255–263. <https://doi.org/10.1016/j.jpowsour.2007.08.077>.
- (152) Chang, A.; Skinner, S. J.; Kilner, J. A. Electrical Properties of GdBaCo<sub>2</sub>O<sub>5+x</sub> for IT-SOFC Applications. *Solid State Ion* **2006**, *177* (19-25 SPEC. ISS.), 2009–2011. <https://doi.org/10.1016/j.ssi.2006.05.047>.
- (153) Li, N.; Lü, Z.; Wei, B.; Huang, X.; Chen, K.; Zhang, Y.; Su, W. Characterization of GdBaCo<sub>2</sub>O<sub>5+δ</sub> Cathode for IT-SOFCs. *J Alloys Compd* **2008**, *454* (1–2), 274–279. <https://doi.org/10.1016/j.jallcom.2006.12.017>.
- (154) Chen, D.; Wang, F.; Shi, H.; Ran, R.; Shao, Z. Systematic Evaluation of Co-Free LnBaFe<sub>2</sub>O<sub>5+δ</sub> (Ln = Lanthanides or Y) Oxides towards the Application as Cathodes for Intermediate-

- Temperature Solid Oxide Fuel Cells. *Electrochim Acta* **2012**, *78*, 466–474. <https://doi.org/10.1016/j.electacta.2012.06.073>.
- (155) Ding, H.; Xue, X. Cobalt-Free Layered Perovskite  $GdBaFe_2O_5+x$  as a Novel Cathode for Intermediate Temperature Solid Oxide Fuel Cells. *J Power Sources* **2010**, *195* (15), 4718–4721. <https://doi.org/10.1016/j.jpowsour.2010.02.027>.
- (156) Muñoz-Gil, D.; Ávila-Brande, D.; Urones-Garrote, E.; García-Martín, S. Ordering Effects in the Crystal Structure and Electrochemical Properties of the  $Gd_0.5Ba_0.5Mn_0.5Fe_0.5O_3-\delta$  Perovskite. *Dalton Transactions* **2015**, *44* (23), 10867–10874. <https://doi.org/10.1039/c4dt03873h>.
- (157) Kim, J.; Jun, A.; Shin, J.; Kim, G. Effect of Fe Doping on Layered  $GdBa_0.5Sr_0.5Co_2O_5+\delta$  Perovskite Cathodes for Intermediate Temperature Solid Oxide Fuel Cells. *Journal of the American Ceramic Society* **2014**, *97* (2), 651–656. <https://doi.org/10.1111/jace.12692>.
- (158) Kim, J. H.; Cassidy, M.; Irvine, J. T. S.; Bae, J. Advanced Electrochemical Properties of  $LnBa_0.5Sr_0.5Co_2O_5+\delta$  ( $Ln=Pr, Sm$ , and  $Gd$ ) as Cathode Materials for IT-SOFC. *J Electrochem Soc* **2009**, *156* (6), B682. <https://doi.org/10.1149/1.3110989>.
- (159) Kim, J. H.; Baek, S. W.; Lee, C.; Park, K.; Bae, J. Performance Analysis of Cobalt-Based Cathode Materials for Solid Oxide Fuel Cell. *Solid State Ion* **2008**, *179* (27–32), 1490–1496. <https://doi.org/10.1016/j.ssi.2008.01.086>.
- (160) Rossignol, C.; Ralph, J. M.; Bae, J. M.; Vaughey, J. T.  $Ln_1-XSr_xCoO_3$  ( $Ln=Gd, Pr$ ) as a Cathode for Intermediate-Temperature Solid Oxide Fuel Cells. In *Solid State Ionics*; 2004; Vol. 175, pp 59–61. <https://doi.org/10.1016/j.ssi.2004.09.021>.
- (161) Ralph, J. M.; Rossignol, C.; Kumar, R. Cathode Materials for Reduced-Temperature SOFCs. *J Electrochem Soc* **2003**, *150* (11), A1518. <https://doi.org/10.1149/1.1617300>.
- (162) Bernuy-Lopez, C.; Rioja-Monllor, L.; Nakamura, T.; Ricote, S.; O’Hayre, R.; Amezawa, K.; Einarsrud, M. A.; Grande, T. Effect of Cation Ordering on the Performance and Chemical Stability of Layered Double Perovskite Cathodes. *Materials* **2018**, *11* (2). <https://doi.org/10.3390/ma11020196>.
- (163) Setevich, C. F.; Mogni, L. v.; Caneiro, A.; Prado, F. D. Optimum Cathode Configuration for IT-SOFC Using  $La_0.4Ba_0.6CoO_3-\delta$  and  $Ce_0.9Gd_0.1O_1.95$ . In *International Journal of Hydrogen Energy*; 2012; Vol. 37, pp 14895–14901. <https://doi.org/10.1016/j.ijhydene.2012.01.155>.
- (164) Setevich, C.; Prado, F.; de Florio, D. Z.; Caneiro, A. Stabilization of the Cubic Perovskite in the System  $La_{1-x}Ba_xCo_1-YFeyO_3-\delta$  ( $0.7 \leq x \leq 0.9$ ) and Its Electrochemical Performance as Cathode Materials for Intermediate-Temperature Solid Oxide Fuel Cells. *J Power Sources* **2014**, *247*, 264–272. <https://doi.org/10.1016/j.jpowsour.2013.08.091>.
- (165) Pang, S.; Jiang, X.; Li, X.; Su, Z.; Xu, H.; Xu, Q.; Chen, C. Characterization of Cation-Ordered Perovskite Oxide  $LaBaCo_2O_5+\delta$  as Cathode of Intermediate-Temperature Solid Oxide Fuel Cells. *Int J Hydrogen Energy* **2012**, *37* (8), 6836–6843. <https://doi.org/10.1016/j.ijhydene.2012.01.056>.
- (166) Bu, Y. F.; Ding, D.; Lai, S. Y.; Chen, D. C.; Xiong, X. H.; Wei, T.; Zhong, Q. Evaluation of  $La_0.4Ba_0.6Fe_0.8Zn_0.2O_3-\delta + Sm_0.2Ce_0.8O_1.9$  as a Potential Cobalt-Free Composite Cathode for Intermediate Temperature Solid Oxide Fuel Cells. *J Power Sources* **2015**, *275*, 808–814. <https://doi.org/10.1016/j.jpowsour.2014.11.085>.

- (167) Li, M.; Ren, Y.; Zhu, Z.; Zhu, S.; Chen, F.; Zhang, Y.; Xia, C. La<sub>0.4</sub>Bi<sub>0.4</sub>Sr<sub>0.2</sub>FeO<sub>3-δ</sub> as Cobalt-Free Cathode for Intermediate-Temperature Solid Oxide Fuel Cell. *Electrochim Acta* **2016**, *191*, 651–660. <https://doi.org/10.1016/j.electacta.2016.01.164>.
- (168) Yasuda, I.; Ogasawara, K.; Hishinuma, M. Oxygen Tracer Diffusion in Polycrystalline Calcium-Doped Lanthanum Chromites. *Journal of the American Ceramic Society* **1997**, *80*.
- (169) Jiang, S. P.; Liu, L.; Ong, K. P.; Wu, P.; Li, J.; Pu, J. Electrical Conductivity and Performance of Doped LaCrO<sub>3</sub> Perovskite Oxides for Solid Oxide Fuel Cells. *J Power Sources* **2008**, *176* (1), 82–89. <https://doi.org/10.1016/j.jpowsour.2007.10.053>.
- (170) van Hassel, B. A.; Kawada, T.; Sakai, N.; Yokokawa, H.; Doldya, M.; Bouwmeester, H. J. M. Oxygen Permeation Modelling of Perovskites. *Solid State Ion* **1993**, *66*, 295–305.
- (171) Yang, G.; Su, C.; Chen, Y.; Tadé, M. O.; Shao, Z. Nano La<sub>0.6</sub>Ca<sub>0.4</sub>Fe<sub>0.8</sub>Ni<sub>0.2</sub>O<sub>3-δ</sub> Decorated Porous Doped Ceria as a Novel Cobalt-Free Electrode for “Symmetrical” Solid Oxide Fuel Cells. *J. Mater. Chem. A* **2014**, *2* (45), 19526–19535. <https://doi.org/10.1039/C4TA03485F>.
- (172) Ortiz-Vitoriano, N.; Hauch, A.; Ruiz De Larramendi, I.; Bernuy-López, C.; Knibbe, R.; Rojo, T. Electrochemical Characterization of La<sub>0.6</sub>Ca<sub>0.4</sub>Fe<sub>0.8</sub>Ni<sub>0.2</sub>O<sub>3-δ</sub> Perovskite Cathode for IT-SOFC. *J Power Sources* **2013**, *239*, 196–200. <https://doi.org/10.1016/j.jpowsour.2013.03.121>.
- (173) Carter, S.; Selcuk, A.; Chater, R. J.; Kajda, J. Oxygen Transport in Selected Nonstoichiometric Perovskite-Structure Oxides. *Solid State Ion* **1992**, *56*, 597–605.
- (174) Berger, C.; Bucher, E.; Sitte, W. Mass and Charge Transport Properties of La<sub>0.9</sub>Ca<sub>0.1</sub>FeO<sub>3-δ</sub>. *Solid State Ion* **2017**, *299*, 46–54. <https://doi.org/10.1016/j.ssi.2016.09.015>.
- (175) Berger, C.; Bucher, E.; Windischbacher, A.; Boese, A. D.; Sitte, W. Strontium-Free Rare Earth Perovskite Ferrites with Fast Oxygen Exchange Kinetics: Experiment and Theory. *J Solid State Chem* **2018**, *259*, 57–66. <https://doi.org/10.1016/j.jssc.2017.12.019>.
- (176) Berger, C.; Bucher, E.; Gspan, C.; Sitte, W. Crystal Structure, Oxygen Nonstoichiometry, and Mass and Charge Transport Properties of the Sr-Free SOFC/SOEC Air Electrode Material La 0.75 Ca 0.25 FeO 3-δ. *J Solid State Chem* **2019**, *273*, 92–100. <https://doi.org/10.1016/j.jssc.2019.02.032>.
- (177) Kong, X.; Zhou, X.; Tian, Y.; Wu, X.; Zhang, J.; Zuo, W. Niobium Doped Lanthanum Calcium Ferrite Perovskite as a Novel Electrode Material for Symmetrical Solid Oxide Fuel Cells. *J Power Sources* **2016**, *326*, 35–42. <https://doi.org/10.1016/j.jpowsour.2016.06.111>.
- (178) Liu, Y. X.; Wang, S. F.; Hsu, Y. F.; Kai, H. W.; Jasinski, P. Characteristics of LaCo<sub>0.4</sub>Ni<sub>0.6-X</sub>Cu<sub>x</sub>O<sub>3-δ</sub> Ceramics as a Cathode Material for Intermediate-Temperature Solid Oxide Fuel Cells. *J Eur Ceram Soc* **2018**, *38* (4), 1654–1662. <https://doi.org/10.1016/j.jeurceramsoc.2017.11.019>.
- (179) Ishigaki, T.; Yamauchi, S.; Mizusaki, J.; Fueki, K.; Tamura, H. Tracer Diffusion Coefficient of Oxide Ions in LaCoO<sub>3</sub> Single Crystal. *J Solid State Chem* **1984**, *54* (1), 100–107. [https://doi.org/10.1016/0022-4596\(84\)90136-1](https://doi.org/10.1016/0022-4596(84)90136-1).
- (180) Armstrong, E. N.; Duncan, K. L.; Wachsman, E. D. Effect of A and B-Site Cations on Surface Exchange Coefficient for ABO<sub>3</sub> Perovskite Materials. *Physical Chemistry Chemical Physics* **2013**, *15* (7), 2298–2308. <https://doi.org/10.1039/c2cp42919e>.

- (181) Takeda, Y.; Kanno, R.; Noda, M.; Tomida, Y.; Yamamoto, O. Cathodic Polarization Phenomena of Perovskite Oxide Electrodes with Stabilized Zirconia. *J Electrochem Soc* **1987**, *134*.
- (182) Kammer, K.; Mikkelsen, L.; Bilde-Sørensen, J. B. Electrical and Electro-Chemical Characterisation of La<sub>0.99</sub>Fe<sub>1-x</sub>Ni<sub>x</sub>O<sub>3-δ</sub> Perovskites. *Journal of Solid State Electrochemistry* **2006**, *10* (11), 934–940. <https://doi.org/10.1007/s10008-006-0153-8>.
- (183) Ishigaki, T.; Yamauchi, S.; Mizusaki, J.; Fueki, K.; Naito, H.; Adachi, T. Diffusion of Oxide Ions in LaFeO<sub>3</sub> Single Crystal. *J Solid State Chem* **1984**, *55* (1), 50–53. [https://doi.org/10.1016/0022-4596\(84\)90246-9](https://doi.org/10.1016/0022-4596(84)90246-9).
- (184) Ioroi, T.; Hara, T.; Uchimoto, Y.; Ogumi, Z.; Takehara, Z. Preparation of Perovskite-Type La<sub>1-X</sub>Sr<sub>X</sub>MnO<sub>3</sub> Films by Vapor-Phase Processes and Their Electrochemical Properties. *J Electrochem Soc* **1998**, *145* (6).
- (185) Horita, T.; Tsunoda, T.; Yamaji, K.; Sakai, N.; Kato, T.; Yokokawa, H. Microstructure and Oxygen Diffusion at the LaMnO<sub>3</sub> Film/Yttria-Stabilized Zirconia Interface. *Solid State Ion* **2002**, *152*–153.
- (186) Bevilacqua, M.; Montini, T.; Tavagnacco, C.; Fonda, E.; Fornasiero, P.; Graziani, M. Preparation, Characterization, and Electrochemical Properties of Pure and Composite LaNi<sub>0.6</sub>Fe<sub>0.4</sub>O<sub>3</sub>-Based Cathodes for IT-SOFC. *Chemistry of Materials* **2007**, *19* (24), 5926–5936. <https://doi.org/10.1021/cm071622n>.
- (187) Hansen, K. K. The Effect of A-Site Deficiency on the Performance of La<sub>1-S</sub>Fe<sub>0.4</sub>Ni<sub>0.6</sub>O<sub>3-δ</sub> Cathodes. *Mater Res Bull* **2010**, *45* (2), 197–199. <https://doi.org/10.1016/j.materresbull.2009.09.024>.
- (188) Raj, E. S.; Kilner, J. A.; Irvine, J. T. S. Oxygen Diffusion and Surface Exchange Studies on (La<sub>0.75</sub>Sr<sub>0.25</sub>)<sub>0.95</sub>Cr<sub>0.5</sub>Mn<sub>0.5</sub>O<sub>3-δ</sub>. *Solid State Ion* **2006**, *177* (19–25 SPEC. ISS.), 1747–1752. <https://doi.org/10.1016/j.ssi.2006.04.011>.
- (189) Li, M.; Wang, Y.; Wang, Y.; Chen, F.; Xia, C. Bismuth Doped Lanthanum Ferrite Perovskites as Novel Cathodes for Intermediate-Temperature Solid Oxide Fuel Cells. *ACS Appl Mater Interfaces* **2014**, *6* (14), 11286–11294. <https://doi.org/10.1021/am5017045>.
- (190) van der Haar, L. M.; den Otter, M. W.; Morskate, M.; Bouwmeester, H. J. M.; Verweij, H. Chemical Diffusion and Oxygen Surface Transfer of La[Sub 1-x]Sr[Sub x]CoO[Sub 3-δ] Studied with Electrical Conductivity Relaxation. *J Electrochem Soc* **2002**, *149* (3), J41. <https://doi.org/10.1149/1.1446874>.
- (191) van Doorn, R.; Fullarton, I. C.; de Souza, R. A.; Kilner, J. A.; Bouwmeester, H. J.; Burggraaf, A. J. Surface Oxygen Exchange of La<sub>0.3</sub>Sr<sub>0.7</sub>CoO<sub>3-d</sub>. *Solid State Ion* **1997**, *96*, 7.
- (192) Egger, A.; Bucher, E.; Yang, M.; Sitte, W. Comparison of Oxygen Exchange Kinetics of the IT-SOFC Cathode Materials La<sub>0.5</sub>Sr<sub>0.5</sub>CoO<sub>3-δ</sub> and La<sub>0.6</sub>Sr<sub>0.4</sub>CoO<sub>3-δ</sub>. In *Solid State Ionics*; 2012; Vol. 225, pp 55–60. <https://doi.org/10.1016/j.ssi.2012.02.050>.
- (193) Wang, S.; Verma, A.; Yang, Y. L.; Jacobson, A. J.; Abeles, B. *The Effect of the Magnitude of the Oxygen Partial Pressure Change in Electrical Conductivity Relaxation Measurements: Oxygen Transport Kinetics in La Sr CoO*; 2001; Vol. 140. [www.elsevier.com/locate/terssi](http://www.elsevier.com/locate/terssi).
- (194) Yang, Y. L.; Chen, C. L.; Chen, S. Y.; Chu, C. W.; Jacobson, A. J. *Impedance Studies of Oxygen Exchange on Dense Thin Film Electrodes of La<sub>0.5</sub>Sr<sub>0.5</sub>CoO<sub>3</sub>*; 2000; Vol. 147.

- (195) Chen, X.; Wang, S.; Yang, Y. L.; Smith, L.; Wu, N. J.; Kim, B.-I.; Perry, S. S.; Jacobson, A. J.; Ignatiev, A. Electrical Conductivity Relaxation Studies of an Epitaxial La<sub>0.5</sub>Sr<sub>0.5</sub>CoO<sub>3-d</sub> Thin Film. *Solid State Ion* **2002**, *146*.
- (196) de Souza, R. A.; Kilner, J. A. Oxygen Transport in La<sub>1-X</sub>Sr<sub>x</sub>Mn<sub>y</sub>Co<sub>1-Y</sub>O<sub>3-d</sub> Perovskites Part II. Oxygen Surface Exchange. *Solid State Ion* **1999**, *126*, 153–161.
- (197) Bucher, E.; Gspan, C.; Sitte, W. Degradation and Regeneration of the SOFC Cathode Material La<sub>0.6</sub>Sr<sub>0.4</sub>CoO<sub>3 - δ</sub> in SO<sub>2</sub>-Containing Atmospheres. *Solid State Ion* **2015**, *272*, 112–120. <https://doi.org/10.1016/j.ssi.2015.01.009>.
- (198) Han, F.; Mücke, R.; van Gestel, T.; Leonide, A.; Menzler, N. H.; Buchkremer, H. P.; Stöver, D. Novel High-Performance Solid Oxide Fuel Cells with Bulk Ionic Conductance Dominated Thin-Film Electrolytes. *J Power Sources* **2012**, *218*, 157–162. <https://doi.org/10.1016/j.jpowsour.2012.06.087>.
- (199) Shiono, M.; Kobayashi, K.; Nguyen, T. L.; Hosoda, K.; Kato, T.; Ota, K.; Dokiya, M. Effect of CeO<sub>2</sub> Interlayer on ZrO<sub>2</sub> Electrolyte/La(Sr)CoO<sub>3</sub> Cathode for Low-Temperature SOFCs. *Solid State Ion* **2004**, *170* (1–2), 1–7. <https://doi.org/10.1016/j.ssi.2004.02.018>.
- (200) Horita, T.; Yamaji, K.; Sakai, N.; Yokokawa, H.; Weber, A.; Ivers-Tiffée, E. Electrode Reaction of La<sub>1-x</sub>Sr<sub>x</sub>CoO<sub>3-d</sub> Cathodes on La<sub>0.8</sub>Sr<sub>0.2</sub>Ga<sub>0.8</sub>Mg<sub>0.2</sub>O<sub>3-y</sub> Electrolyte in Solid Oxide Fuel Cells. *J Electrochem Soc* **2001**, *148* (5), A456. <https://doi.org/10.1149/1.1362540>.
- (201) Zhao, Z.; Liu, L.; Zhang, X.; Wu, W.; Tu, B.; Ou, D.; Cheng, M. A Comparison on Effects of CO<sub>2</sub> on La<sub>0.8</sub>Sr<sub>0.2</sub>MnO<sub>3+δ</sub> and La<sub>0.6</sub>Sr<sub>0.4</sub>CoO<sub>3-δ</sub> Cathodes. *J Power Sources* **2013**, *222*, 542–553. <https://doi.org/10.1016/j.jpowsour.2012.09.023>.
- (202) de Souza, R.; Kilner, J. A. Oxygen Transport in La<sub>1-X</sub>Sr<sub>x</sub>Mn<sub>1-Y</sub>CoyO<sub>3+-δ</sub> Perovskites Part I. Oxygen Tracer Diffusion. *Solid State Ion* **1998**, *106*, 175–187. [https://doi.org/10.1016/S0167-2738\(97\)00499-2](https://doi.org/10.1016/S0167-2738(97)00499-2).
- (203) Deganello, F.; Esposito, V.; Miyayama, M.; Traversa, E. Cathode Performance of Nanostructured La<sub>1-ASr</sub>Co<sub>1-B</sub>Fe<sub>2</sub>O<sub>3-x</sub> on a Ce<sub>0.8</sub>Sm<sub>0.2</sub>O<sub>2</sub> Electrolyte Prepared by Citrate-Nitrate Autocombustion. *J Electrochem Soc* **2007**, *154* (2), A89. <https://doi.org/10.1149/1.2400611>.
- (204) Lee, C.; Baek, S. W.; Bae, J. Cathodic Behavior of La<sub>0.8</sub>Sr<sub>0.2</sub>Co<sub>1-X</sub>Mn<sub>X</sub>O<sub>3 - δ</sub> Perovskite Oxide on YSZ Electrolyte for Intermediate Temperature-Operating Solid Oxide Fuel Cells. *Solid State Ion* **2008**, *179* (27–32), 1465–1469. <https://doi.org/10.1016/j.ssi.2008.01.009>.
- (205) Ishigaki, T.; Yamauchi, S.; Kishio, K.; Mizusaki, J.; Fueki, K. Diffusion of Oxide Ion Vacancies in Perovskite-Type Oxides. *J Solid State Chem* **1988**, *73* (1), 179–187. [https://doi.org/10.1016/0022-4596\(88\)90067-9](https://doi.org/10.1016/0022-4596(88)90067-9).
- (206) Katsuki, M.; Wang, S.; Dokiya, M.; Hashimoto, T. High Temperature Properties of La<sub>0.6</sub>Sr<sub>0.4</sub>Co<sub>0.8</sub>Fe<sub>0.2</sub>O<sub>3-d</sub> Oxygen Nonstoichiometry and Chemical Diffusion Constant. *Solid State Ion* **2003**, *156*.
- (207) Endler-Schuck, C.; Joos, J.; Niedrig, C.; Weber, A.; Ivers-Tiffée, E. The Chemical Oxygen Surface Exchange and Bulk Diffusion Coefficient Determined by Impedance Spectroscopy of Porous La<sub>0.58</sub>Sr<sub>0.4</sub>Co<sub>0.2</sub>Fe<sub>0.8</sub>O<sub>3 - δ</sub> (LSCF) Cathodes. *Solid State Ion* **2015**, *269*, 67–79. <https://doi.org/10.1016/j.ssi.2014.11.018>.

- (208) Bouwmeester, H. J. M.; den Otter, M. W.; Boukamp, B. A. Oxygen Transport in La<sub>0.6</sub>Sr<sub>0.4</sub>Co<sub>1</sub>-YFe YO<sub>3</sub>- $\delta$ . In *Journal of Solid State Electrochemistry*; Springer New York, 2004; Vol. 8, pp 599–605. <https://doi.org/10.1007/s10008-003-0488-3>.
- (209) Wang, S.; van der Heide, P. A. W.; Chavez, C.; Jacobson, A. J.; Adler, S. B. An Electrical Conductivity Relaxation Study of La<sub>0.6</sub>Sr<sub>0.4</sub>Fe<sub>0.8</sub>Co<sub>0.2</sub>O<sub>3</sub>- $\delta$ . *Solid State Ion* **2003**, *156* (1–2), 201–208. [https://doi.org/10.1016/s0167-2738\(02\)00178-9](https://doi.org/10.1016/s0167-2738(02)00178-9).
- (210) Leonide, A.; Rüger, B.; Weber, A.; Meulenberg, W. A.; Ivers-Tiffée, E. Impedance Study of Alternative (La,Sr)FeO[Sub 3- $\delta$ ] and (La,Sr)(Co,Fe)O[Sub 3- $\delta$ ] MIEC Cathode Compositions. *J Electrochem Soc* **2010**, *157* (2), B234. <https://doi.org/10.1149/1.3265473>.
- (211) Benson, S. J.; Waller, D.; Kilner, J. A. *Degradation of La 0.6 Sr 0.4 Fe 0.8 Co 0.2 O 3 in Carbon Dioxide and Water Atmospheres*; 1999; Vol. 146.
- (212) Sahibzada, M.; Benson, S. J.; Rudkin, R. A.; Kilner, J. A. Pd-Promoted La<sub>0.6</sub>Sr<sub>0.4</sub>Co<sub>0.2</sub>Fe<sub>0.8</sub>O<sub>3</sub> Cathodes. *Solid State Ion* **1998**, 285–290.
- (213) Esquirol, A.; Kilner, J.; Brandon, N. Oxygen Transport in La<sub>0.6</sub>Sr<sub>0.4</sub>Co<sub>0.2</sub>Fe<sub>0.8</sub>O<sub>3</sub>- $\delta$ /Ce<sub>0.8</sub>Ge<sub>0.2</sub>O<sub>2-x</sub> Composite Cathode for IT-SOFCs. In *Solid State Ionics*; 2004; Vol. 175, pp 63–67. <https://doi.org/10.1016/j.ssi.2004.09.013>.
- (214) Nadeem, M.; Wan, Y.; Xia, C. The Effect of Group IIIA Oxides on the Oxygen Reduction Reaction at Cathodes for Intermediate-Temperature Solid Oxide Fuel Cells. *Compos B Eng* **2020**, *189*. <https://doi.org/10.1016/j.compositesb.2020.107924>.
- (215) Nie, L.; Liu, M.; Zhang, Y.; Liu, M. La<sub>0.6</sub>Sr<sub>0.4</sub>Co<sub>0.2</sub>Fe<sub>0.8</sub>O<sub>3</sub>- $\delta$  Cathodes Infiltrated with Samarium-Doped Cerium Oxide for Solid Oxide Fuel Cells. *J Power Sources* **2010**, *195* (15), 4704–4708. <https://doi.org/10.1016/j.jpowsour.2010.02.049>.
- (216) Esquirol, A.; Brandon, N. P.; Kilner, J. A.; Mogensen, M. Electrochemical Characterization of La<sub>0.6</sub>Sr<sub>0.4</sub>Co<sub>0.2</sub>Fe<sub>0.8</sub>O<sub>3</sub> Cathodes for Intermediate-Temperature SOFCs. *J Electrochem Soc* **2004**, *151* (11), A1847. <https://doi.org/10.1149/1.1799391>.
- (217) Philippeau, B.; Mauvy, F.; Mazataud, C.; Fourcade, S.; Grenier, J. C. Comparative Study of Electrochemical Properties of Mixed Conducting Ln<sub>2</sub>NiO<sub>4</sub> +  $\delta$  (Ln = La, Pr and Nd) and La<sub>0.6</sub>Sr<sub>0.4</sub>Fe<sub>0.8</sub>Co<sub>0.2</sub>O. *Solid State Ion* **2013**, *249–250*, 17–25. <https://doi.org/10.1016/j.ssi.2013.06.009>.
- (218) Celikbilek, O.; Thieu, C. A.; Agnese, F.; Calì, E.; Lenser, C.; Menzler, N. H.; Son, J. W.; Skinner, S. J.; Djurado, E. Enhanced Catalytic Activity of Nanostructured, A-Site Deficient (La<sub>0.7</sub>Sr<sub>0.3</sub>)<sub>0.95</sub>(Co<sub>0.2</sub>Fe<sub>0.8</sub>)O<sub>3</sub>- $\delta$  for SOFC Cathodes. *J Mater Chem A Mater* **2019**, *7* (43), 25102–25111. <https://doi.org/10.1039/c9ta07697b>.
- (219) Zurlo, F.; di Bartolomeo, E.; D'Epifanio, A.; Felice, V.; Natali Sora, I.; Tortora, L.; Licoccia, S. La<sub>0.8</sub>Sr<sub>0.2</sub>Fe<sub>0.8</sub>Cu<sub>0.2</sub>O<sub>3</sub>- $\delta$  as “Cobalt-Free” Cathode for La<sub>0.8</sub>Sr<sub>0.2</sub>Ga<sub>0.8</sub>Mg<sub>0.2</sub>O<sub>3</sub>- $\delta$  Electrolyte. *J Power Sources* **2014**, *271*, 187–194. <https://doi.org/10.1016/j.jpowsour.2014.07.183>.
- (220) Hong, T.; Zhang, L.; Chen, F.; Xia, C. Oxygen Surface Exchange Properties of La<sub>0.6</sub>Sr<sub>0.4</sub>Co<sub>0.8</sub>Fe<sub>0.2</sub>O<sub>3</sub>- $\delta$  Coated with Sm<sub>x</sub>Ce<sub>1-x</sub>O<sub>2</sub>- $\delta$ . *J Power Sources* **2012**, *218*, 254–260. <https://doi.org/10.1016/j.jpowsour.2012.07.004>.
- (221) Porotnikova, N. M.; Antonova, E. P.; Khodimchuk, A. v.; Tropin, E. S.; Farlenkov, A. S.; Ananyev, M. v. Oxygen Diffusion and Surface Exchange Kinetics for the Mixed-Conducting

- Oxide La<sub>0.6</sub> Sr<sub>0.4</sub> Co<sub>0.8</sub> Fe<sub>0.2</sub> O<sub>3-δ</sub>. *Chimica Techno Acta* **2018**, 5 (4), 196–204.  
<https://doi.org/10.15826/chimtech.2018.5.04.04>.
- (222) Yang, Z.; Xu, N.; Han, M.; Chen, F. Performance Evaluation of La0.4Sr0.6Co0.2Fe0.7Nb0.1O3-δ as Both Anode and Cathode Material in Solid Oxide Fuel Cells. *Int J Hydrogen Energy* **2014**, 39 (14), 7402–7406.  
<https://doi.org/10.1016/j.ijhydene.2014.01.009>.
- (223) Yoo, S.; Kim, J.; Song, S. Y.; Lee, D. W.; Shin, J.; Ok, K. M.; Kim, G. Structural, Electrical and Electrochemical Characteristics of La<sub>0.1</sub>Sr<sub>0.9</sub>Co<sub>1-X</sub>NbxO<sub>3-δ</sub> as a Cathode Material for Intermediate Temperature Solid Oxide Fuel Cells. *RSC Adv* **2014**, 4 (36), 18710–18717.  
<https://doi.org/10.1039/c4ra02061h>.
- (224) Ftikos, C.; Carter, S.; Steele, B. C. H. Mixed Electronic/Ionic Conductivity of the Solid Solution La<sub>1-X</sub>SrxCo<sub>1-Y</sub>NiyO<sub>3-d</sub> (x: 0.4, 0-5, 0-6 and y: 0.2, 0.4, 0.6). *J Eur Ceram Soc* **1993**, 12, 79–86.
- (225) Hjalmarsson, P.; Søgaard, M.; Mogensen, M. Oxygen Transport Properties of Dense and Porous (La<sub>0.8</sub>Sr<sub>0.2</sub>)<sub>0.99</sub>Co<sub>0.8</sub>Ni<sub>0.2</sub>O<sub>3-δ</sub>. *Solid State Ion* **2009**, 180 (23–25), 1290–1297.  
<https://doi.org/10.1016/j.ssi.2009.07.012>.
- (226) Yoo, J.; Verma, A.; Wang, S.; Jacobson, A. J. Oxygen Transport Kinetics in SrFeO<sub>3-d</sub>, La<sub>0.5</sub>Sr<sub>0.5</sub>FeO<sub>3-d</sub>, and La<sub>0.2</sub>Sr<sub>0.8</sub>Cr<sub>0.2</sub>Fe<sub>0.8</sub>O<sub>3-d</sub> Measured by Electrical Conductivity Relaxation. *J Electrochem Soc* **2005**, 152 (3), A497. <https://doi.org/10.1149/1.1854617>.
- (227) Chen, M.; Paulson, S.; Thangadurai, V.; Birss, V. Sr-Rich Chromium Ferrites as Symmetrical Solid Oxide Fuel Cell Electrodes. *J Power Sources* **2013**, 236, 68–79.  
<https://doi.org/10.1016/j.jpowsour.2013.02.024>.
- (228) Ramos, T.; Atkinson, A. Oxygen Diffusion and Surface Exchange in La<sub>1-X</sub>SrXFe<sub>0.8</sub>Cr<sub>0.2</sub>O<sub>3-δ</sub> (X=0.2, 0.4 and 0.6). *Solid State Ion* **2004**, 170 (3–4), 275–286.  
<https://doi.org/10.1016/j.ssi.2004.03.001>.
- (229) Atkinson, A.; Chater, R. J.; Rudkin, R. Oxygen Diffusion and Surface Exchange in La<sub>0.8</sub>Sr<sub>0.2</sub>Fe<sub>0.8</sub>Cr<sub>0.2</sub>O<sub>3-d</sub> under Reducing Conditions. *Solid State Ion* **2001**, 139, 233–240.
- (230) Ruiz-Morales, J. C.; Canales-Vázquez, J.; Peña-Martínez, J.; López, D. M.; Núñez, P. On the Simultaneous Use of La<sub>0.75</sub>Sr<sub>0.25</sub>Cr<sub>0.5</sub>Mn<sub>0.5</sub>O<sub>3-δ</sub> as Both Anode and Cathode Material with Improved Microstructure in Solid Oxide Fuel Cells. *Electrochim Acta* **2006**, 52 (1), 278–284. <https://doi.org/10.1016/j.electacta.2006.05.006>.
- (231) Bastidas, D. M.; Tao, S.; Irvine, J. T. S. A Symmetrical Solid Oxide Fuel Cell Demonstrating Redox Stable Perovskite Electrodes. *J Mater Chem* **2006**, 16 (17), 1603–1605.  
<https://doi.org/10.1039/b600532b>.
- (232) Ding, X.; Cui, C.; Du, X.; Guo, L. Electrical Conductivity, Thermal Expansion and Electrochemical Properties of Fe-Doped La<sub>0.7</sub>Sr<sub>0.3</sub>CuO<sub>3-δ</sub> Cathodes for Solid Oxide Fuel Cells. *J Alloys Compd* **2009**, 475 (1–2), 418–421.  
<https://doi.org/10.1016/j.jallcom.2008.07.044>.
- (233) Zhou, Q.; Xu, L.; Guo, Y.; Jia, D.; Li, Y.; Wei, W. C. J. La<sub>0.6</sub>Sr<sub>0.4</sub>Fe<sub>0.8</sub>Cu<sub>0.2</sub>O<sub>3-δ</sub> Perovskite Oxide as Cathode for IT-SOFC. *Int J Hydrogen Energy* **2012**, 37 (16), 11963–11968. <https://doi.org/10.1016/j.ijhydene.2012.05.114>.

- (234) Ia O', G. J.; Shao-Horn, Y. Oxygen Surface Exchange Kinetics on Sr-Substituted Lanthanum Manganite and Ferrite Thin-Film Microelectrodes. *J Electrochem Soc* **2009**, *156* (7), B816. <https://doi.org/10.1149/1.3123214>.
- (235) Martínez-Amesti, A.; Larrañaga, A.; Rodríguez-Martínez, L. M.; Aguayo, A. T.; Pizarro, J. L.; Nó, M. L.; Laresgoiti, A.; Arriortua, M. I. Reactivity between La(Sr)FeO<sub>3</sub> Cathode, Doped CeO<sub>2</sub> Interlayer and Yttria-Stabilized Zirconia Electrolyte for Solid Oxide Fuel Cell Applications. *J Power Sources* **2008**, *185* (1), 401–410. <https://doi.org/10.1016/j.jpowsour.2008.06.049>.
- (236) Søgaard, M.; Vang Hendriksen, P.; Mogensen, M. Oxygen Nonstoichiometry and Transport Properties of Strontium Substituted Lanthanum Ferrite. *J Solid State Chem* **2007**, *180* (4), 1489–1503. <https://doi.org/10.1016/j.jssc.2007.02.012>.
- (237) Pang, S.; Wang, W.; Chen, T.; Shen, X.; Wang, Y.; Xu, K.; Xi, X. Systematic Evaluation of Cobalt-Free Ln<sub>0.5</sub>Sr<sub>0.5</sub>Fe<sub>0.8</sub>Cu<sub>0.2</sub>O<sub>3-δ</sub> (Ln = La, Pr, and Nd) as Cathode Materials for Intermediate-Temperature Solid Oxide Fuel Cells. *J Power Sources* **2016**, *326*, 176–181. <https://doi.org/10.1016/j.jpowsour.2016.06.134>.
- (238) Kim, S.; Wang, S.; Chen, X.; Yang, Y. L.; Wu, N.; Ignatiev, A.; Jacobson, A. J.; Abeles, B. Oxygen Surface Exchange in Mixed Ionic Electronic Conductors: Application to La<sub>0.5</sub>Sr<sub>0.5</sub>Fe<sub>0.8</sub>Ga<sub>0.2</sub>O<sub>3-δ</sub>. *J Electrochem Soc* **2000**, *147*.
- (239) Yadollahi Farsani, F.; Jafari, M.; Shahsavari, E.; Shakeripour, H.; Salamati, H. Investigation of Structural, Electrical and Electrochemical Properties of La<sub>0.6</sub>Sr<sub>0.4</sub>Fe<sub>0.8</sub>Mn<sub>0.2</sub>O<sub>3-δ</sub> as an Intermediate Temperature Solid Oxide Fuel Cell Cathode. *Int J Hydrogen Energy* **2020**, *45* (15), 8915–8929. <https://doi.org/10.1016/j.ijhydene.2020.01.030>.
- (240) Bian, L.; Duan, C.; Wang, L.; Zhu, L.; O’Hayre, R.; Chou, K. C. Electrochemical Performance and Stability of La<sub>0.5</sub>Sr<sub>0.5</sub>Fe<sub>0.9</sub>Nb<sub>0.1</sub>O<sub>3-Δ</sub> Symmetric Electrode for Solid Oxide Fuel Cells. *J Power Sources* **2018**, *399*, 398–405. <https://doi.org/10.1016/j.jpowsour.2018.07.119>.
- (241) Yasuda, I.; Hishinuma, M.; Dokiyab, M. Oxygen Tracer Diffusion Coefficient of (La, Sr)MnO<sub>3+d</sub>. *Solid State Ion* **1996**, *86*, 1197–1201.
- (242) Bak, T. A Manometric Method for the Determination of Chemical Diffusion in Non-Stoichiometric Oxides: Example of (La,Sr)MnO<sub>3</sub>. *Solid State Ion* **2000**, *135* (1–4), 557–561. [https://doi.org/10.1016/S0167-2738\(00\)00636-6](https://doi.org/10.1016/S0167-2738(00)00636-6).
- (243) Murray, E. P.; Barnett, S. A. (La, Sr)MnO<sub>3</sub>-(Ce, Gd)O<sub>2-x</sub> Composite Cathodes for Solid Oxide Fuel Cells. *Solid State Ion* **2001**, *143*, 265–273.
- (244) Luo, X.; Yang, Y.; Yang, Y.; Tian, D.; Lu, X.; Chen, Y.; Huang, Q.; Lin, B. Reduced-Temperature Redox-Stable LSM as a Novel Symmetrical Electrode Material for SOFCs. *Electrochim Acta* **2018**, *260*, 121–128. <https://doi.org/10.1016/j.electacta.2017.11.071>.
- (245) Murray, E. P.; Tsai, T.; Barnett, S. A. *Oxygen Transfer Processes in (La,Sr)MnO / YO-Stabilized ZrO<sub>3</sub> 2 3 2 Cathodes: An Impedance Spectroscopy Study*; 1998; Vol. 110.
- (246) Kim, J.-D.; Kim, G.-D.; Moon, J.-W.; Park, Y.-I.; Lee, W.-H.; Kobayashi, K.; Nagai, M.; Kim, C.-E. Characterization of LSM-YSZ Composite Electrode by Ac Impedance Spectroscopy. *Solid State Ion* **2001**, *143*.
- (247) Petitjean, M.; Caboche, G.; Siebert, E.; Dessemond, L.; Dufour, L. C. (La<sub>0.8</sub>Sr<sub>0.2</sub>)(Mn<sub>1-Y</sub>Fey) O<sub>3±δ</sub> Oxides for ITSOFC Cathode Materials? Electrical and Ionic Transport

- Properties. *J Eur Ceram Soc* **2005**, *25* (12 SPEC. ISS.), 2651–2654.  
<https://doi.org/10.1016/j.jeurceramsoc.2005.03.117>.
- (248) Barbucci, A.; Paola Carpanese, M.; Viviani, M.; Vatistas, N.; Nicolella, C. Morphology and Electrochemical Activity of SOFC Composite Cathodes: I. Experimental Analysis. In *Journal of Applied Electrochemistry*; 2009; Vol. 39, pp 513–521. <https://doi.org/10.1007/s10800-008-9708-y>.
- (249) Gu, H.; Zheng, Y.; Ran, R.; Shao, Z.; Jin, W.; Xu, N.; Ahn, J. Synthesis and Assessment of La<sub>0.8</sub>Sr<sub>0.2</sub>Sc YMn<sub>1</sub>-YO<sub>3</sub>- $\delta$  as Cathodes for Solid-Oxide Fuel Cells on Scandium-Stabilized Zirconia Electrolyte. *J Power Sources* **2008**, *183* (2), 471–478.  
<https://doi.org/10.1016/j.jpowsour.2008.05.053>.
- (250) Yan, L.; Balasubramaniam, K. R.; Wang, S.; Du, H.; Salvador, P. Electrical Conductivity Relaxation Study of Solid Oxide Fuel Cell Cathodes Using Epitaxial (001)-Oriented Strontium-Doped Lanthanum Manganite Thin Films. In *Materials Research Society Symposium Proceedings*; Materials Research Society, 2010; Vol. 1255, pp 11–16.  
<https://doi.org/10.1557/proc-1255-m02-02>.
- (251) Yan, L.; Salvador, P. A. Substrate and Thickness Effects on the Oxygen Surface Exchange of La 0.7Sr 0.3MnO 3 Thin Films. *ACS Appl Mater Interfaces* **2012**, *4* (5), 2541–2550.  
<https://doi.org/10.1021/am300194n>.
- (252) Yan, L.; Balasubramaniam, K. R.; Wang, S.; Du, H.; Salvador, P. A. Effects of Crystallographic Orientation on the Oxygen Exchange Rate of La<sub>0.7</sub>Sr<sub>0.3</sub>MnO<sub>3</sub> Thin Films. *Solid State Ion* **2011**, *194* (1), 9–16. <https://doi.org/10.1016/j.ssi.2011.05.004>.
- (253) Gan, L.; Zhong, Q.; Zhao, X.; Song, Y.; Bu, Y. Structural and Electrochemical Properties of B-Site Mg-Doped La<sub>0.7</sub>Sr<sub>0.3</sub>MnO<sub>3</sub>- $\delta$  Perovskite Cathodes for Intermediate Temperature Solid Oxide Fuel Cells. *J Alloys Compd* **2016**, *655*, 99–105.  
<https://doi.org/10.1016/j.jallcom.2015.09.136>.
- (254) Noh, T.; Ryu, J.; Kim, J.; Kim, Y. N.; Lee, H. Structural and Impedance Analysis of Copper Doped LSM Cathode for IT-SOFCs. *J Alloys Compd* **2013**, *557*, 196–201.  
<https://doi.org/10.1016/j.jallcom.2013.01.002>.
- (255) Zheng, Y.; Zhang, C.; Ran, R.; Cai, R.; Shao, Z.; Farrusseng, D. A New Symmetric Solid-Oxide Fuel Cell with La<sub>0.8</sub>Sr<sub>0.2</sub>Sc<sub>0.2</sub>Mn<sub>0.8</sub>O<sub>3</sub>- $\delta$  Perovskite Oxide as Both the Anode and Cathode. *Acta Mater* **2009**, *57* (4), 1165–1175.  
<https://doi.org/10.1016/j.actamat.2008.10.047>.
- (256) Zhu, G.; Fang, X.; Xia, C.; Liu, X. Preparation and Electrical Properties of La<sub>0.4</sub>Sr<sub>0.6</sub>Ni<sub>0.2</sub>Fe<sub>0.8</sub>O<sub>3</sub> Using a Glycine Nitrate Process. *Ceram Int* **2005**, *31* (1), 115–119.  
<https://doi.org/10.1016/j.ceramint.2004.03.042>.
- (257) Cao, Z.; Zhang, Y.; Miao, J.; Wang, Z.; Lü, Z.; Sui, Y.; Huang, X.; Jiang, W. Titanium-Substituted Lanthanum Strontium Ferrite as a Novel Electrode Material for Symmetrical Solid Oxide Fuel Cell. *Int J Hydrogen Energy* **2015**, *40* (46), 16572–16577.  
<https://doi.org/10.1016/j.ijhydene.2015.10.010>.
- (258) Yoo, S.; Jun, A.; Ju, Y. W.; Odkhuu, D.; Hyodo, J.; Jeong, H. Y.; Park, N.; Shin, J.; Ishihara, T.; Kim, G. Development of Double-Perovskite Compounds as Cathode Materials for Low-Temperature Solid Oxide Fuel Cells. *Angewandte Chemie - International Edition* **2014**, *53* (48), 13064–13067. <https://doi.org/10.1002/anie.201407006>.

- (259) Kim, C.; Kim, J.; Shin, J.; Kim, G. Effects of Composite Cathode on Electrochemical and Redox Properties for Intermediate-Temperature Solid Oxide Fuel Cells. *Int J Hydrogen Energy* **2014**, *39* (35), 20812–20818. <https://doi.org/10.1016/j.ijhydene.2014.07.007>.
- (260) Kong, X.; Feng, S.; Sun, H.; Yi, Z.; Liu, G. Effect of Mn on the Characterization of Layered Perovskite  $\text{NdBaCo}_2\text{-XMn}_x\text{O}_5+\delta$  ( $X=0.5, 1, 1.5, 2$ ) as Cathode Materials for IT-SOFCs. *Int J Electrochem Sci* **2018**, *13* (8), 7939–7948. <https://doi.org/10.20964/2018.08.68>.
- (261) Yoo, S.; Choi, S.; Kim, J.; Shin, J.; Kim, G. Investigation of Layered Perovskite Type  $\text{NdBa}_1\text{-XSr XCo}_2\text{O}_5+\delta$  ( $x = 0, 0.25, 0.5, 0.75$ , and  $1.0$ ) Cathodes for Intermediate-Temperature Solid Oxide Fuel Cells. *Electrochim Acta* **2013**, *100*, 44–50. <https://doi.org/10.1016/j.electacta.2013.03.041>.
- (262) Donazzi, A.; Pelosato, R.; Cordaro, G.; Stucchi, D.; Cristiani, C.; Dotelli, G.; Sora, I. N. Evaluation of Ba Deficient  $\text{NdBaCo}_2\text{O}_5+\delta$  Oxide as Cathode Material for IT-SOFC. *Electrochim Acta* **2015**, *182*, 573–587. <https://doi.org/10.1016/j.electacta.2015.09.117>.
- (263) Kim, J. H.; Irvine, J. T. S. Characterization of Layered Perovskite Oxides  $\text{NdBa}_1\text{-XSr XCo}_2\text{O}_5+\delta$  ( $x = 0$  and  $0.5$ ) as Cathode Materials for IT-SOFC. *Int J Hydrogen Energy* **2012**, *37* (7), 5920–5929. <https://doi.org/10.1016/j.ijhydene.2011.12.150>.
- (264) Kong, X.; Liu, G.; Yi, Z.; Ding, X.  $\text{NdBaCu}_2\text{O}_5+\delta$  and  $\text{NdBa}_0.5\text{Sr}_0.5\text{Cu}_2\text{O}_5+\delta$  Layered Perovskite Oxides as Cathode Materials for IT-SOFCs. *Int J Hydrogen Energy* **2015**, *40* (46), 16477–16483. <https://doi.org/10.1016/j.ijhydene.2015.09.006>.
- (265) Kim, J.; Choi, S.; Park, S.; Kim, C.; Shin, J.; Kim, G. Effect of Mn on the Electrochemical Properties of a Layered Perovskite  $\text{NdBa}_0.5\text{Sr}_0.5\text{Co}_2 - \text{XMn}_x\text{O}_5 + \delta$  ( $x = 0, 0.25$ , and  $0.5$ ) for Intermediate-Temperature Solid Oxide Fuel Cells. *Electrochim Acta* **2013**, *112*, 712–718. <https://doi.org/10.1016/j.electacta.2013.09.014>.
- (266) Kim, J.; Seo, W. Y.; Shin, J.; Liu, M.; Kim, G. Composite Cathodes Composed of  $\text{NdBa}_0.5\text{Sr}_0.5\text{Co}_2\text{O}_5+\delta$  and  $\text{Ce}_0.9\text{Gd}_0.1\text{O}_1.95$  for Intermediate-Temperature Solid Oxide Fuel Cells. *J Mater Chem A Mater* **2013**, *1* (3), 515–519. <https://doi.org/10.1039/c2ta00025c>.
- (267) Subardi, A.; Liao, K. Y.; Fu, Y. P. Oxygen Transport, Thermal and Electrochemical Properties of  $\text{NdBa}_0.5\text{Sr}_0.5\text{Co}_2\text{O}_5+\delta$  Cathode for SOFCs. *J Eur Ceram Soc* **2019**, *39* (1), 30–40. <https://doi.org/10.1016/j.jeurceramsoc.2018.01.022>.
- (268) Zhu, X.; Qian, C.; Sun, F.; Zhang, L.; Liu, X.; Li, D. Perovskite-Type  $\text{Nd}_0.5\text{Sr}_0.5\text{Co}_0.5\text{Fe}_0.5\text{O}_3-\delta$  as a Novel Cathode Material for Intermediate-Temperate Solid Oxide Fuel Cell. *J Alloys Compd* **2019**, *802*, 415–421. <https://doi.org/10.1016/j.jallcom.2019.06.231>.
- (269) Lim, C.; Sengodan, S.; Jeong, D.; Shin, J.; Kim, G. Investigation of the Fe Doping Effect on the B-Site of the Layered Perovskite  $\text{PrBa}_0.8\text{Ca}_0.2\text{Co}_2\text{O}_{5+\Delta}$  for a Promising Cathode Material of the Intermediate-Temperature Solid Oxide Fuel Cells. *Int J Hydrogen Energy* **2019**, *44* (2), 1088–1095. <https://doi.org/10.1016/j.ijhydene.2018.10.182>.
- (270) Grimaud, A.; Bassat, J. M.; Mauvy, F.; Pollet, M.; Wattiaux, A.; Marrony, M.; Grenier, J. C. Oxygen Reduction Reaction of  $\text{PrBaCo}_2\text{-XFexO}_5+\delta$  Compounds as H<sup>+</sup>-SOFC Cathodes: Correlation with Physical Properties. *J Mater Chem A Mater* **2014**, *2* (10), 3594–3604. <https://doi.org/10.1039/c3ta13956e>.

- (271) Kim, G.; Wang, S.; Jacobson, A. J.; Yuan, Z.; Donner, W.; Chen, C. L.; Reimus, L.; Brodersen, P.; Mims, C. A. Oxygen Exchange Kinetics of Epitaxial PrBaCo<sub>2O</sub><sub>5+δ</sub> Thin Films. *Appl Phys Lett* **2006**, *88* (2), 1–3. <https://doi.org/10.1063/1.2163257>.
- (272) Liu, J.; Collins, G.; Liu, M.; Chen, C.; He, J.; Jiang, J.; Meletis, E. I. Ultrafast Oxygen Exchange Kinetics on Highly Epitaxial PrBaCo<sub>2O</sub><sub>5+δ</sub> Thin Films. *Appl Phys Lett* **2012**, *100* (19), 193903. <https://doi.org/10.1063/1.4712123>.
- (273) Kim, G.; Wang, S.; Jacobson, A. J.; Reimus, L.; Brodersen, P.; Mims, C. A. Rapid Oxygen Ion Diffusion and Surface Exchange Kinetics in PrBaCo<sub>2O</sub><sub>5+x</sub> with a Perovskite Related Structure and Ordered a Cations. *J Mater Chem* **2007**, *17* (24), 2500–2505. <https://doi.org/10.1039/b618345j>.
- (274) Cox-Galhotra, R. A.; McIntosh, S. Electrical Conductivity Relaxation of Polycrystalline PrBaCo<sub>2O</sub><sub>5 + δ</sub> Thin Films. *Solid State Ion* **2012**, *228*, 14–18. <https://doi.org/10.1016/j.ssi.2012.09.001>.
- (275) Frison, R.; Portier, S.; Martin, M.; Conder, K. Study of Oxygen Tracer Diffusion in PrBaCo<sub>2O</sub><sub>5.74</sub> by SIMS. In *Nuclear Instruments and Methods in Physics Research, Section B: Beam Interactions with Materials and Atoms*; 2012; Vol. 273, pp 142–145. <https://doi.org/10.1016/j.nimb.2011.07.060>.
- (276) Chen, D.; Ran, R.; Zhang, K.; Wang, J.; Shao, Z. Intermediate-Temperature Electrochemical Performance of a Polycrystalline PrBaCo<sub>2O</sub><sub>5+δ</sub> Cathode on Samarium-Doped Ceria Electrolyte. *J Power Sources* **2009**, *188* (1), 96–105. <https://doi.org/10.1016/j.jpowsour.2008.11.045>.
- (277) Zhu, C.; Liu, X.; Yi, C.; Yan, D.; Su, W. Electrochemical Performance of PrBaCo<sub>2O</sub><sub>5+δ</sub> Layered Perovskite as an Intermediate-Temperature Solid Oxide Fuel Cell Cathode. *J Power Sources* **2008**, *185* (1), 193–196. <https://doi.org/10.1016/j.jpowsour.2008.06.075>.
- (278) Jeong, D.; Kim, J.; Kwon, O.; Lim, C.; Sengodan, S.; Shin, J.; Kim, G. Scandium Doping Effect on a Layered Perovskite Cathode for Low-Temperature Solid Oxide Fuel Cells (LT-SOFCs). *Applied Sciences* **2018**, *8* (11). <https://doi.org/10.3390/app812217>.
- (279) Zhang, L.; Li, S.; Xia, T.; Sun, L.; Huo, L.; Zhao, H. Co-Deficient PrBaCo<sub>2-x</sub>O<sub>6-Δ</sub> Perovskites as Cathode Materials for Intermediate-Temperature Solid Oxide Fuel Cells: Enhanced Electrochemical Performance and Oxygen Reduction Kinetics. *Int J Hydrogen Energy* **2018**, *43* (7), 3761–3775. <https://doi.org/10.1016/j.ijhydene.2018.01.018>.
- (280) Park, S.; Choi, S.; Kim, J.; Shin, J.; Kim, G. Strontium Doping Effect on High-Performance PrBa<sub>1-X</sub>Sc<sub>X</sub>Co<sub>2O</sub><sub>5+δ</sub> as a Cathode Material for IT-SOFCs. *ECS Electrochemistry Letters* **2012**, *1* (5). <https://doi.org/10.1149/2.007205eel>.
- (281) Dong, G.; Yang, C.; He, F.; Jiang, Y.; Ren, C.; Gan, Y.; Lee, M.; Xue, X. Tin Doped PrBaFe<sub>2O</sub><sub>5+δ</sub> Anode Material for Solid Oxide Fuel Cells. *RSC Adv* **2017**, *7* (37), 22649–22661. <https://doi.org/10.1039/c7ra03143b>.
- (282) Chen, T.; Pang, S.; Shen, X.; Jiang, X.; Wang, W. Evaluation of Ba-Deficient PrBa<sub>1-X</sub>Fe<sub>2O</sub><sub>5+δ</sub> Oxides as Cathode Materials for Intermediateerature Solid Oxide Fuel Cells. *RSC Adv* **2016**, *6* (17), 13829–13836. <https://doi.org/10.1039/c5ra19555a>.
- (283) He, W.; Wu, X.; Dong, F.; Ni, M. A Novel Layered Perovskite Electrode for Symmetrical Solid Oxide Fuel Cells: PrBa(Fe0.8Sc0.2)2O<sub>5+Δ</sub>. *J Power Sources* **2017**, *363*, 16–19. <https://doi.org/10.1016/j.jpowsour.2017.07.059>.

- (284) Zhao, L.; Chen, K.; Liu, Y.; He, B. A Novel Layered Perovskite as Symmetric Electrode for Direct Hydrocarbon Solid Oxide Fuel Cells. *J Power Sources* **2017**, *342*, 313–319. <https://doi.org/10.1016/j.jpowsour.2016.12.066>.
- (285) Choi, S.; Park, S.; Shin, J.; Kim, G. The Effect of Calcium Doping on the Improvement of Performance and Durability in a Layered Perovskite Cathode for Intermediate-Temperature Solid Oxide Fuel Cells. *J Mater Chem A Mater* **2015**, *3* (11), 6088–6095. <https://doi.org/10.1039/c4ta05684a>.
- (286) Park, S.; Choi, S.; Shin, J.; Kim, G. Tradeoff Optimization of Electrochemical Performance and Thermal Expansion for Co-Based Cathode Material for Intermediate-Temperature Solid Oxide Fuel Cells. *Electrochim Acta* **2014**, *125*, 683–690. <https://doi.org/10.1016/j.electacta.2014.01.112>.
- (287) Choi, S.; Yoo, S.; Kim, J.; Park, S.; Jun, A.; Sengodan, S.; Kim, J.; Shin, J.; Jeong, H. Y.; Choi, Y.; Kim, G.; Liu, M. Highly Efficient and Robust Cathode Materials for Low-Temperature Solid Oxide Fuel Cells:  $\text{PrBa}_{0.5}\text{Sr}_{0.5}\text{Co}_{2-x}\text{Fe}_{\text{XO}}{5+\delta}$ . *Sci Rep* **2013**, *3*. <https://doi.org/10.1038/srep02426>.
- (288) Lü, S.; Long, G.; Meng, X.; Ji, Y.; Lü, B.; Zhao, H.  $\text{PrBa}_{0.5}\text{Sr}_{0.5}\text{Co}_{2\text{O}5+\delta}$  as Cathode Material Based on LSGM and GDC Electrolyte for Intermediate-Temperature Solid Oxide Fuel Cells. *Int J Hydrogen Energy* **2012**, *37* (7), 5914–5919. <https://doi.org/10.1016/j.ijhydene.2011.12.134>.
- (289) Fu, D.; Jin, F.; He, T. A-Site Calcium-Doped  $\text{Pr}_{1-\text{Cax}}\text{BaCo}_{2\text{O}5+\delta}$  Double Perovskites as Cathodes for Intermediate-Temperature Solid Oxide Fuel Cells. *J Power Sources* **2016**, *313*, 134–141. <https://doi.org/10.1016/j.jpowsour.2016.02.071>.
- (290) Huang, S.; Lu, Q.; Feng, S.; Li, G.; Wang, C.  $\text{PrNi}_{0.6}\text{Co}_{0.4}\text{O}_3\text{-Ce}_{0.8}\text{Sm}_{0.2}\text{O}_{1.9}$  Composite Cathodes for Intermediate Temperature Solid Oxide Fuel Cells. *J Power Sources* **2012**, *199*, 150–154. <https://doi.org/10.1016/j.jpowsour.2011.10.025>.
- (291) Park, K.; Lee, C.; Bae, J.; Yoo, Y. Structural and Electrochemical Properties of  $\text{Pr}_{0.3}\text{Sr}_{0.7}\text{Co}_{0.3}\text{Fe}_{0.7}\text{O}_3-\delta$  Cathode for IT-SOFC. *Int J Hydrogen Energy* **2009**, *34* (16), 6852–6860. <https://doi.org/10.1016/j.ijhydene.2009.05.138>.
- (292) Zhang, P.; Guan, G.; Khaerudini, D. S.; Hao, X.; Xue, C.; Han, M.; Kasai, Y.; Abudula, A. B-Site Mo-Doped Perovskite  $\text{Pr}_{0.4}\text{Sr}_{0.6}(\text{Co}_{0.2}\text{Fe}_{0.8})_1\text{-XMoxO}_3-\sigma$  ( $x = 0, 0.05, 0.1$  and  $0.2$ ) as Electrode for Symmetrical Solid Oxide Fuel Cell. *J Power Sources* **2015**, *276*, 347–356. <https://doi.org/10.1016/j.jpowsour.2014.11.141>.
- (293) Yin, Y. M.; Xiong, M. W.; Yang, N. T.; Tong, Z.; Guo, Y. Q.; Ma, Z. F.; Sun, E.; Yamanis, J.; Jing, B. Y. Investigation on Thermal, Electrical, and Electrochemical Properties of Scandium-Doped  $\text{Pr}_{0.6}\text{Sr}_{0.4}(\text{Co}_{0.2}\text{Fe}_{0.8})(1-x)\text{ScxO}_3-\delta$  as Cathode for IT-SOFC. *Int J Hydrogen Energy* **2011**, *36* (6), 3989–3996. <https://doi.org/10.1016/j.ijhydene.2010.12.113>.
- (294) Zhang, P.; Guan, G.; Khaerudini, D. S.; Hao, X.; Han, M.; Kasai, Y.; Sasagawa, K.; Abudula, A. Properties of A-Site Nonstoichiometry  $(\text{Pr}_{0.4})\text{X}\text{Sr}_{0.6}\text{Co}_{0.2}\text{Fe}_{0.7}\text{Nb}_{0.1}\text{O}_{3-\sigma}$  ( $0.9 \leq x \leq 1.1$ ) as Symmetrical Electrode Material for Solid Oxide Fuel Cells. *J Power Sources* **2014**, *248*, 163–171. <https://doi.org/10.1016/j.jpowsour.2013.09.077>.
- (295) Piao, J.; Sun, K.; Zhang, N.; Chen, X.; Xu, S.; Zhou, D. Preparation and Characterization of  $\text{Pr}_{1-X}\text{Sr}_x\text{FeO}_3$  Cathode Material for Intermediate Temperature Solid Oxide Fuel Cells. *J Power Sources* **2007**, *172* (2), 633–640. <https://doi.org/10.1016/j.jpowsour.2007.05.023>.

- (296) Lu, J.; Yin, Y. M.; Ma, Z. F. Preparation and Characterization of New Cobalt-Free Cathode Pr<sub>0.5</sub>Sr<sub>0.5</sub>Fe<sub>0.8</sub>Cu<sub>0.2</sub>O<sub>3-δ</sub> for IT-SOFC. *Int J Hydrogen Energy* **2013**, *38* (25), 10527–10533. <https://doi.org/10.1016/j.ijhydene.2013.05.164>.
- (297) Hashimoto, S. I.; Kammer, K.; Larsen, P. H.; Poulsen, F. W.; Mogensen, M. A Study of Pr<sub>0.7</sub>Sr<sub>0.3</sub>Fe<sub>1-X</sub>Ni<sub>X</sub>O<sub>3-δ</sub> as a Cathode Material for SOFCs with Intermediate Operating Temperature. *Solid State Ion* **2005**, *176* (11–12), 1013–1020. <https://doi.org/10.1016/j.ssi.2004.09.010>.
- (298) Ding, X.; Gao, Z.; Ding, D.; Zhao, X.; Hou, H.; Zhang, S.; Yuan, G. Cation Deficiency Enabled Fast Oxygen Reduction Reaction for a Novel SOFC Cathode with Promoted CO<sub>2</sub> Tolerance. *Appl Catal B* **2019**, *243*, 546–555. <https://doi.org/10.1016/j.apcatb.2018.10.075>.
- (299) Zhu, Y.; Zhou, W.; Ran, R.; Chen, Y.; Shao, Z.; Liu, M. Promotion of Oxygen Reduction by Exsolved Silver Nanoparticles on a Perovskite Scaffold for Low-Temperature Solid Oxide Fuel Cells. *Nano Lett* **2016**, *16* (1), 512–518. <https://doi.org/10.1021/acs.nanolett.5b04160>.
- (300) Zhou, Q.; He, T.; Ji, Y. SmBaCo<sub>2</sub>O<sub>5+x</sub> Double-Perovskite Structure Cathode Material for Intermediate-Temperature Solid-Oxide Fuel Cells. *J Power Sources* **2008**, *185* (2), 754–758. <https://doi.org/10.1016/j.jpowsour.2008.07.064>.
- (301) Kim, J. H.; Kim, Y.; Connor, P. A.; Irvine, J. T. S.; Bae, J.; Zhou, W. Structural, Thermal and Electrochemical Properties of Layered Perovskite SmBaCo<sub>2</sub>O<sub>5+d</sub>, a Potential Cathode Material for Intermediate-Temperature Solid Oxide Fuel Cells. *J Power Sources* **2009**, *194* (2), 704–711. <https://doi.org/10.1016/j.jpowsour.2009.06.024>.
- (302) Jun, A.; Kim, J.; Shin, J.; Kim, G. Optimization of Sr Content in Layered SmBa<sub>1-X</sub>Sr<sub>X</sub>Co<sub>2</sub>O<sub>5+δ</sub> Perovskite Cathodes for Intermediate-Temperature Solid Oxide Fuel Cells. *Int J Hydrogen Energy* **2012**, *37* (23), 18381–18388. <https://doi.org/10.1016/j.ijhydene.2012.09.048>.
- (303) Jun, A.; Shin, J.; Kim, G. High Redox and Performance Stability of Layered SmBa<sub>0.5</sub>Sr<sub>0.5</sub>Co<sub>1.5</sub>Cu<sub>0.5</sub>O<sub>5+δ</sub> Perovskite Cathodes for Intermediate-Temperature Solid Oxide Fuel Cells. *Physical Chemistry Chemical Physics* **2013**, *15* (45), 19906–19912. <https://doi.org/10.1039/c3cp53883d>.
- (304) Jun, A.; Lim, T. H.; Shin, J.; Kim, G. Electrochemical Properties of B-Site Ni Doped Layered Perovskite Cathodes for IT-SOFCs. *Int J Hydrogen Energy* **2014**, *39* (35), 20791–20798. <https://doi.org/10.1016/j.ijhydene.2014.06.136>.
- (305) Kim, J. H.; Cassidy, M.; Irvine, J. T. S.; Bae, J. Electrochemical Investigation of Composite Cathodes with SmBa<sub>0.5</sub>Sr<sub>0.5</sub>Co<sub>2</sub>O<sub>5-δ</sub> Cathodes for Intermediate Temperature-Operating Solid Oxide Fuel Cell. *Chemistry of Materials* **2010**, *22* (3), 883–892. <https://doi.org/10.1021/cm901720w>.
- (306) Ding, X.; Kong, X.; Wu, H.; Zhu, Y.; Tang, J.; Zhong, Y. SmBa<sub>0.5</sub>Sr<sub>0.5</sub>Cu<sub>2</sub>O<sub>5+δ</sub> and SmBa<sub>0.5</sub>Sr<sub>0.5</sub>Cu<sub>2</sub>O<sub>5+δ</sub> Layered Perovskite Oxides as Cathodes for IT-SOFCs. *Int J Hydrogen Energy* **2012**, *37* (3), 2546–2551. <https://doi.org/10.1016/j.ijhydene.2011.10.080>.
- (307) Huang, S.; Feng, S.; Lu, Q.; Li, Y.; Wang, H.; Wang, C. Cerium and Niobium Doped SrCo<sub>3-δ</sub> as a Potential Cathode for Intermediate Temperature Solid Oxide Fuel Cells. *J Power Sources* **2014**, *251*, 357–362. <https://doi.org/10.1016/j.jpowsour.2013.11.096>.

- (308) Song, Y.; Chen, Y.; Xu, M.; Wang, W.; Zhang, Y.; Yang, G.; Ran, R.; Zhou, W.; Shao, Z. A Cobalt-Free Multi-Phase Nanocomposite as Near-Ideal Cathode of Intermediate-Temperature Solid Oxide Fuel Cells Developed by Smart Self-Assembly. *Advanced Materials* **2020**, 32 (8), 1906979. <https://doi.org/10.1002/adma.201906979>.
- (309) Gu, H.; Chen, H.; Gao, L.; Zheng, Y.; Zhu, X.; Guo, L. Effect of Co Doping on the Properties of Sr<sub>0.8</sub>Ce<sub>0.2</sub>MnO<sub>3-δ</sub> Cathode for Intermediate-Temperature Solid-Oxide Fuel Cells. *Int J Hydrogen Energy* **2008**, 33 (17), 4681–4688. <https://doi.org/10.1016/j.ijhydene.2008.06.025>.
- (310) Gu, H.; Chen, H.; Gao, L.; Zheng, Y.; Zhu, X.; Guo, L. Electrochemical Characterization of Co-Doped Sr<sub>0.8</sub>Ce<sub>0.2</sub>MnO<sub>3-δ</sub> Cathodes on Sm<sub>0.2</sub>Ce<sub>0.8</sub>O<sub>1.9</sub>-Electrolyte for Intermediate-Temperature Solid Oxide Fuel Cells. *Electrochim Acta* **2009**, 54 (13), 3532–3537. <https://doi.org/10.1016/j.electacta.2008.12.039>.
- (311) Li, M.; Zhou, W.; Xu, X.; Zhu, Z. SrCo<sub>0.85</sub>Fe<sub>0.1</sub>P<sub>0.05</sub>O<sub>3-δ</sub> Perovskite as a Cathode for Intermediate-Temperature Solid Oxide Fuel Cells. *J Mater Chem A Mater* **2013**, 1 (43), 13632–13639. <https://doi.org/10.1039/c3ta12781h>.
- (312) Zhu, Y.; Sunarso, J.; Zhou, W.; Jiang, S.; Shao, Z. High-Performance SrNb<sub>0.1</sub>Co<sub>0.9</sub>-XFexO<sub>3-δ</sub> Perovskite Cathodes for Low-Temperature Solid Oxide Fuel Cells. *J Mater Chem A Mater* **2014**, 2 (37), 15454–15462. <https://doi.org/10.1039/c4ta03208j>.
- (313) Ding, L.; Wang, L.; Ding, D.; Zhang, S.; Ding, X.; Yuan, G. Promotion on Electrochemical Performance of a Cation Deficient SrCo<sub>0.7</sub>Nb<sub>0.1</sub>Fe<sub>0.2</sub>O<sub>3-Δ</sub> Perovskite Cathode for Intermediate-Temperature Solid Oxide Fuel Cells. *J Power Sources* **2017**, 354, 26–33. <https://doi.org/10.1016/j.jpowsour.2017.04.009>.
- (314) Yoo, C. Y.; Park, J. H.; Yun, D. S.; Lee, Y. A.; Yun, K. S.; Lee, J. H.; Yoon, H.; Joo, J. H.; Yu, J. H. Unraveling Crystal Structure and Transport Properties of Fast Ion Conducting SrCo<sub>0.9</sub>Nb<sub>0.1</sub>O<sub>3-δ</sub>. *Journal of Physical Chemistry C* **2016**, 120 (39), 22248–22256. <https://doi.org/10.1021/acs.jpcc.6b07615>.
- (315) Zhou, W.; Shao, Z.; Ran, R.; Jin, W.; Xu, N. A Novel Efficient Oxide Electrode for Electrocatalytic Oxygen Reduction at 400–600°C. *Chemical Communications* **2008**, No. 44, 5791–5793. <https://doi.org/10.1039/b813327a>.
- (316) Wang, F.; Zhou, Q.; He, T.; Li, G.; Ding, H. Novel SrCo<sub>1-Y</sub>Nb<sub>y</sub>O<sub>3-δ</sub> Cathodes for Intermediate-Temperature Solid Oxide Fuel Cells. *J Power Sources* **2010**, 195 (12), 3772–3778. <https://doi.org/10.1016/j.jpowsour.2009.12.081>.
- (317) Zhu, Y.; Lin, Y.; Shen, X.; Sunarso, J.; Zhou, W.; Jiang, S.; Su, D.; Chen, F.; Shao, Z. Influence of Crystal Structure on the Electrochemical Performance of A-Site-Deficient Sr<sub>1-S</sub>Nb<sub>0.1</sub>Co<sub>0.9</sub>O<sub>3-Δ</sub>Perovskite Cathodes. *RSC Adv* **2014**, 4 (77), 40865–40872. <https://doi.org/10.1039/c4ra06191h>.
- (318) Li, M.; Zhou, W.; Peterson, V. K.; Zhao, M.; Zhu, Z. A Comparative Study of SrCo<sub>0.8</sub>Nb<sub>0.2</sub>O<sub>3-δ</sub> and SrCo<sub>0.8</sub>Ta<sub>0.2</sub>O<sub>3-δ</sub> as Low-Temperature Solid Oxide Fuel Cell Cathodes: Effect of Non-Geometry Factors on the Oxygen Reduction Reaction. *J Mater Chem A Mater* **2015**, 3 (47), 24064–24070. <https://doi.org/10.1039/c5ta07178j>.
- (319) Chen, D.; Chen, C.; Zhang, Z.; Baiyee, Z. M.; Ciucci, F.; Shao, Z. Compositional Engineering of Perovskite Oxides for Highly Efficient Oxygen Reduction Reactions. *ACS Appl Mater Interfaces* **2015**, 7 (16), 8562–8571. <https://doi.org/10.1021/acsami.5b00358>.

- (320) An, B.; Zhou, W.; Guo, Y.; Ran, R.; Shao, Z. A Composite Oxygen-Reduction Electrode Composed of SrSc<sub>0.2</sub>Co<sub>0.8</sub>O<sub>3-δ</sub> Perovskite and Sm<sub>0.2</sub>Ce<sub>0.8</sub>O<sub>1.9</sub> for an Intermediate-Temperature Solid-Oxide Fuel Cell. *Int J Hydrogen Energy* **2010**, *35* (11), 5601–5610. <https://doi.org/10.1016/j.ijhydene.2010.03.044>.
- (321) Zhou, W.; Shao, Z.; Ran, R.; Cai, R. Novel SrSc<sub>0.2</sub>Co<sub>0.8</sub>O<sub>3-δ</sub> as a Cathode Material for Low Temperature Solid-Oxide Fuel Cell. *Electrochim commun* **2008**, *10* (10), 1647–1651. <https://doi.org/10.1016/j.elecom.2008.08.033>.
- (322) Zhou, W.; Sunarso, J.; Zhao, M.; Liang, F.; Klande, T.; Feldhoff, A. A Highly Active Perovskite Electrode for the Oxygen Reduction Reaction below 600 °c. *Angewandte Chemie - International Edition* **2013**, *52* (52), 14036–14040. <https://doi.org/10.1002/anie.201307305>.
- (323) Chen, G.; Sunarso, J.; Wang, Y.; Ge, C.; Yang, J.; Liang, F. Evaluation of A-Site Deficient Sr<sub>1-x</sub>Sc<sub>0.175</sub>Nb<sub>0.025</sub>Co<sub>0.8</sub>O<sub>3-δ</sub> (X=0, 0.02, 0.05 and 0.1) Perovskite Cathodes for Intermediate-Temperature Solid Oxide Fuel Cells. *Ceram Int* **2016**, *42* (11), 12894–12900. <https://doi.org/10.1016/j.ceramint.2016.05.057>.
- (324) Shen, Y.; Wang, F.; Ma, X.; He, T. SrCo<sub>1-Y</sub>Ti<sub>y</sub>O<sub>3-δ</sub> as Potential Cathode Materials for Intermediate-Temperature Solid Oxide Fuel Cells. *J Power Sources* **2011**, *196* (18), 7420–7425. <https://doi.org/10.1016/j.jpowsour.2011.04.025>.
- (325) Li, M.; Zhou, W.; Zhu, Z. Comparative Studies of SrCo<sub>1-X</sub>TaxO<sub>3-δ</sub> (X=0.05-0.4) Oxides as Cathodes for Low-Temperature Solid-Oxide Fuel Cells. *ChemElectroChem* **2015**, *2* (9), 1331–1338. <https://doi.org/10.1002/celc.201500157>.
- (326) Jiang, L.; Wang, J.; Xiong, X.; Jin, X.; Pei, Q.; Huang, K. Thermal and Electrical Stability of Sr<sub>0.9</sub>Y<sub>0.1</sub>CoO<sub>2.5+δ</sub> as a Promising Cathode for Intermediate-Temperature Solid Oxide Fuel Cells . *J Electrochem Soc* **2016**, *163* (5), F330–F335. <https://doi.org/10.1149/2.0361605jes>.
- (327) Fernández-Ropero, A. J.; Porras-Vázquez, J. M.; Cabeza, A.; Slater, P. R.; Marrero-López, D.; Losilla, E. R. High Valence Transition Metal Doped Strontium Ferrites for Electrode Materials in Symmetrical SOFCs. *J Power Sources* **2014**, *249*, 405–413. <https://doi.org/10.1016/j.jpowsour.2013.10.118>.
- (328) Zhang, Z.; Chen, D.; Wang, J.; Tan, S.; Yu, X.; Shao, Z. Highly Active and Stable Cobalt-Free Hafnium-Doped SrFe<sub>0.9</sub>Hf<sub>0.1</sub>O<sub>3-δ</sub> Perovskite Cathode for Solid Oxide Fuel Cells. *ACS Appl Energy Mater* **2018**, *1* (5), 2134–2142. <https://doi.org/10.1021/acsaem.8b00198>.
- (329) Jiang, S.; Sunarso, J.; Zhou, W.; Shen, J.; Ran, R.; Shao, Z. Cobalt-Free SrNb<sub>x</sub>Fe<sub>1-x</sub>O<sub>3-δ</sub> (x = 0.05, 0.1 and 0.2) Perovskite Cathodes for Intermediate Temperature Solid Oxide Fuel Cells. *J Power Sources* **2015**, *298*, 209–216. <https://doi.org/10.1016/j.jpowsour.2015.08.063>.
- (330) Zhou, Q.; Zhang, L.; He, T. Cobalt-Free Cathode Material SrFe<sub>0.9</sub>Nb<sub>0.1</sub>O<sub>3-δ</sub> for Intermediate-Temperature Solid Oxide Fuel Cells. *Electrochim commun* **2010**, *12* (2), 285–287. <https://doi.org/10.1016/j.elecom.2009.12.016>.
- (331) Jiang, S.; Zhou, W.; Niu, Y.; Zhu, Z.; Shao, Z. Phase Transition of a Cobalt-Free Perovskite as a High-Performance Cathode for Intermediate-Temperature Solid Oxide Fuel Cells. *ChemSusChem* **2012**, *5* (10), 2023–2031. <https://doi.org/10.1002/cssc.201200264>.

- (332) Jiang, S.; Liang, F.; Zhou, W.; Shao, Z. Hierarchical Porous Cobalt-Free Perovskite Electrode for Highly Efficient Oxygen Reduction. *J Mater Chem* **2012**, *22* (32), 16214–16218. <https://doi.org/10.1039/c2jm33311b>.
- (333) Liang, F.; Wang, Z.; Wang, Z.; Mao, J.; Sunarso, J. Electrochemical Performance of Cobalt-Free Nb and Ta Co-Doped Perovskite Cathodes for Intermediate-Temperature Solid Oxide Fuel Cells. *ChemElectroChem* **2017**, *4* (9), 2366–2372. <https://doi.org/10.1002/celc.201700236>.
- (334) Rehman, A. U.; Li, M.; Knibbe, R.; Khan, M. S.; Peterson, V. K.; Brand, H. E. A.; Li, Z.; Zhou, W.; Zhu, Z. Enhancing Oxygen Reduction Reaction Activity and CO<sub>2</sub> Tolerance of Cathode for Low-Temperature Solid Oxide Fuel Cells by in Situ Formation of Carbonates. *ACS Appl Mater Interfaces* **2019**, *11* (30), 26909–26919. <https://doi.org/10.1021/acsami.9b07668>.
- (335) Jung, W. C.; Tuller, H. L. A New Model Describing Solid Oxide Fuel Cell Cathode Kinetics: Model Thin Film SrTi 1-XFe XO 3-Δmixed Conducting Oxides - A Case Study. *Adv Energy Mater* **2011**, *1* (6), 1184–1191. <https://doi.org/10.1002/aenm.201100164>.
- (336) dos Santos-Gómez, L.; Compana, J. M.; Bruque, S.; Losilla, E. R.; Marrero-López, D. Symmetric Electrodes for Solid Oxide Fuel Cells Based on Zr-Doped SrFeO<sub>3</sub>- $\delta$ . *J Power Sources* **2015**, *279*, 419–427. <https://doi.org/10.1016/j.jpowsour.2015.01.043>.
- (337) Porras-Vazquez, J. M.; Pike, T.; Hancock, C. A.; Marco, J. F.; Berry, F. J.; Slater, P. R. Investigation into the Effect of Si Doping on the Performance of SrFeO 3- $\delta$  SOFC Electrode Materials. *J Mater Chem A Mater* **2013**, *1* (38), 11834–11841. <https://doi.org/10.1039/c3ta12113e>.
- (338) Chen, G.; Wang, Y.; Sunarso, J.; Liang, F.; Wang, H. A New Scandium and Niobium Co-Doped Cobalt-Free Perovskite Cathode for Intermediate-Temperature Solid Oxide Fuel Cells. *Energy* **2016**, *95*, 137–143. <https://doi.org/10.1016/j.energy.2015.11.061>.
- (339) Gu, H.; Sunarso, J.; Yang, G.; Zhou, C.; Song, Y.; Zhang, Y.; Wang, W.; Ran, R.; Zhou, W.; Shao, Z. Turning Detrimental Effect into Benefits: Enhanced Oxygen Reduction Reaction Activity of Cobalt-Free Perovskites at Intermediate Temperature via CO<sub>2</sub>-Induced Surface Activation. *ACS Appl Mater Interfaces* **2020**, *12* (14), 16417–16425. <https://doi.org/10.1021/acsami.0c00975>.
- (340) Yang, G.; Su, C.; Chen, Y.; Dong, F.; Tade, M. O.; Shao, Z. Cobalt-Free SrFe0.9Ti0.1O<sub>3</sub>- $\delta$  as a High-Performance Electrode Material for Oxygen Reduction Reaction on Doped Ceria Electrolyte with Favorable CO<sub>2</sub> Tolerance. *J Eur Ceram Soc* **2015**, *35* (9), 2531–2539. <https://doi.org/10.1016/j.jeurceramsoc.2015.03.005>.
- (341) Yu, X.; Long, W.; Jin, F.; He, T. Cobalt-Free Perovskite Cathode Materials SrFe<sub>1-X</sub>Ti<sub>X</sub>O<sub>3</sub>- $\delta$  and Performance Optimization for Intermediate-Temperature Solid Oxide Fuel Cells. *Electrochim Acta* **2014**, *123*, 426–434. <https://doi.org/10.1016/j.electacta.2014.01.020>.
- (342) Wang, Z.; Yang, Z.; Song, Y.; Mao, J.; Liang, F.; Zhou, W. Alkaline Metal Doped Strontium Cobalt Ferrite Perovskites as Cathodes for Intermediate-Temperature Solid Oxide Fuel Cells. *Int J Hydrogen Energy* **2018**, *43* (29), 13420–13429. <https://doi.org/10.1016/j.ijhydene.2018.05.057>.
- (343) Fullarton, I. C.; Jacobs, J.-P.; van Benthem, H. E.; Kilner, J. A.; Brongersma, H. H.; Scanlon, P. J.; Steele, B. C. H. *Study of Oxygen Ion Transport in Acceptor Doped Samarium Cobalt Oxide*; 1995; Vol. 1.

- (344) Guo, Y.; Chen, D.; Shi, H.; Ran, R.; Shao, Z. Effect of Sm<sup>3+</sup> Content on the Properties and Electrochemical Performance of Sm<sub>x</sub>Sr<sub>1-x</sub>CoO<sub>3-δ</sub> (0.2 ≤ x ≤ 0.8) as an Oxygen Reduction Electrodes on Doped Ceria Electrolytes. *Electrochim Acta* **2011**, *56* (7), 2870–2876. <https://doi.org/10.1016/j.electacta.2010.12.075>.
- (345) Yeh, T. C.; Routbort, J. L.; Mason, T. O. Oxygen Transport and Surface Exchange Properties of Sr<sub>0.5</sub>Sm<sub>0.5</sub>CoO<sub>3-δ</sub>. *Solid State Ion* **2013**, *232*, 138–143. <https://doi.org/10.1016/j.ssi.2012.11.024>.
- (346) Dong, F.; Chen, D.; Ran, R.; Park, H.; Kwak, C.; Shao, Z. A Comparative Study of Sm<sub>0.5</sub>Sr<sub>0.5</sub>MO<sub>3-δ</sub> (M = Co and Mn) as Oxygen Reduction Electrodes for Solid Oxide Fuel Cells. *Int J Hydrogen Energy* **2012**, *37* (5), 4377–4387. <https://doi.org/10.1016/j.ijhydene.2011.11.150>.
- (347) Yoo, S.; Lim, T. H.; Shin, J.; Kim, G. Comparative Characterization of Thermodynamic, Electrical, and Electrochemical Properties of Sm<sub>0.5</sub>Sr<sub>0.5</sub>Co<sub>1-x</sub>NbxO<sub>3-δ</sub> (x = 0, 0.05, and 0.1) as Cathode Materials in Intermediate Temperature Solid Oxide Fuel Cells. *J Power Sources* **2013**, *226*, 1–7. <https://doi.org/10.1016/j.jpowsour.2012.10.069>.
- (348) Baek, S. W.; Kim, J. H.; Bae, J. Characteristics of ABO<sub>3</sub> and A<sub>2</sub>BO<sub>4</sub> (A=Sm, Sr; B=Co, Fe, Ni) Samarium Oxide System as Cathode Materials for Intermediate Temperature-Operating Solid Oxide Fuel Cell. *Solid State Ion* **2008**, *179* (27–32), 1570–1574. <https://doi.org/10.1016/j.ssi.2007.12.010>.
- (349) Lv, H.; Wu, Y. ji; Huang, B.; Zhao, B. yuan; Hu, K. ao. Structure and Electrochemical Properties of Sm<sub>0.5</sub>Sr<sub>0.5</sub>Co<sub>1-x</sub>Fe<sub>x</sub>O<sub>3-δ</sub> Cathodes for Solid Oxide Fuel Cells. *Solid State Ion* **2006**, *177* (9–10), 901–906. <https://doi.org/10.1016/j.ssi.2006.01.038>.
- (350) Duong, A. T.; Mumm, D. R. On the Interaction of SSC and LSGM in Composite SOFC Electrodes. *J Power Sources* **2013**, *241*, 281–287. <https://doi.org/10.1016/j.jpowsour.2013.04.046>.
- (351) Zhang, H.; Chen, G.; Tang, L. Cubic Perovskite-Type Sm<sub>0.3</sub>Sr<sub>0.7</sub>Nb<sub>0.08</sub>Co<sub>0.92</sub>O<sub>3-δ</sub> as a Novel Cathode Material for Intermediate Temperature Solid Oxide Fuel Cells. *Chemical Communications* **2020**, *56* (9), 1361–1364. <https://doi.org/10.1039/c9cc07374d>.
- (352) Zhang, Y.; Gao, X.; Sunarso, J.; Liu, B.; Zhou, W.; Ni, M.; Shao, Z. Significantly Improving the Durability of Single-Chamber Solid Oxide Fuel Cells: A Highly Active CO<sub>2</sub>-Resistant Perovskite Cathode. *ACS Appl Energy Mater* **2018**, *1* (3), 1337–1343. <https://doi.org/10.1021/acsaem.8b00051>.
- (353) Ling, Y.; Zhao, L.; Lin, B.; Dong, Y.; Zhang, X.; Meng, G.; Liu, X. Investigation of Cobalt-Free Cathode Material Sm<sub>0.5</sub>Sr<sub>0.5</sub>Fe<sub>0.8</sub>Cu<sub>0.2</sub>O<sub>3-δ</sub> for Intermediate Temperature Solid Oxide Fuel Cell. *Int J Hydrogen Energy* **2010**, *35* (13), 6905–6910. <https://doi.org/10.1016/j.ijhydene.2010.04.021>.
- (354) Li, Y.; Kim, Y. N.; Cheng, J.; Alonso, J. A.; Hu, Z.; Chin, Y. Y.; Takami, T.; Fernández-Díaz, M. T.; Lin, H. J.; Chen, C. te; Tjeng, L. H.; Manthiram, A.; Goodenough, J. B. Oxygen-Deficient Perovskite Sr<sub>0.7</sub>Y<sub>0.3</sub>CoO<sub>2.65-δ</sub> as a Cathode for Intermediate-Temperature Solid Oxide Fuel Cells. *Chemistry of Materials* **2011**, *23* (22), 5037–5044. <https://doi.org/10.1021/cm202542q>.
- (355) Meng, F.; Xia, T.; Wang, J.; Shi, Z.; Lian, J.; Zhao, H.; Bassat, J. M.; Grenier, J. C. Evaluation of Layered Perovskites YBa<sub>1-x</sub>Sr<sub>x</sub>Co<sub>2</sub>O<sub>5+δ</sub> as Cathodes for Intermediate-Temperature

Solid Oxide Fuel Cells. *Int J Hydrogen Energy* **2014**, *39* (9), 4531–4543.  
<https://doi.org/10.1016/j.ijhydene.2014.01.008>.

- (356) Xue, J.; Shen, Y.; He, T. Double-Perovskites  $\text{YBaCo}_2\text{-}\text{XFexO}_5+\delta$  Cathodes for Intermediate-Temperature Solid Oxide Fuel Cells. *J Power Sources* **2011**, *196* (8), 3729–3735.  
<https://doi.org/10.1016/j.jpowsour.2010.12.071>.